DEWATERING OF ACTIVATED SLUDGE - A GLOBAL APPROACH

Adrian-Gabriel Ghiaus[1,2], Jean Vaxelaire[1], Michel Roques[1] and Didier Anglerot[2]

1. Université de Pau et des Pays de l'Adour, Laboratoire de Génie des Procédés de Pau
Rue Jules Ferry, 64000 Pau, France, E-mail: ghiaus@mech.upatras.gr
2. Elf-Atochem, Groupement de Recherches de Lacq,
R.N. 117, B.P. 34, 64170 Lacq, France

Keywords: activated sludge, waste treatment, filtration-compression, convective drying

ABSTRACT

Dewatering of sludge is requested in order to achieve small transportation and storage volumes and/or enough calorific value to enable self-supporting combustion of the biomass. Due to its much low energy costs, mechanical dewatering is used as a first step to eliminate the water. However, the final moisture content reached through this method, generally, is not sufficient and drying becomes obligatory.
Four processes of water elimination, i.e. decantation, filtration, compression and convective drying, were examined in order to evaluate, by laboratory experiments, the dewatering of fresh activated sludge (both flocculated and unflocculated), supplied by a wastewater treatment pilot-station in operation at Lacq, France (Elf-G.R.L.). The processes are depending on each other as well as on the sludge characteristics and on the filtration-compression and drying operation parameters. Their dynamic analysis and interpretation should lead to a global optimization and provide data for designing high-performance treatment plants.

INTRODUCTION

Wastewater treatment processes, using the biologic oxidation as cleanup method, generate huge amount of waste activated sludge. In the aerobic treatment plants, the activated sludge is produced as the microorganisms convert some of the oxidizable matter from the wastewater to microbial cell mass. Much of this biomass is recycled through the aeration unit but, in order to maintain constant concentration of microorganisms inside the reactor, the excess of biomass must be withdrawn and it has to be wasted. In actual industrial practice, the waste biomass is eliminated through various ways, e.g. incineration, sanitary landfill, composting for agricultural valorization, rejection in oceans and seas, and others (Vasilind, 1979). In the near future, new environmental regulations will prohibit the sewage sludge to be dumped in

nature and only minimal wastes will be accepted (OTV, 1997). Therefore, quasi-total elimination methods, such as incineration and land application, are of obvious interest, and very low moisture content of the waste sludge is required to be achieved.
For example, in the case of incineration, heat will be consumed in evaporating water before any combustion heat is released from the process. Excess moisture content in the dewatered sludge will lead to losses in boiler efficiency during the incineration process. Thus, efficient dewatering prior to combustion is desirable.
Mechanical dewatering has found extensive industrial applications in solid-liquid separation mainly due to its low energy consumption in comparison with classical thermal methods. Waste activated sludge is difficult to dewater and usually the addition of coagulants and/or flocculants is essential before the mechanical pressure is applied to force out the water. On the other hand, these polymeric chemicals can contribute significantly to the operation cost of the wastewater treatment plants (Rehmat *et al.*, 1997).
The filtration-compression of suspensions has received extensive theoretical and experimental investigation (Shirato *et al*., 1986; Novak *et al.,* 1999; Tiller *et al.,* 1999). Techniques were developed and corroborated in order to evaluate and explain the internal and macroscopic characteristics of the filter cakes. Recently, Lee *et al.* (2000) have proposed a review of the various theories dealing with filtration and compression and their implications to sludge dewatering. However, in the case of activated sludge, experimental data is still generally lacking due to the variability and the complexity of this kind of material. As is commonly known, biological sludge samples substantially differ from particulate sludge samples, exhibiting a higher porous and fractal-like structure, a high dewatering resistance, and a large amount of bound water.

FILTRATION-COMPRESSION PROCESS

The mechanical dewatering process comprises two consecutive phases: *filtration,* where the elimination of the liquid from a thin sludge (suspension) generates the formation of a filter cake, and *compression,* where the built-up cake is squeezed and extra liquid faces expulsion due and according to the applied pressure. A very dense, saturated with liquid particle-packing is obtained. Usually, the filtration-compression (expression) process is carried out under constant pressure and a graphical representation of the ratio t/V (time / filtrate volume) versus V (filtrate volume) is used to describe the process behavior.

Filtration phase

Ruth's equation generally well describes the filtration sub-process:

$$\frac{t}{V} = \frac{\mu \alpha W}{2A^2 \Delta p} \cdot V + \frac{\mu R_s}{A \Delta p} \tag{1}$$

It is typically considered for industrial design and simulation analysis. The specific resistance (α) is an index that can be used to characterize dewaterability of the suspension; higher it is, more difficult is to dewater the sludge. For compressible sludge, the specific resistance of the cake also depends on the applied pressure. Different empirical relationships are proposed in the literature to correlate α to the applied pressure. In this study the experimental data is well characterized by the function:

$$\alpha = \alpha_o \cdot (\Delta p)^n \tag{2}$$

where the compressibility coefficient (n) describes the sludge ability to be compressed during the filtration phase.

Compression phase

A convenient way to describe the compression process using experimental results is to plot the consolidation ratio (U_c) against time. For processes having elastic behavior, the mathematical model based on Terzaghi's approach, well outlines the compression phase (Shirato *et al.*, 1986):

$$U_c = \frac{z_o - z}{z_o - z_\infty} = 1 - \exp\left(- \frac{\pi^2 C_e}{4{\omega_o}^2} \cdot t \right) \tag{3}$$

C_e is the consolidation coefficient, which in a first approach, can be considered as a constant. ω_o is the total volume of solids in the cake per unit of filtration area. In the case of filtration-compression experiments, its value depends on the quantity of biomass introduced into the cell:

$$\omega_o = \frac{m_s}{\rho_s \cdot A} \tag{4}$$

Based on fundamental investigation of constant-pressure expression both in theory and practice, Shirato *et al.* (1986) have adopted the combined Terzaghi-Voigt's rheological model to describe the consolidation process that exhibits a visco-elastic behavior. According to this model, the compression phase has two stages (primary and secondary) and is mathematically described by the equation (5):

$$U_c = \frac{z_o - z}{z_o - z_\infty} = (1 - B)\left[1 - \exp\left(- \frac{\pi^2 C'_e}{4{\omega_o}^2} \cdot t \right) \right] + B[1 - \exp(-\eta \cdot t)] \tag{5}$$

where, in addition to equation (3), B is the fraction of moisture removed during the secondary consolidation stage; C'_e is the modified consolidation coefficient; and η the creep factor.
Assuming that the rate of primary consolidation is much faster than the rate of secondary consolidation, which is normally the case in practice, a reduced form of the equation (5), under the infinite consolidation time limit, is derived as follows (Chu *et al.*, 1999):

$$U_c = \frac{z_o - z}{z_o - z_\infty} = 1 - B\exp(-\eta \cdot t) \tag{6}$$

These relationships enable an estimation of the time of compression needed to reach a given moisture content into the cake and then a satisfactory design of industrial filters. This approach requires experimental investigations on a filtration-compression cell followed by a mathematical fitting procedure in order to derive the parameters B, C_e, C'_e and η.

CONVECTIVE DRYING PROCESS

After the mechanical dewatering step, thermal drying is used to lower the moisture content of the consolidated sludge (up to 0.05 kg/kg can be achieved). Elimination of free and bound water by convective drying is relatively well characterized by the evaporated vapor flux (Vaxelaire *et al.*, 1999):

$$\dot{m}_v = m_c \frac{dX_{av}}{dt} \tag{7}$$

where m_c is the mass of the cake, X_{av} is the average moisture content and t is the time.
The plotted graph of the water evaporation rate versus the mean moisture content of the cake, under defined conditions, represents the drying rate curve. The analysis of these curves gives information about the drying characteristics (periods, critical and equilibrium moisture content, maximum rate of evaporation).

MATERIALS AND METHODS

Waste Activated Sludge

Aiming to have similar test samples, the activated sludge was picked up from the aeration tank of a wastewater treatment pilot-station in operation at Lacq, France (Elf-Atochem, G.R.L.), that works under controlled conditions. Because of the high degree of dilution (99.6 % water content), prior to the filtration-compression process, all the sludge samples were thickened by gravitational sedimentation, the water content lowering up to 96 %.

Sludge Conditioning

A variety of polymer application options are available to aid in improving the dewaterability of sludge. The addition of long chain flocculant polymers binds the solid particles into large flocs. In this study, the sludge was flocculated with a solution of 1 g/l of cationic polymer (FO4800MPM), manufactured by SNF-Floerger, with a dose of 4 g flocculant per kg of biomass.

Filtration-compression cell

Mechanical dewatering was carried out using a laboratory-scale filtration-compression cell. It allows up to 500 ml of diluted sludge to be expressed under constant pressure, ranging from 0 to 30 bar. Filtrate mass, piston position and applied pressure were on-line recorded by a personal computer. Diagrams representing the time evolution of the significant parameters were plotted and analyzed to interpret the measured data and to evaluate the mathematical model constants.

Convective drying rig

Thermal dewatering was performed with a convective drying rig. A data acquisition system adjusts and controls the drying air parameters, i.e. velocity, temperature and humidity, and records the mass and the temperature of the humid cake to be dried. Reduction of cake dimensions due to shrinkage effect can be identified by visual observation.

EXPERIMENTS, RESULTS AND DISCUSSIONS

The computation of experimental data allows the analysis of several characteristic parameters of the sludge behavior during the dewatering processes.
One of the series of measurements has concerned the examination of the biomass unitary-load and cake thickness influences on the filtration-compression and drying processes, respectively.
The diluted sludge ($C_{ds} \approx 4$ g/kg) was flocculated with FO4800MPM and decanted until different concentrations. Filtration-compression tests were done for samples of 200 ml under applied pressure of 2 bar. For three significant samples, the main results are presented in Table 1.
Figure 1 gives the filtration-compression curves for the three presented cases. The filterability increases with the decrease in biomass load of the sludge.

Table 1: Main parameters for filtration-compression of flocculated sludge

Parameters	**Sample 1**	**Sample 2**	**Sample 3**
Biomass unitary load, kg/m^2	0.542	1.114	1.623
Initial concentration, kg/m^3	10.4	21.4	31.3
Filtration time, min	3	11	14
Compression time, min	70	311	337
Specific resistance of the cake, m/kg	$5.166 \cdot 10^{12}$	$8.528 \cdot 10^{12}$	$7.394 \cdot 10^{12}$

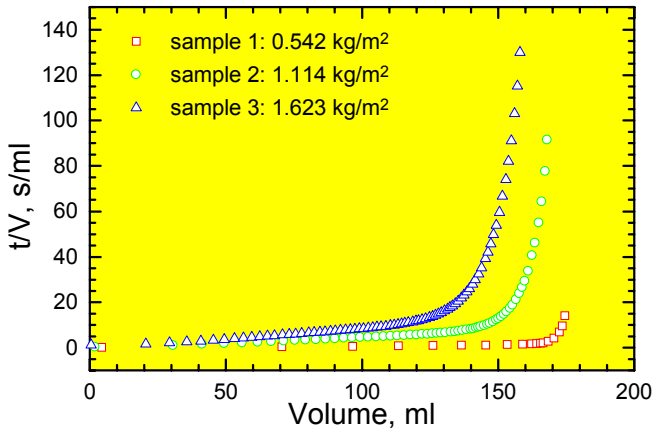

Figure 1. Filtration-compression characteristic curves

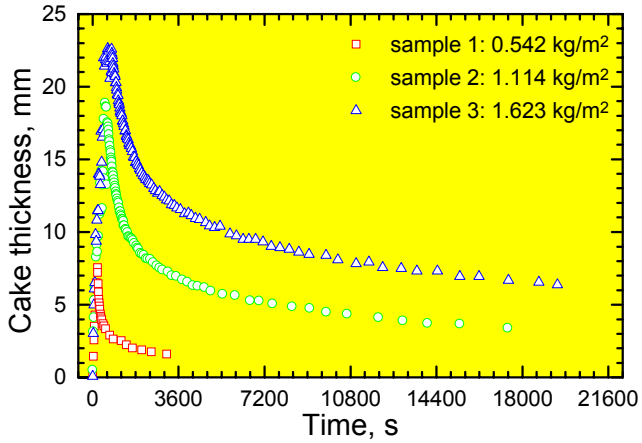

Figure 2. Evolution of the cake thickness

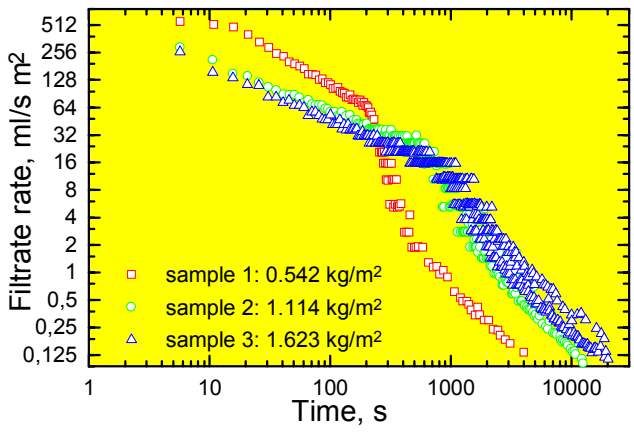

Figure 3. Unitary filtrate rate during expression

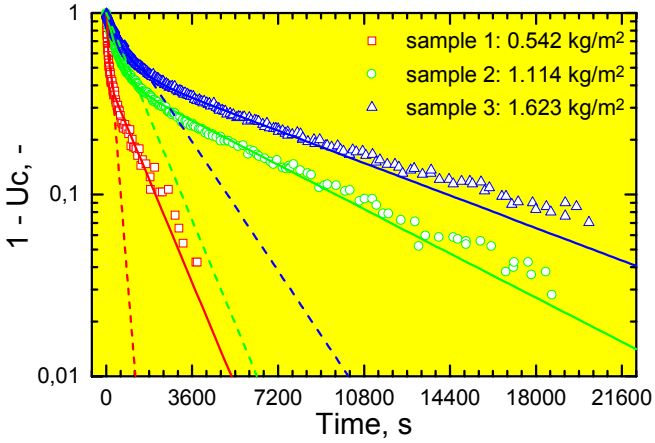

Figure 4. Characterization of compression phase
symbol = experimental data
dash line = elastic model of Terzaghi
solid line = visco-elastic model of Shirato

During the filtration phase, the cake is built up, reaching a maximum thickness at the transition between filtration and compression (Figure 2). Filtration period can be easily identified from the diagram of filtrate-rate versus time (Figure 3), plotted in logarithmic scale. The slope, which is constant for the filtration, obviously changes at transition to the compression phase. The instruments allow accurate measurement of filtrate apparent velocity up to 50 µm/s. For the investigated sludge, the transition point can be analytically computed from the second derivate solution of the function V = f(t), equation (8), where the coefficients are obtained by fitting the experimental data.

$$V = c_1\left(1 - \frac{1}{1 + c_1 c_2 \cdot t}\right) + c_3\left(1 - \frac{1}{1 + c_3 c_4 \cdot t}\right) \quad (8)$$

The visco-elastic approach enables a good characterization of the compression of activated sludge in the laboratory cell (Figure 4). The concentration of the sludge to be dewatered has a relatively significant impact on the experimental result and thus on the model parameters (Table 2). So one must be careful when designing compression units based on process modeling. Moreover, the accuracy of the result needs a good evaluation of the cake thickness at infinite compression time. For the studied sludge, the best results for the z_∞ estimation are given by regressing the cake thickness with the following function:

$$z = z_\infty + \frac{c_1}{\exp(c_2 \cdot t)} + \frac{c_3}{\exp(c_4 \cdot t)} \quad (9)$$

After compression, the humid cake was dried under a hot air-stream (2 m/s, 68 °C, 6 %) until it reached the equilibrium moisture content (around 0.05 kg/kg). The main parameters of drying process are given in the Table 3. The evolution in time of the cake moisture content is given in Figure 5 and the cake surface temperature in Figure 6. Drying kinetics can be analyzed by representing the mass flux of water vapors as a function of time and moisture content, Figure 7 and 8, respectively.

Table 2: Compression modeling: model parameters

Flocculated Sludge	**Sample 1**	**Sample 2**	**Sample 3**
Initial concentration, kg/m^3	10.4	21.4	31.3
Model of Terzaghi			
π^2 C_e (ρ_s. A)^2/ 4, kg^2/s	$1.64 \cdot 10^{-8}$	$1.34 \cdot 10^{-8}$	$1.77 \cdot 10^{-8}$
Model of Shirato			
π^2 C'_e (ρ_s. A)^2/ 4, kg^2/s	$6.18 \cdot 10^{-8}$	$2.86 \cdot 10^{-9}$	$4.35 \cdot 10^{-9}$
B, -	0.446	0.553	0.489
η, s^{-1}	$0.724 \cdot 10^{-3}$	$2.248 \cdot 10^{-3}$	$1.489 \cdot 10^{-3}$

Table 3: Main parameters of humid cake drying

Parameters	**Sample 1**	**Sample 2**	**Sample 3**
Initial mass of the cake, g	8.187	15.358	27.562
Initial thickness of the cake, mm	1.8	3.2	6.3
Initial moisture content, %	74.30	71.84	77.07
Final thickness of the cake, mm	1.3	2.6	4.0
Final diameter, mm	51	53	52
Final mass, g	2.221	4.550	6.573
Final moisture content, %	5.268	4.950	3.864
Maximum evaporation rate, g/s m^2	0.560	0.495	0.500
Constant rate period, min	18	18	33
Total drying time, min	100	200	420

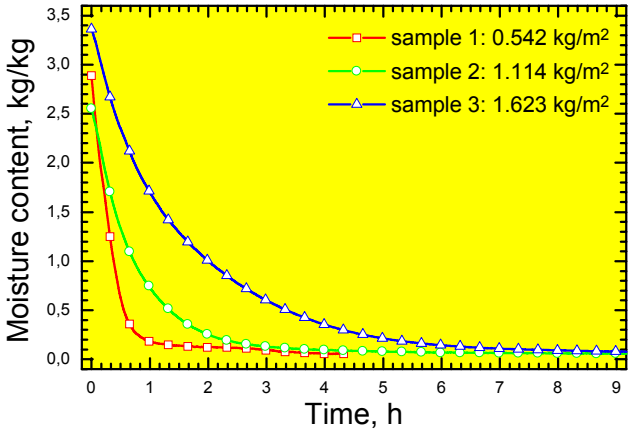

Figure 5: Evolution of moisture content

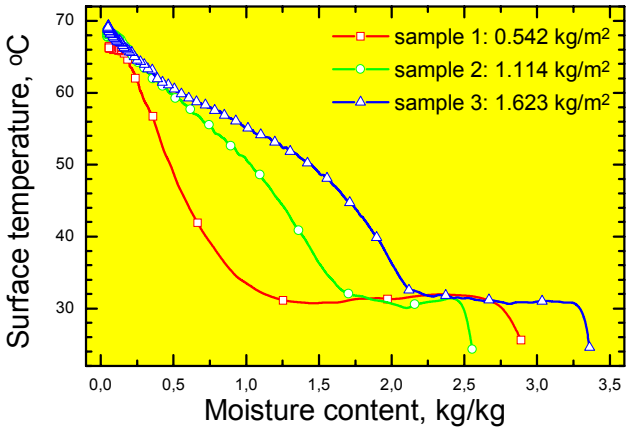

Figure 6: Surface temperature vs. moisture content

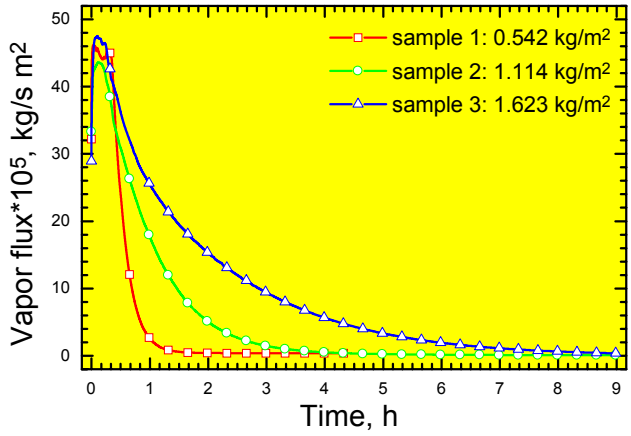

Figure 7: Evolution of vapor mass flux

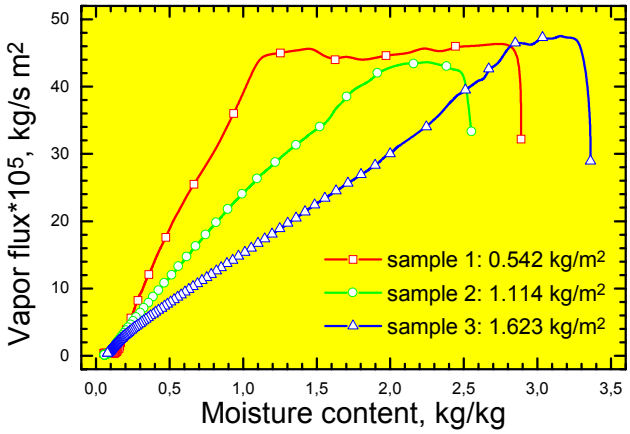

Figure 8: Evaporation mass flux vs. moisture content

The kinetic curves (Figures 7 and 8) exhibit classical behavior starting with a constant evaporation mass flux density period (around 20 minutes) which is controlled by the external conditions (temperature, velocity and humidity of the drying air). During the second drying step (falling rate period) the water transfer depends both on the external conditions and on the migration ability of the water within the material. Experimental data have indicated different duration of falling rate periods depending on the sample initial characteristics (thickness, moisture content, etc.). This fact could be due to different migration rates and/or to the pertinence of the "characteristic" parameters. Throughout the second drying period, one has observed that the surface of the material was very dry while the core of the cake remains wet. The thickness of the surface dry layer increases as drying occurs. The moisture content of the cake at each time is calculated as a global parameter even if different parts contain different moisture content. Thus the average moisture content masks some information and a local approach based on moisture content profiles into the material should give interesting data for the study of sludge drying.

CONCLUSIONS

Experimental investigations were carried out to evaluate the mechanical and thermal dewatering of activated sludge. To avoid variability problem (generally observed with this kind of material) experiments were performed on sludge issued from a laboratory pilot plant working under controlled conditions The diluted sludge, with a water content of 99.6 % in the aeration tank, was conditioned with cationic polymer and thickened up to 96 % by gravitational sedimentation. After the filtration-compression process, a

compact cake with approx. 75 % water content is obtained. The overall specific resistance of the cake, built up during the filtration phase, was found around $6 \cdot 10^{12}$ m/kg, and the average filtrate flow rate at transition between filtration and compression, about 50 ml/s·m^2. The compression of activated sludge can be characterized by the Shirato model (viscoelastic behavior). The model was validated by experimental data and the impact of sludge concentration on the model parameters must be noted.
Convective drying was carried out using a stream of hot air (2 m/s, 68 °C, 6 %). At the end of the process, the final cake moisture content was about 5 %. The maximum reached value of evaporation rate was around 0.5 g/s·m^2. Mass transfer coefficient for the constant rate period of drying was measured to be about $1.656 \cdot 10^{-4}$ g/s m^2 Pa. The shrinkage effect during drying was important, leading to a decrease in sample volume with more than 60 %. The drying study indicates an influence of the initial thickness of the sample on the results.
The constant-pressure filtration-compression and the drying laboratory tests provide valuable information for the design and optimum operation of dewatering plants. Nevertheless, one must be careful with the use of laboratory experimental data in process design.

ACKNOWLEDGMENT

This work was carried out in the framework of a post-doctoral research grant awarded to Adrian-Gabriel GHIAUS by Elf-Aquitaine Society.

NOTATION

A	filtration area	m^2
B	constant	-
C	total concentration (suspension and disolved)	g/kg
C_e	consolidation coefficient	m^2/s
C'_e	modified consolidation coefficient	m^2/s
$c_{1,2,\ldots}$	coefficients	-
m	mass	kg
n	compressibility coefficient	-
R_s	resistance of filtration support	m^{-1}
t	time	s
U_c	consolidation ratio	-
V	volume of filtrate	m^3
W	specific mass of dry cake per unit of filtrate volume	kg/m^3
X	moisture content	kg/kg
z	cake thickness	m

Greek Symbols

α	specific resistance	m/kg
α_o	unitary specific resistance	m/kg Pa^n
Δp	filtration-compression applied pressure	Pa
η	creep factor (secondary compression coefficient)	s^{-1}
μ	viscosity of filtrate	Pa s
ρ	density	Kg/m^3
ω_o	specific volume of wet cake	m

Subscripts

av	average
c	cake
ds	diluted sludge
o	filtration-compression transition state
s	solids of biomass
v	vapor
∞	infinite consolidation state

Superscripts

Over dot	derivate in regard to time

LITERATURE

Chu, C.P. and Lee, D.J., (1999), Three stages of consolidation dewatering of sludges, Journal of Environmental Engineering, no. 10, pp. 959-965

Lee, D. J. and Wang, C. H., (2000), Theories of cake filtration and consolidation and implications to sludge dewatering, Water Research, vol. 34(1), pp. 1-20

Novak, J.T., Agerbaek, M.L., Sorensen, B.L. and Hansen J.A., (1999), Conditiong, filtering, and expressing waste activated sludge, Journal of Environmental Engineering, sept, pp. 816-824

OTV, (1997), Traiter et valoriser les boues, OTV collection (France)

Rehmat, T., Branion, R., Duff, S. and Groves, M., (1997), A laboratory sludge press for characterizing sludge dewatering, Water Science Technology, vol. 35, no. 2-3, pp. 189-196

Shirato, M., Murase, T., Iwata, M. and Nakatsuka, S., (1986), The Terzaghi-Voigt combined model for constant pressure consolidation of filter cakes and homogeneous semi-solid materials, Chemical Engineering Science, vol. 41(12), pp. 3213-3218

Tiller, F.M., Lu, R., Kwon, J. H. and Lee, D. J., (1999) Variable flow rate in compactible filter cakes, Water Research, vol. 33(1), pp. 15-22

Vasilind, P.A., (1979), Treatment and disposal of wastewater sludge, Ann Arbor Science, Ann Arbor, Mich.

Vaxelaire, J., Bongiovanni, J.-M. and Puiggali, J.-R., (1999), Mechanical dewatering and thermal drying of residual sludge, Environmental Technology, vol. 20, pp. 29-36

Available online at www.sciencedirect.com
SCIENCE DIRECT®
Journal of Food Engineering 75 (2006) 542–550
JOURNAL OF FOOD ENGINEERING
www.elsevier.com/locate/jfoodeng

Dried product quality improvement by air flow manipulation in tray dryers

Dionissios P. Margaris *, Adrian-Gabriel Ghiaus

University of Patras, Fluid Mechanics Laboratory, GR-265 00 Patras, Hellas, Greece

Received 20 October 2004; accepted 27 April 2005
Available online 29 June 2005

Abstract

This paper presents the numerical simulation inside complex geometry drying spaces having hundreds of trays. A set of measurements taken in a laboratory experimental rig above one single tray, was used to validate the turbulence model most appropriate for the analysed configuration. Due to the change of the flow direction inside the investigated domain, the evaluation of velocity components was done using a five-hole tube connected with a ''scanivalve'' device and a differential pressure transducer. The comparison between the measured data and the predicted results from the numerical simulation of an identical arrangement, led to the conclusion that the standard k–ε is the most adequate turbulence model. Extensive simulation of the air flow inside the full-scale industrial dryer and the prediction of its parameters for different configuration helped in the optimisation of the drying space and finally led to a substantial improvement of the quality of the dried product together with considerable reduction of energy consumption.

Keywords: Batch drying units; Drying process; Tray dryer; Numerical simulation; Flow measurements

1. Introduction

Phase separation processes are often associated with industrial units having complex geometry configuration. Whenever a fluid is involved in a separation process, the main factor that affects the overall system efficiency is the flow behaviour. In the case of fluid passages having complicated geometry aspect, the use of computational fluid dynamics (CFD) codes is a convenient way to evaluate the gas flow parameters. However, to obtain trustful results from numerical simulations, the codes have to be validated by means of experimental measurements.

Experimental fluid dynamics has played an important role in validating and delineating the limits of the various approximations to the governing equations. For example, wind tunnels provide an effective means of reproducing actual flows at laboratory scale. Traditionally, this has conferred a cost effective alternative to full-scale measurement. However, in the design of such equipment that critically depends on the flow behaviour (e.g. in phase separation processes), as part of the design process, measurements are economically impractical. On the other hand, the use of computational fluid dynamics codes leads to numerical solutions of the governing equations and to a complete description of the flow field of interest.

One of the biggest requirements in drying processes is the achievement of uniform moisture content of the final product. This becomes more difficult for large batch drying systems used especially for dehydration of agricultural products. Uniformity of the moisture content inside the final product could be obtained through a proper distribution and guidance of the drying air inside the drying space (Ghiaus, Margaris, & Papanikas, 1998). This implies the insertion of special devices that

* Corresponding author. Tel.: +30 2610997193; fax: +30 2610997202.
E-mail address: margaris@mech.upatras.gr (D.P. Margaris).

0260-8774/$ - see front matter © 2005 Elsevier Ltd. All rights reserved.
doi:10.1016/j.jfoodeng.2005.04.037

Nomenclature

C	conversion factor, Pa/V	u	velocity component in x-direction, m/s
C_i	constant	v	velocity component in y-direction, m/s
g	gravitational acceleration, m/s^2	w	velocity component in z-direction, m/s
k	kinetic energy, J/kg	$\vec{w}$	velocity vector, m/s
k_i	coefficient	Γ_Φ	diffusion coefficient
l_c	characteristic length, m	ε	dissipation rate, W/m^3
p	pressure, Pa	μ_t	dynamic turbulent viscosity, kg/m s
Pr	Prandtl number	ν_l	kinematic laminar viscosity, m^2/s
p_s	static pressure	ν_t	kinematic turbulent viscosity, m^2/s
S_Φ	source term	ρ	density, kg/m^3
t	time, s	Φ	conserved property

will complicate even more the geometry of the space where the flow is developed.

For the case presented in this paper, numerical simulation is carried out using the well-known PHOENICS CFD code in order to predict the airflow parameters and to optimise the design of the dryer. A set of measurements taken in a laboratory experimental rig, constructed to reproduce the actual flow above one single tray inside the full-scale dryer, is used to validate the turbulence model most appropriate for the analysed configuration.

2. Mathematical modelling of the flow

In a general form, the transport equation for momentum, kinetic energy, dissipation rate, etc. can be written as:

$$\frac{\partial}{\partial t}(\rho\Phi) + \mathrm{div}(\rho\vec{w}\Phi) = \mathrm{div}(\Gamma_\Phi \,\mathrm{grad}(\Phi)) + S_\Phi \qquad (1)$$

transient + convection = diffusion + source

where ρ is the density, $\vec{w}$ is the velocity vector, Φ the variable in question, Γ_Φ the diffusive exchange coefficient for Φ and S_Φ the source term (Bird, Stewart, & Lightfoot, 1960). For our purpose, it is necessary to solve the momentum and continuity equations. In the momentum equation, the particular transport parameters are: $\Phi = u,\ v,\ w$ (velocity components), $\Gamma_\Phi = \rho(\nu_t + \nu_l)$ and $S_\Phi = -\frac{\partial p}{\partial x}$, where ν_t and ν_l are the turbulent and laminar viscosities. In the continuity equation, $\Phi = 1$ and $\Gamma_\Phi = S_\Phi = 0$.

The Navier–Stokes equations together with the continuity equation comprise a closed set of equations, the solution of which provides a valid description of laminar and turbulent flows. Turbulence fluctuations can generate rates of momentum transfer far greater than those due to molecular diffusion. The turbulent motion has a wide spectrum of eddy sizes, and large and small eddies can coexist in the same volume of fluid. Several models were developed to define the turbulence, most of them using the eddy-viscosity concept ($\mu_t = \rho\nu_t$), which is a property of the local state of turbulence.

2.1. Constant-viscosity turbulence model

The turbulence model that uses a constant value for the eddy viscosity is the simplest one (Launder, Reynolds, Rodi, Mathieu, & Jeandel, 1984). For dimensional reasons, the effective kinematic viscosity associated with the local turbulence is proportional to the typical velocity and to the characteristic length, given as:

$$\nu_t = Cwl_c \qquad (2)$$

Estimation of a reasonable value for ν_t can be made by taking $C = 0.01$, typical velocity as the mean-flow velocity (the bulk value) and characteristic length as 10% of the flow width.

It is often convenient to use this simple model whilst the main features of the CFD simulation are being put together. Once the other aspects of the flow are well represented, a more accurate turbulence model can be activated.

2.2. k–ε turbulence model

The k–ε turbulence model has proved the most popular, mainly because it does not require a near-wall correction term (Lam & Bremhorst, 1981; Menter, 1994; Pope, 2000). The typical velocity is calculated from the solution of the transport equation for turbulent kinetic energy, k. The dependent variable of the second transport equation is not usually l_c itself, but rather the variable $k^m l_c^n$. The standard high-Re form of the k–ε model employs the following turbulence transport equations:

Kinetic-energy equation:

$$\frac{\partial}{\partial t}(\rho k) + \mathrm{div}(\rho\vec{w}k) = \mathrm{div}\left(\rho\frac{\nu_t}{\sigma_k}\mathrm{grad}(k)\right) + \rho(P_k + G_b - \varepsilon) \qquad (3)$$

Dissipation rate equation:

$$\frac{\partial}{\partial t}(\rho\varepsilon) + \mathrm{div}(\rho\vec{w}\varepsilon) = \mathrm{div}\left(\rho\frac{v_t}{\sigma_\varepsilon}\mathrm{grad}(\varepsilon)\right) + \rho\frac{\varepsilon}{k}(C_1P_k + C_3G_b - C_2\varepsilon) \quad (4)$$

where k is the kinetic energy of turbulence, ε is the dissipation rate, σ_k and σ_ε are effective Prandtl–Schmidt numbers (Launder & Spalding, 1972).

The two-equation models account for the transport effects of velocity and characteristic length, and the model determines the distribution of the last. The constant C_3 has been found to depend on the flow situation. It should be close to zero for stably stratified flow, and close to 1.0 for un-stably stratified flows.

P_k is the volumetric production rate of turbulent kinetic energy by shear forces and G_b (buoyancy production) is the volumetric production rate of turbulent kinetic energy by gravitational forces interacting with density gradients. G_b is negative for stably stratified (dense below light) layers, so that k is reduced and turbulence damped. G_b is positive for un-stably stratified (dense above light) layers, in which therefore k increases at the expense of gravitational potential energy.

The model forms a good compromise between generality and economy of use for many CFD problems.

3. Validation of the turbulence model

While computer models have been increasingly successful in simulating an ever-widening range of engineering problems, it is nevertheless essential that these models are validated and verified against experiment.

A laboratory arrangement was set up to reproduce the most important part of the actual drying room, i.e. one isolated tray, where the air, flowing above it, has a mean velocity between 2 and 3 m/s. The experimental rig consists of a low-speed wind tunnel having several settling chambers, followed by a nozzle (93 cm long and 1 m × 20 cm outlet rectangular cross-section), to provide a uniform flow. To the nozzle was attached the test section, a rectangular channel having the same cross-section as the nozzle and 1.5 m length. Inside the test section, the tray was simulated by inserted two fences of 10 cm height (half of the channel's height) on the entire width of the channel. The distance between the two fences is 0.5 m. A centrifugal blower with airfoil backward curved blades, type BSA 560, manufactured by Vencon Varsos, was set up to deliver the air at the inlet of the test section with 2.86 m/s.

The measurements were taken using a five-hole tube with a spherical head of 8 mm diameter and bent shaft (type Schiltknecht f.881), which permits the evaluation of all three components of the velocity vector at a space point and, in the same time, the direct measurement of total and static pressure (Kjelgaard, 1988). Its simplicity in handling, its accuracy and the possibility to measure the direction of the flow over a wide range, are the outstanding advantages of this instrument.

The spherical head of the five-hole tube is provided with five apertures, arranged in two meridians at right angles, enclosing an angle of 45° in its respective plane (Fig. 1). Five capillary tubes connect the five apertures with their respective numbered tube connections. A flange gives possibilities for assembly and a circular, turntable dial divided from 0° to 360° in steps of 1°, is incorporated into the flange. The dial can be locked on the shaft of the pressure tube with an arresting device. The spherical head is aligned with the zero-position on the dial by adjusting a sighting device (two red dots marked on the bottom of the pressure tube).

The measuring procedure is as follows: the probe head has to be initially yawed into the flow by nulling the difference between the pressures from the two horizontal plane holes. The yaw angle can then be read from

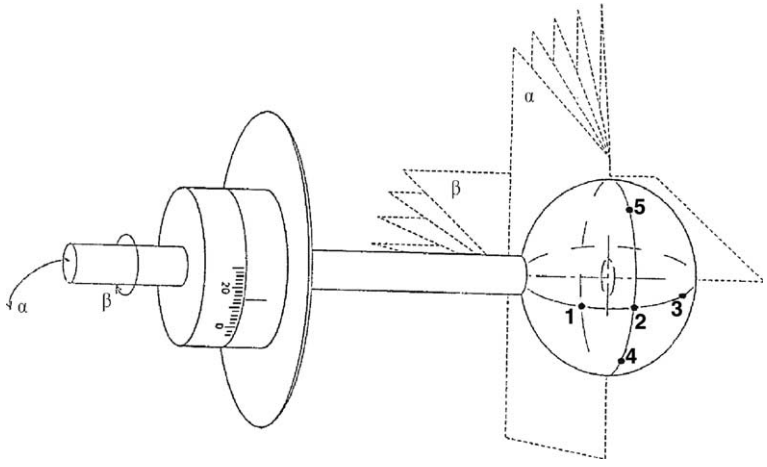

Fig. 1. Spherical pressure tube with five holes.

the probe holder. The pressure readings of the five ports are used to calculate the total pressure and the absolute velocity from a calibration chart. For accurate results to be obtained with this kind of instrument, an individual calibrated diagram is required to be constructed for each probe (Bryer & Pankhurst, 1971).

The five ports of the instrument were connected, through a fluid switch wafer manufactured by Scanivalve Corp., with a differential pressure transducer type FCO 44, manufactured by Furness Control Limited having a range of ±200 Pa. The output signal (voltage, in volts) of the transducer was read by a readout unit FCO 70-1, connected in parallel with a digital multi-meter Fluke 8840A. The pressure, in Pa, is a linear function of the transducer output signal and can be calculated from the following equation:

$$p\ [\mathrm{Pa}] = C\ [\mathrm{Pa/V}]p\ [\mathrm{V}] \tag{5}$$

where C is the conversion factor and has the value 19.89425 Pa/V.

To determine the torsional angle "β" (yaw angle), the spherical head is turned on its guide until the pressure on aperture 4 equals the pressure on aperture 5, and therefore, the output reading of the differential transducer connected to these two ports is zero. The angle "β" can be read from the fixed marks on the dial. The magnitude of the velocity resultant can be calculated from:

$$w = \sqrt{\frac{2(p_2 - p_4)}{\rho k_{24}}} \tag{6}$$

where p_2 and p_4 are the pressures measured at ports 2 and 4, ρ is the air density, and coefficient k_{24} is determined with the aid of the individual calibration diagram provided for each five-hole tube instrument. When the pressures on aperture 1 and 3 are equal, as it is in our case, the pitch angle "α" is zero, the flow is two-dimensional and the coefficient k_{24} is a constant that can be calculated based on the flow theory around a sphere (Ower & Pankhurst, 1977).

Static pressure of the air can be calculated at the measuring point using the following

$$p_s = p_2 - k_2 \frac{\rho w^2}{2} \tag{7}$$

where p_2 is the pressure measured by port 2 of the instrument, k_2 is determined from the individual calibration diagram with reference to the pitch angle, ρ is the air density and w the air velocity. For the specific measurement conditions of this research, the coefficients k_{24} and k_2 were experimentally validated by calibrating the instrument in a known air stream. The values were found to be: $k_{24} = 0.883$ and $k_2 = 0.998$.

The measurement accuracy of pressure tubes increases with speed. The average deviation for the yaw angle is 0.1°, while those for speed of air flow and static pressure are 0.5% and 1%, respectively. The uncertainty estimates for velocity vectors is within ±5% and for pressure, less than 3%.

The measurements were taken within a vertical plane in 255 points with a step of 5 cm on the horizontal side and 1 cm on the vertical side, corresponding to a grid of

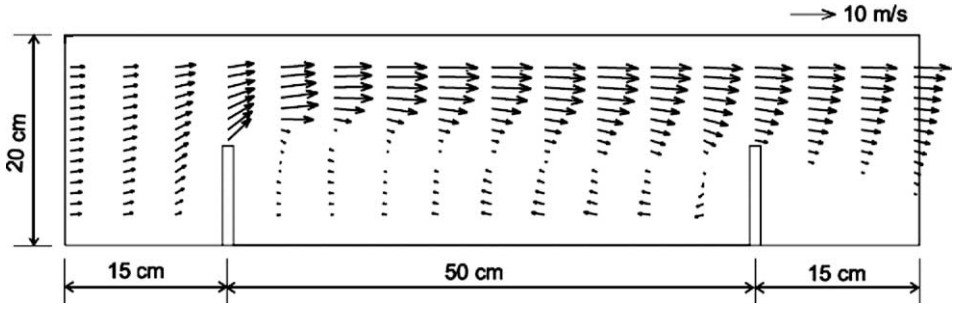

Fig. 2. Velocity distribution over one tray experimentally measured.

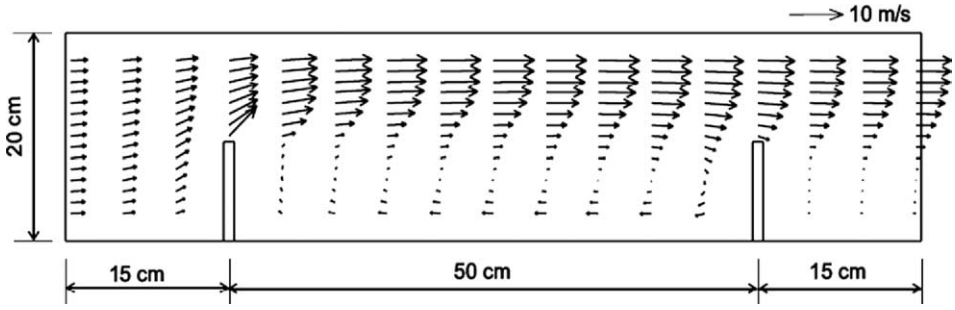

Fig. 3. Velocity distribution over one tray simulated with constant viscosity turbulence model.

17×15 cells. In all measurement points, the pressure difference between the two apertures associated with the pitch angle was zero, which means that the pitch angle is zero and the flow is two-dimensional. The instrument indicator gives the direction of the flow (the yaw angle) and a specific algorithm computes the velocity magnitude according to the pressure measured through the ports. The resultant mean velocity distribution within

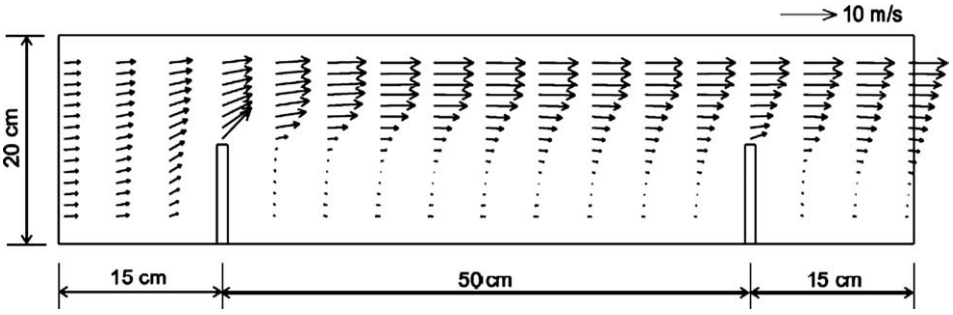

Fig. 4. Velocity distribution over one tray simulated with k–ε turbulence model.

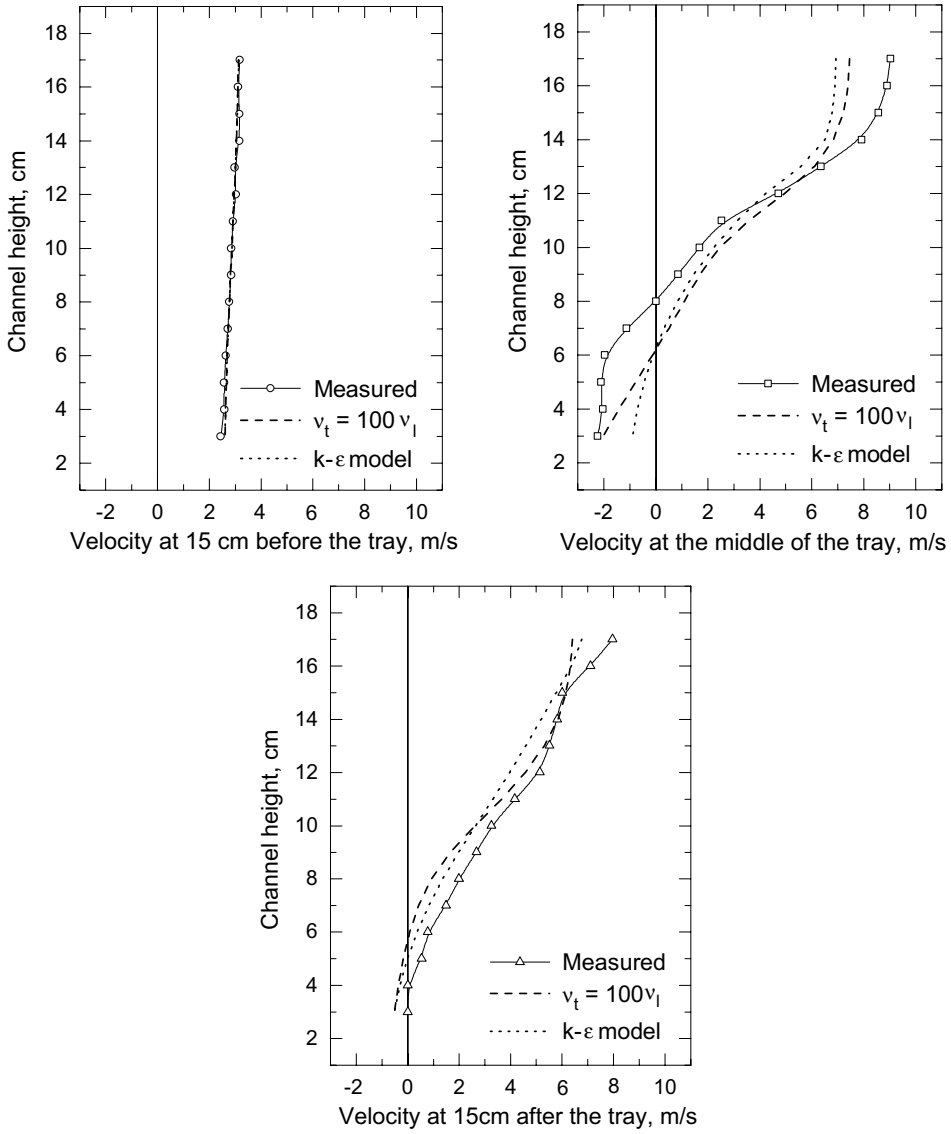

Fig. 5. Profiles of the velocity horizontal components.

the measured frame is graphically presented in Fig. 2. Recirculation of the air inside the tray (between the two walls) can be easily observed.

An identical arrangement like the experimental model, having the same boundary conditions, was numerically simulated with the well-known CFD code PHOENICS developed by CHAM. The flow is considered to be steady-state. The particular governing equations are solved numerically by a finite-volume formulation. The computational domain is assumed to be 2-D having a grid of 3200 (160×20) cells within a frame of 160×20 cm with a step of 1 cm in both directions. Finite difference equations are obtained by integrating the differential equations over the control volume surrounding the grid nodes. Interpolation assumptions are required to obtain scalar values at cell faces and vector quantities at cell centres. The solution procedure is the SIMPLE algorithm of Patankar and Spalding (1972) employing pressure and velocity as the main variables. The method is iterative, the finite-difference equations being solved for each variable in turn by applying the tri-diagonal matrix algorithm.

Wall-boundary conditions are represented as linearized sources for cells adjacent to the tray surfaces. In turbulent flow, as in our case, the near-wall grid nodes are in the fully turbulent region. The normal practice for flows without heat transfer is to bridge the laminar sub-layer with equilibrium logarithmic wall functions (Bradshaw, Cebeci, & Whitelaw, 1981).

Numerical simulation was carried out using different turbulence models that are provided by the code. Constant viscosity turbulence model was validated for different values of the ratio (ν_t/ν_l) in the range 20–5000. From all the tested cases, the closest results to the measured data were obtained for (ν_t/ν_l) = 100. For this case, the velocity distribution given by numerical simulation is presented in Fig. 3.

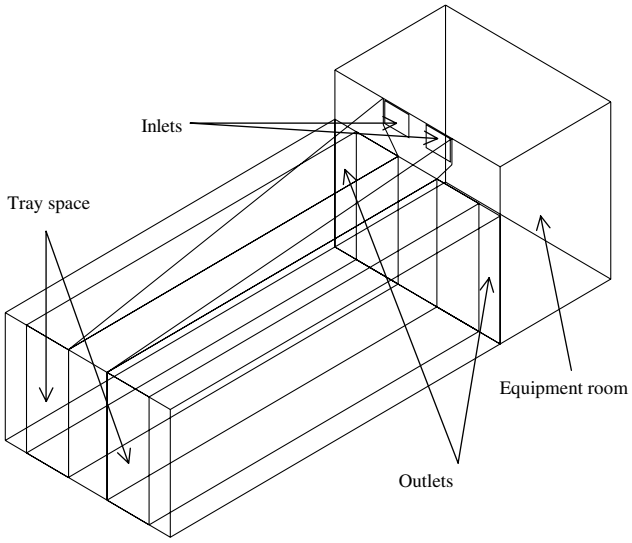

Fig. 6. Outline of the industrial dryer.

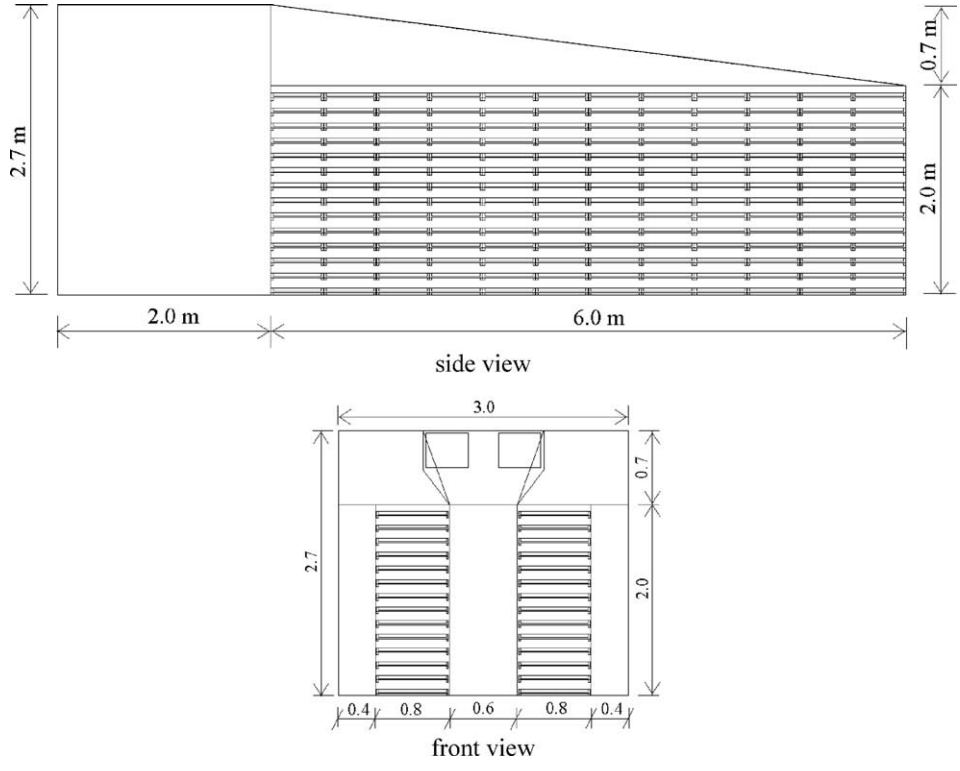

Fig. 7. Side and front view of the industrial dryer with 14 trays per column.

Validation of two-equation models was focused on the following four models: k–ε, 2-scale k–ε, RNG k–ε, and Chen–Kim k–ε (Goldberg, 1996). Analysing the simulation results for each case and comparing them with the measurements, we found out that the best agreement was given by the k–ε model. The velocity distribution predicted with the k–ε model is given in Fig. 4. Even if the number of computational nodes is much greater, the vectors are plotted only in those nodes where the measurements were taken.

The results given by the two selected turbulence models, i.e. constant viscosity ($\nu_t/\nu_l = 100$) and k–ε, were compared with the measurements and the profiles of the velocity horizontal components from each model and from the measurements, in three characteristic cross-sections, were plotted and are presented in Fig. 5. The conclusion is that the k–ε model gives a better agreement, and therefore it was used in the following for numerical simulation of the airflow inside the full-scale drying room.

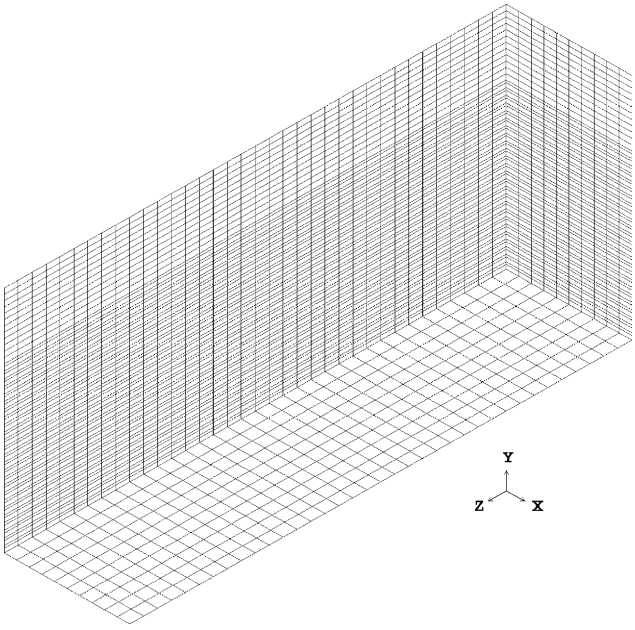

Fig. 8. Grid of the computational domain for 25 trays per column.

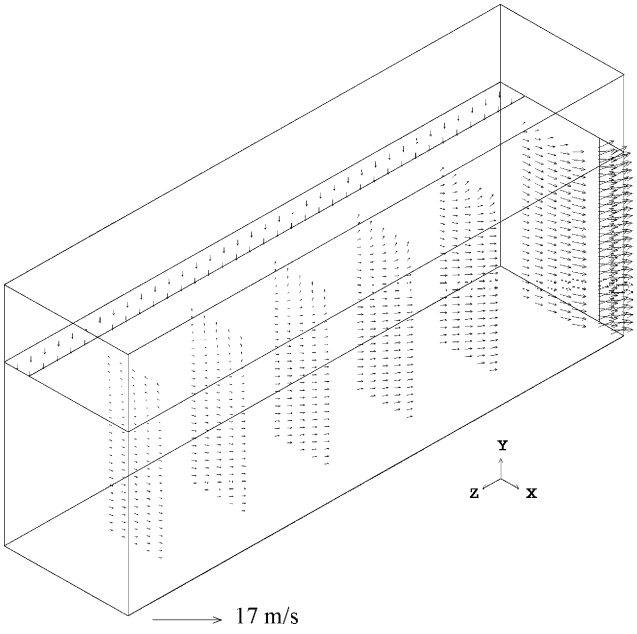

Fig. 10. 3-D velocity distribution in vertical planes after optimisation.

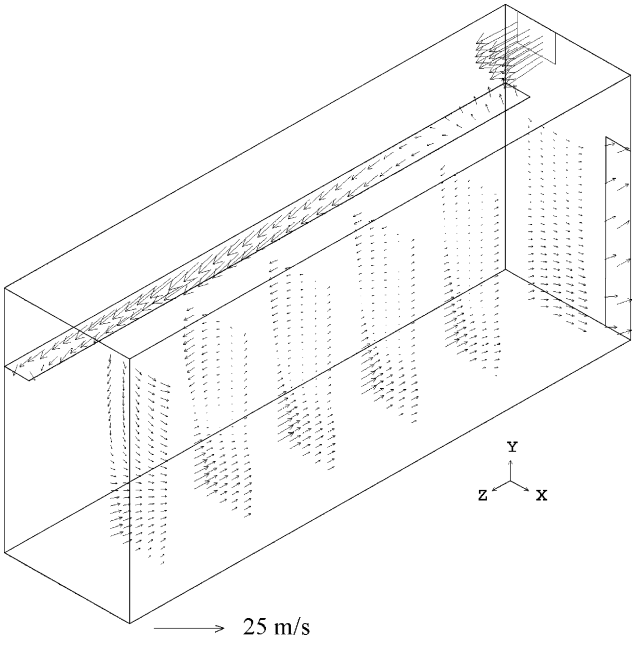

Fig. 9. 3-D velocity distribution inside drying room.

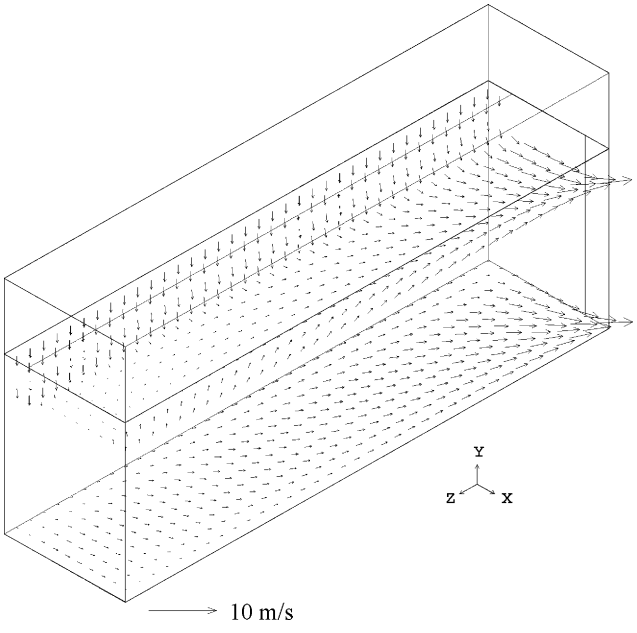

Fig. 11. 3-D velocity distribution in horizontal planes after optimisation.

4. Optimisation of an industrial dryer

The drying space of the full-scale unit has overall dimensions $3 \times 2 \times 6$ m (width, height and length). Two rows of trays are placed symmetrically from the longitudinal vertical plane of the room. The length of one tray is 75 cm, and the width can be either 50 or 75 cm. Therefore, each row will have 12 columns by using 50 cm trays, and 8 columns by using 75 cm trays.

The shelf system, constructed to support the trays, permits the adjustment of the distance between trays according to technological needs. One column can contain up to 25 trays. Above the drying room, in the direction of the longitudinal axis, there is a wedge shape distribution channel. Next to the drying space is the equipment room containing fans, heat exchangers, a burner and the control panel. The inlet and outlet openings for the drying air are on the back wall: the two inlets at the centre-upper part of the distribution channel, each of 44 cm width and 36 cm height, and the two outlets at the lateral-bottom sides of the drying room, each of 2 m height and 30 cm width (see Fig. 6). An example of tray arrangement (with 14 trays per column) is given in Fig. 7.

The airflow inside this complicated geometry space was simulated with the PHOENICS CFD code. The computational domain (half of the space due to its longitudinal plane of symmetry) has the overall dimensions $1.5 \times 2.7 \times 6$ m and was divided in 22,320 cells as follows: 10 cells in x-direction, 62 cells in y-direction from which 50 cells for the drying room containing 25 trays and 12 cells for the distribution channel, and 36 cells in z-direction. Therefore, each cell has 15 cm and 16.5 cm for x and z-direction respectively, whereas in y-direction has 24 mm for those cells corresponding to the tray thickness, 16 mm between the trays and 58 mm inside the distribution channel. The grid for the computational domain is given in Fig. 8. Because the flow between the trays is horizontal, the velocity has only two components (in x and z directions) and the grid has only one cell between two trays. Each tray is considered to be a blockage for the flow. No-slip boundary conditions and appropriate wall functions apply on the solid surfaces. The selected turbulence model was the standard 2-equation k–ε. For an inlet flow rate of 3.33 m^3/s, which corresponds to a mean inlet velocity of 21 m/s and a mean velocity over the trays of 2.86 m/s, a typical example of 3-D representation of the velocity vector distribution inside the drying room is given in Fig. 9. It can be observed a non-uniform flow inside the drying space associated with re-circulation regions.

Graphical representations of the flow parameters for different geometrical configuration and their interpretation led to the optimisation of the tray arrangement, size and position of the inlet opening, opportunity of using separation walls between rows of trays and directing wings inside the distribution channel and central corridor. For example, the optimisation of the distribution channel geometry led to a uniform inlet air for the drying space, thus more uniform flow and no re-circulation are achieved between the trays as can be seen in Figs. 10 and 11. An up-view of the flow above several trays (first tray starts from the bottom) is presented in Fig. 12. The proposed improvements were implemented into practice on an industrial dryer that operates in Kimi, Evia Island

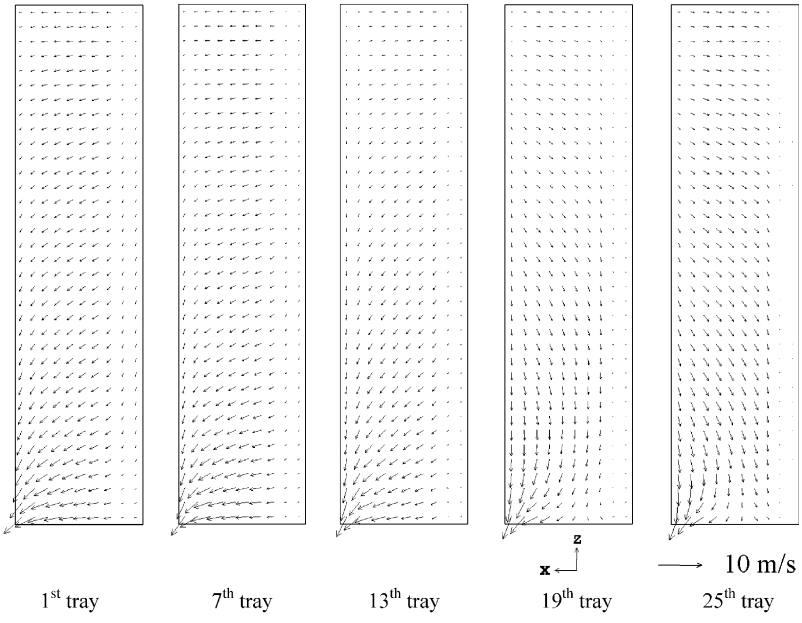

Fig. 12. 2-D velocity distribution for several trays (first tray starts from the bottom).

of Greece (Ghiaus, 1998). The design improvements resulted from the numerical simulation led to an increment of 23% in the uniformity of the humidity inside the final product, when 3 tons of Corinthian grapes were dried during the monitoring period.

5. Conclusions

The evaluation of the airflow parameters inside drying units is a very important task. In some cases, the air has to be removed, while in others, it just helps the separation of the other two phases. Experimental investigations give valuable information for the understanding of a specific phenomenon and help to validate general CFD codes that are afterward used to extensively analyse the phenomenon by numerical simulation. Improvement solutions by flow manipulation techniques using CFD codes can be given to both, dryers that are already in operation and new units under design.

References

Bird, R. B., Stewart, W. E., & Lightfoot, E. N. (1960). *Transport phenomena*. New York: John Wiley & Sons.

Bradshaw, P., Cebeci, T., & Whitelaw, J. H. (1981). *Engineering calculation methods for turbulent flow*. London: Academic Press.

Bryer, D. W., & Pankhurst, R. C. (1971). *Pressure probe methods for determining wind speed and flow direction*. London: National Physical Lab.

Ghiaus, A. -G. (1998). *Momentum, heat and mass transfer in convective drying processes*, PhD thesis, University of Patras, Patras, Greece.

Ghiaus, A. -G., Margaris, D. P., Papanikas, D. G. (1998). Improvement of food drying quality by flow manipulation techniques. In *Proceedings of Second Trabzon International Energy and Environment Symposium*, Trabzon (pp. 359–362).

Goldberg, U. C. (1996). Exploring a three-equation R–k-ε turbulence model, ASME. *Journal of Fluids Engineering, 118-4*, 795–799.

Kjelgaard, S. O. (1988). Theoretical derivation and calibration technique of hemispherical-tipped five-hole probe, NASA Technical Memorandum 4047.

Lam, C. K. G., & Bremhorst, K. A. (1981). Modified form of k–ε model for predicting wall turbulence, ASME. *Journal of Fluids Engineering, 103*, 456–460.

Launder, B. E., Reynolds, W. C., Rodi, W., Mathieu, J., & Jeandel, D. (1984). *Turbulence models and their applications*. Editions Eyrolles.

Launder, B. E., & Spalding, D. B. (1972). *Mathematical models of turbulence*. London: Academic Press.

Menter, F. R. (1994). Two-equation eddy-viscosity turbulence models for engineering applications. *AIAA Journal, 32-8*, 1598–1605.

Ower, E., & Pankhurst, R. C. (1977). *The measurement of air flow*. London: Pergamon Press.

Patankar, S. V., & Spalding, D. B. (1972). A calculation procedure for heat, mass and momentum transfer in three dimensional parabolic flows. *International Journal of Heat and Mass Transfer, 15*, 1787.

Pope, S. B. (2000). *Turbulent flows*. Cambridge University Press.

Available online at www.sciencedirect.com
ScienceDirect
Journal of Food Engineering 79 (2007) 1115–1121
JOURNAL OF FOOD ENGINEERING
www.elsevier.com/locate/jfoodeng

Experimental study of hot air dehydration of Sultana grapes

Dionissios P. Margaris [a,*], Adrian-Gabriel Ghiaus [b]

[a] Fluid Mechanics Laboratory, University of Patras, 265 00 Rio-Patras, Hellas, Greece
[b] Thermal Engineering Department, Technical University of Civil Engineering – Bucharest, Bd. P. Protopopescu 66, 021414 Bucharest, Romania

Received 31 August 2005; accepted 21 March 2006
Available online 18 April 2006

Abstract

A laboratory drying unit was designed and constructed at Fluid Mechanics Laboratory, University of Patras, Greece, in order to evaluate the essential drying characteristics of various fruits and vegetables. The paper presents results of experiments done in the case of hot air drying of Sultana grapes. Time evolution of measured parameters is cross analyzed and presented in diagrams. Moisture content, drying rates and relative moisture content are calculated and also presented in diagrams. Thin-layer model and Page's equation were used for modelling the drying of Sultana grapes up to the water moisture content usually required to attain the shelf stability. The drying constants, effective diffusivity of the bed and product constant were evaluated upon the analytical solution of the thin-layer and Page's equations. The resulted curves were plotted in diagrams and graphically compared with experimental data. A good agreement was found between measurements and Page's equation prediction. Another aim of this research was to validate the in-house DrySAC numerical code, developed for effective design and control of industrial drying units. A very good agreement between predictions and measurements was found.

Keywords: Dehydration; Grapes; Drying curves; Measurements; Prediction

1. Introduction

Dehydration of agricultural products in tray drying units involves great energy consumption mainly because the operation control and maintenance are made heuristically (Bruin & Luyben, 1980). For increasing the process efficiency and reducing the energy consumption, the process parameters have to be optimized. A convenient way to do this is to numerically simulate the total system behaviour and to predict the main parameter evolution for different operation conditions (Chirife, 1983, chap. 3). Simulation codes for drying process are used to design, control and improve new and existing drying systems (Ghiaus, Margaris, & Papanikas, 1997). The main obstacle for extensive analysis of the dehydration process by numerical simulation is the lack of thermo-physical properties for most of the agricultural products. On the other hand, the results from numerical simulation have to be validated by means of experimental investigation (Ghiaus, Margaris, & Papanikas, 2000). Many researches have pointed out that the discrepancies between predictions and experimental data have been a result of the diffusion coefficient being determined when sample temperature gradients are presents. With the temperature not being constant, the determination of effective diffusivity becomes difficult (Srikiatden & Roberts, 2006).

The drying operation involves inter-phase mass (i.e. moisture) transfer from the wet material to the gaseous drying agent (heated air), which may be illustrated as a transport of moisture from the material core to its surface, followed by evaporation from the surface of the material, and dissipation of water vapour into the bulk of the gaseous drying agent. Drying causes irreversible structural damage to the cellular structure of foods. The structure of dried foods depends on the drying methods and conditions, such as temperature, relative humidity, air velocity and initial physico-chemical characteristics of the product (Rahman, Guizani, & Al-Zakwani, 2005).

* Corresponding author. Tel.: +30 2610 997193; fax: +30 2610 997202.
E-mail address: margaris@mech.upatras.gr (D.P. Margaris).

0260-8774/$ - see front matter © 2006 Elsevier Ltd. All rights reserved.
doi:10.1016/j.jfoodeng.2006.03.024

Nomenclature

C_{ex}	transforming factor, N/V	X	moisture content (dry basis), kg water/kg dry solid
D_{eff}	effective diffusivity, m^2/s	X_e	equilibrium moisture content (dry basis), kg water/kg dry solid
F	force, N	X_i	initial moisture content (dry basis), kg water/kg dry solid
K	drying constant, s^{-1}	X^*	relative moisture content, –
N	product constant, –	z	vertical coordinate, m
R^2	coefficient of determination, –	δ	half-thickness of the bed, m
t	time, s		
T	temperature, °C		
U	voltage, V		
ΔU	deviation voltage, V		

The drying of food materials mostly occurs in the falling rate period (the period for which the rate of evaporated water decreases continuously), and moisture transfer during drying is controlled by internal diffusion (Wang & Brennan, 1992). The drying kinetics may be completely described using material and drying medium properties, such as thermal conductivity, thermal and moisture diffusivity, interface heat and mass transfer coefficients. The drying rate and heat flux depend on air humidity and temperature, as well as on heat and mass transfer coefficients in interaction with the moisture and temperature distribution inside the product (Hallstrom & Skjoldebrand, 1983). Diffusion phenomena are extremely complex due to the wide diversity of chemical composition and physical structure of food materials, so reliable data concerning agricultural product properties are scarce (Yusheng & Poulse, 1988).

The paper presents results of experiments done in the case of hot air drying of Sultana grapes. Time evolution of measured parameters is cross analyzed and presented in diagrams. The drying constants, effective diffusivity of the bed and product constant were evaluated upon the analytical solution of the thin-layer and Page's equations.

2. Food drying modelling

Fick's second law of diffusion (Eq. (1)) has been widely used to describe the drying process during the falling rate period for most biological materials (Saravacos & Maroulis, 2001). The differential form of the equation is

$$\frac{\partial X}{\partial t} = \nabla(D_{eff} \cdot \nabla(X)) \tag{1}$$

where X is the moisture content (dry basis), t is the time and D_{eff} is the effective moisture diffusivity representing the conductive term of all moisture transfer mechanisms. In the case of bed dryers, where the edge effects can be neglected and a constant effective diffusivity can be assumed, Eq. (1) will take the following form:

$$\frac{\partial X}{\partial t} = D_{eff} \cdot \frac{\partial^2 X}{\partial z^2} \tag{2}$$

where z is the vertical coordinate. The approximate analytical solution of Eq. (2) which moreover assumes uniform initial moisture distribution and negligible external resistance reduces to:

$$X = X_e + \frac{8}{\pi^2} \cdot (X_i - X_e) \cdot \exp\left(-\frac{\pi^2 \cdot D_{eff} \cdot t}{4\delta^2}\right) \tag{3}$$

where X_e is the equilibrium moisture content (dry basis), X_i the initial moisture content (dry basis) and δ is the half-thickness of the bed. Eq. (3) is frequently written in a dimensionless form as

$$X^* = \frac{X - X_e}{X_i - X_e} = \frac{8}{\pi^2} \cdot \exp\left(-\frac{\pi^2 \cdot D_{eff} \cdot t}{4\delta^2}\right) \tag{4}$$

where X^* is called the (dimensionless) relative moisture content.

The effective moisture diffusivity is usually determined from experimental drying curves with the assumption that drying is mass transfer limited and the temperature remains constant throughout the whole sample during the entire course of drying (Roberts & Tong, 2003). However, mainly in case of food dehydration, where assumptions of thin-layer can be made, the rate of change of moisture content (drying rate) is proportional to the difference between instantaneous moisture content and equilibrium moisture content of the material.

$$\frac{dX}{dt} = -K \cdot (X - X_e) \tag{5}$$

where K is called the drying constant or rate constant, and it is a combination of the transport properties (Mujaffar & Sankat, 2005):

$$K = \frac{\pi^2 \cdot D_{eff}}{4\delta^2} \tag{6}$$

With appropriate initial conditions, the particular solution of the thin-layer equation becomes:

$$X^* = \frac{X - X_e}{X_i - X_e} = \exp(-K \cdot t) \tag{7}$$

Hall (1980) described a procedure for determining the drying constant, K, by drawing a semi logarithmic plot of relative moisture content, X^* vs. time, t. Since Eq. (7) is an exponential relationship, the data should plot as a straight line, the slope of which gives the numerical value of K. Knowing the drying constant, it is convenient to estimate the moisture content as a function of time or the drying time after which the product reaches a certain moisture content.

The limitation of the thin-layer equation in predicting drying process, has necessitated the introduction of a secondary parameter called the product constant, N. The relative moisture content expression takes in this case the well-known form of Page's equation (Morey & Li, 1984).

$$X^* = \frac{X - X_e}{X_i - X_e} = \exp(-K \cdot t^N) \tag{8}$$

When Page's equation is applied to experimental drying data, the graph should be a straight line. The two parameters, i.e. drying constant, K and product constant, N, are graphically evaluated from measurements, by writing Page's equation in a linearized form:

$$\ln(-\ln X^*) = \ln K + N \cdot \ln t \tag{9}$$

The above equations have been used for estimation and prediction of drying time for specific products under given operation conditions. They were also used to generalize the drying curves and to optimize the design and operation of industrial units. The prediction is accurate only in cases where product weight reduction is mainly due to water evaporation. Deviation occurs where there is a further reduction due to the decomposition of sugars.

3. Materials and methods

3.1. Experimental drying unit

The experimental laboratory-scale facility for convective hot air drying is schematically illustrated in Fig. 1. It is a forced-circulation, batch-type tray dryer having the following main components: drying room, centrifugal fan, electrical resistance heater, drying tray, data acquisition system, personal computer, dampers and orifice-plate devices. An overall view of the facility is presented in the photograph taken at the Fluid Mechanics Laboratory of the University of Patras, where the lab-drying unit is located (Fig. 2).

The rectangular-shape drying room has 117 cm length, 25 cm width and 17 cm height with a free cross-section area of 425 cm^2. Its walls are made of Plexiglas plates with 5 mm thickness. The room is thermally insulated at the base with polystyrene plates of 10 cm thickness, and of 5 cm thickness for the lateral and top sides. The drying room contains one sample tray having dimensions $75 \times 24 \times 2$ cm and constructed from aluminium frame with metal wire mesh at the bottom. The tray load is up to 8 kg of fresh product, depending on the bulk density and the thickness of the product bed. Drying air is flowing parallel with the tray surface, in its longitudinal direction. With minor constructive modifications, the circulation can be changed to through-flow, i.e. the drying air is passing through the product bed, from down to up. In the case of parallel-flow, the adjustment of the free space above the tray allows to set various velocities by maintaining the same amount of supplied inlet airflow rate.

The centrifugal fan works with variable power supply of max. 12 V DC and can deliver air into the system at flow rates ranging from 0 to 55 m^3/h according to the input voltage that modifies the motor RPM. The fan has two admission ways: one for fresh air, and the other for the amount of air that is recirculated in the system. The ratio between fresh and recirculated air can be adjusted from 0% to 100% according to the baffle positions. State parameters of the air at the fan exit are established by two thermocouples that measure dry- and wet-bulb temperatures.

The electrical resistance, with a maximum power of 2 kW at 220 V AC, is placed on the axis of two coaxial galvanized iron tubes and can rise the drying air temperature up to 80 °C. The electrical resistance power can be modified in five steps from 0 to 2 kW, in this way obtaining different drying air temperatures. The fan and the electrical heater operation are carried on from an electrical control panel. The drying room, centrifugal fan and electrical heater are connected through Plexiglas pipes of 100 mm ID. Two cross-section conversion pieces (from rectangular to circular) make the connection between the edges of the drying

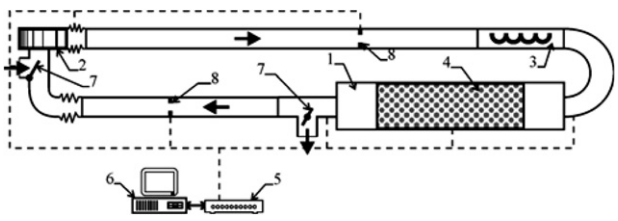

Fig. 1. Schematic representation of the drying facility. 1 – drying room; 2 – centrifugal fan; 3 – electrical resistance heater; 4 – drying tray; 5 – data acquisition system; 6 – personal computer; 7 – dampers; 8 – orifice-plate devices.

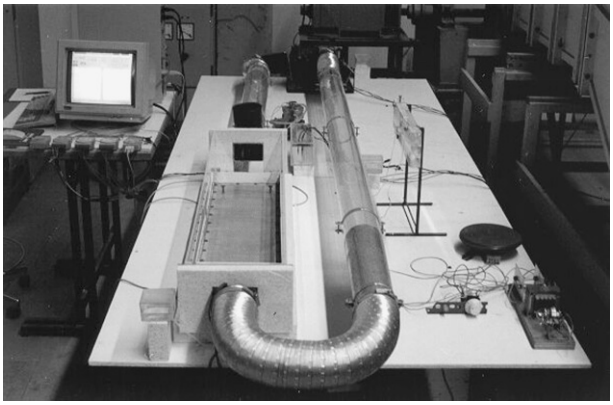

Fig. 2. Overall view of the laboratory drying facility.

room and the pipes. Each one incorporates pairs of thermocouples for measuring the dry- and wet-bulb air temperatures at the inlet and outlet of the drying room.

3.2. Product

Drying experiments were carried out using 3.3 kg of fresh Sultana grapes (golden-colored raisins) purchased from the local market. The grape bunches were manually arranged in the tray with the average bed thickness of 2.2 cm, without any previous pre-treatment. Sultana berries were about 8 mm in size and had an initial moisture content of 3 kg of water/kg dry solid (equivalent with 75% wet basis), which is a common value for fresh Sultana grapes.

3.3. Methods

A system of three load cells, type 8523-100 N, manufactured by "burster" company, was used to measure on-line the weight of the tray containing the product, continuously and without removing the sample from the drying room. Inaccuracy is less than ±0.5% F.S. and sensitivity tolerance ±0.5%. The load cells operate by the approved strain gauge method (Pavese & Molinar, 1992). The force to be measured must be centred. The load cells were calibrated for different excitation voltages and for loading ranging between 0 and 2 kg. The signal output (in volts) depends linearly on the measured force, according to the excitation voltage. The analytical expression used to calculate the force from the signal output is given by

$$F = C_{ex} \cdot U \tag{10}$$

where F is the measured force, in N or in kg force, C_{ex} is a transforming factor depending on the excitation voltage in N/V or in kg force/V, and U is the output signal voltage, in V. The reference signal output depends on the environment temperature in which the load cell operates. The actual output signal for a temperature T is then $(U - \Delta U)_T$ where the deviation of the signal output, ΔU can be calculated from the following relation provided by the manufacturer:

$$\Delta U = 0.02315 \cdot (T - 20) \tag{11}$$

Drying air parameters were evaluated by measuring the dry- and wet-bulb temperatures using type "J" thermocouples with a tolerance value, expressed as a deviation in degrees Celsius, of ±1.5 °C under tolerance class 1. The measurement points were the followings: laboratory environment, exit of the fan, inlet and outlet of the drying room. The wet-bulb temperature was measured by covering the thermocouple hot junctions with a wick wetted in distilled-water.

The thermocouples and the load cells were connected to several analog input modules type "ADAM-4018" of a PC-based "ADVANTECH" data acquisition system. The accuracy of the modules is ±0.05% or better. The data acquisition hardware converts the analog voltage or current levels into digital information so that the computer can process and store the signals. For this application, a comprehensive and flexible designed package, "Advantech Genie", running under the Microsoft Windows environment was chosen as data acquisition and control software. During the entire period of the drying experiment, the real time, the temperatures and the weight of the tray were online displayed on the monitor and were also stored in a .log text file.

The airflow rates, entering the drying room and recirculated in the system, were measured by means of standard orifice-plate devices constructed from 5 mm thickness Plexiglas according to ISO 5167-1980, with upstream internal pipe diameter (D) of 10 cm and orifice diameter (d) of 4 cm. The volume flow rate of the air delivered to the drying room was kept constant at 55 m^3/h. The airflow direction was parallel to the product bed surface and had an average velocity of 0.45 m/s. By proper arrangement of the two dampers, the recirculation ratio of the drying air was set up to 75%. Recirculation ratio was calculated from recirculated and inlet flow rates measured by orifice-plate devices (see position 8 in Fig. 1). Air velocity inside drying room was calculated knowing the inlet flow rate, the air temperature and the actual cross-section of the drying room.

Drying conditions were initially setup and monitored during the entire duration of the process. The values were maintained within ±1.5 °C for dry- and wet-bulb temperatures and within ±5% for the instantaneous air velocity.

Moisture contents at each time interval were calculated by correlating the weight loss data with the dry solid weight of the sample. The drying constants, product constant and effective moisture diffusivity were determined experimentally from the drying curves. Equilibrium moisture content, X_e, was obtained by extending the drying time until no measurable weight loss was observed. The above calculated values were then used in appropriate mathematical models to predict the moisture content at various drying stages.

4. Results and discussion

The environmental conditions had slight fluctuation during the whole drying period, with the dry-bulb temperature oscillating with ±1.5 °C around the value of 22 °C. At the inlet of the drying room, the air dry-bulb temperature was almost constant (69 ± 1 °C). At the outlet of the drying room, three periods were observed: first one, of about 2 h, corresponding to a warm-up period with temperature rising from 53 °C to 60 °C, the second one of 40 h during which the temperature was almost constant at 60 °C, and the last one of 30 h, when a little increase in temperature, up to 62 °C was recorded. The evolution of dry-bulb temperatures during the whole process is illustrated in Fig. 3.

After a drying period of 72 h, the weight of the grapes decreased from 3.3 kg to almost 1 kg, which corresponded to a final moisture content of 0.18 kg water/kg dry solid.

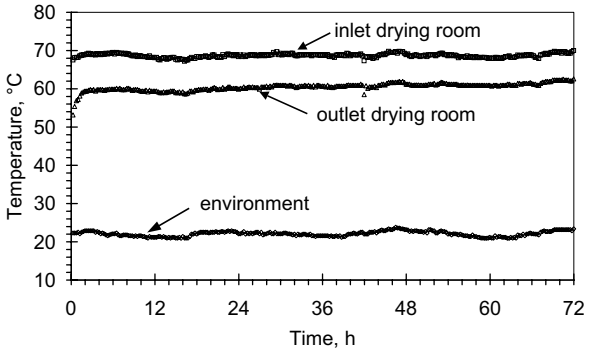

Fig. 3. Evolution of dry-bulb temperatures during drying process.

The evolution of the product weight due to the water loss is represented in Fig. 4. A useful parameter for design and operation of industrial dryers is the drying rate, defined as the water rate evaporated from each square meter of drying surface. This is calculated from measured data of the mass product versus time and is shown in Fig. 5. The drying rate increased during the first 4 h (warm-up period) and afterwards decreased continuously. Uniform oscillations can be observed due to the no-smoothing measured data and the relative short time sampling rate. Graphical interpretation of the rate of moisture loss led to the conclusion that the drying process is not characterized by a constant-rate period.

Experimental drying curves of Sultana grapes, representing the time evolution of moisture content and relative moisture content during the dehydration process, are illustrated in Figs. 6 and 7, respectively.

The DrySAC numerical code (Ghiaus et al., 2000) was used to simulate, under the same operation conditions, the drying process of a same quantity of fresh Sultana grapes. The numerical simulation prediction of product and process parameters was compared with the experimental data in graphical representation. A very good agreement between measurements and simulation can be observed.

The normalized drying curve, Fig. 8, showing the relationship between the natural logarithm of the relative moisture content and time, was constructed in order to determine the drying constant of the thin-layer solution. The measurement data are not so close to the fitting straight-line relationship (coefficient of determination $R^2 = 0.9852$). However, the evaluated drying constant for Sultana grapes, $K_1 = 4.7222 \times 10^{-2}\ \mathrm{h}^{-1}$ ($K_1 = 1.3117 \times 10^{-5}\ \mathrm{s}^{-1}$), could be used in engineering predictions as a first approximation. In this case, the effective diffusivity value of the grape bed was calculated as $D_{\mathrm{eff}} = 6.439210^{-10}\ \mathrm{m}^2/\mathrm{s}$.

Fig. 9 shows the experimental curve relating $\ln(-\ln X^*)$ vs. $\ln t$, for Sultana grapes dried at a mean temperature of 65 °C. The curve comes very close to the fitting straight-line correlation (coefficient of determination $R^2 = 0.9971$). The

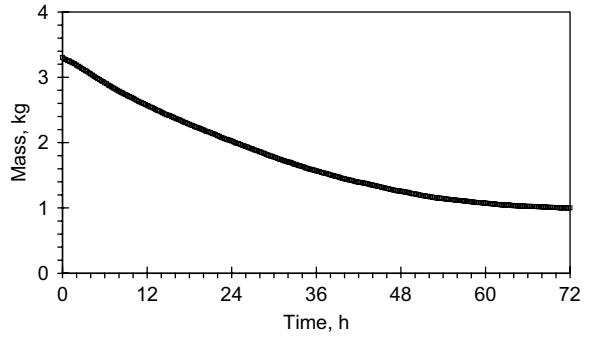

Fig. 4. Decrease of mass product during drying.

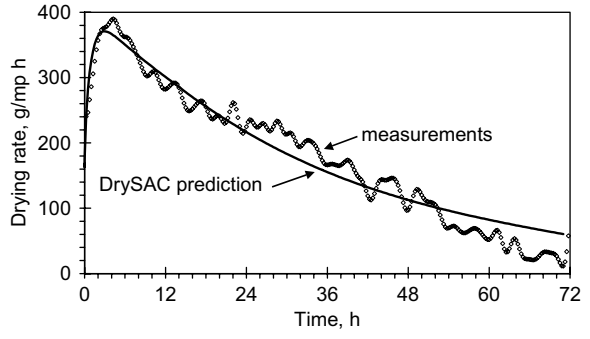

Fig. 5. Drying rate – rate of evaporated water from each square meter of drying surface.

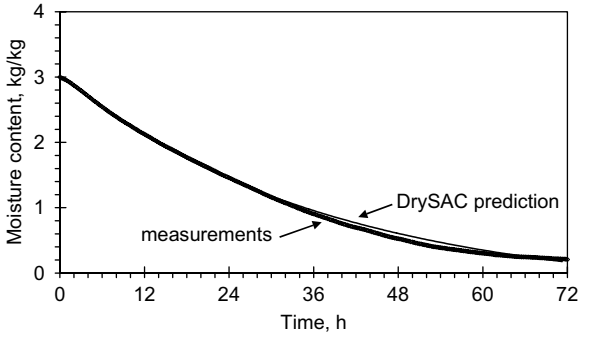

Fig. 6. Evolution of moisture content – dry basis during drying.

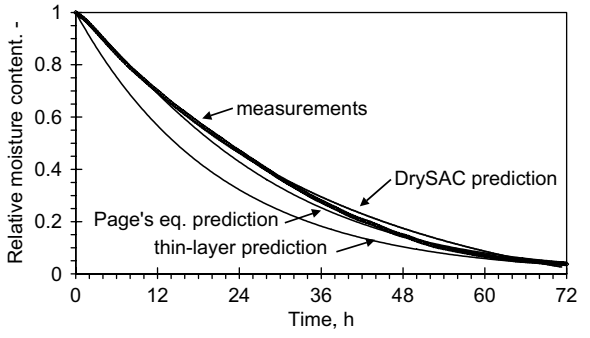

Fig. 7. Relative moisture content vs. time: (a) experimental; (b) one-constant model prediction; (c) two-constant model prediction; (d) DrySAC numerical code.

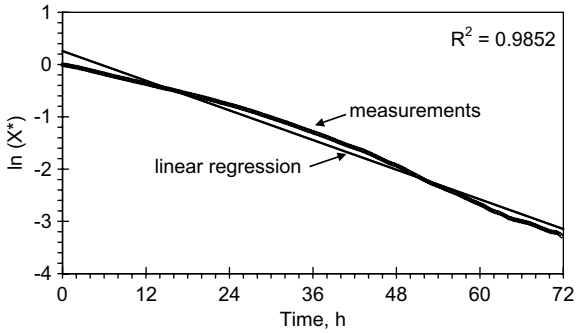

Fig. 8. Determining the drying constant K_1.

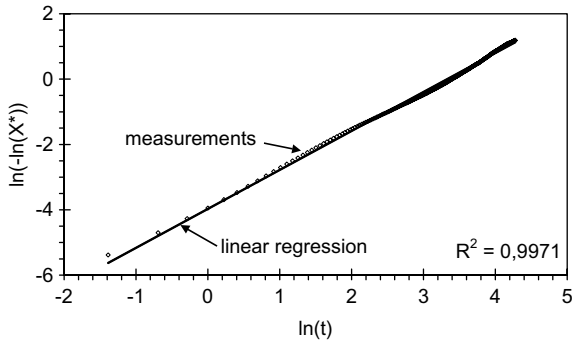

Fig. 9. Determining the drying constant K_2 and product constant N.

application of Page's equation resulted in determining the drying parameters: drying constant $K_2 = 1.9255 \times 10^{-2}\ h^{-1}$ ($K_2 = 0.5348 \times 10^{-5}\ s^{-1}$), and product constant $N = 1.1908$. The obtained values are in the range reported in literature (Karathanos & Belessiotis, 1999).

Based on assumptions of an uniform initial moisture distribution, constant diffusion coefficient, negligible external resistance, negligible temperature gradients and negligible shrinkage during drying, the solution of the thin-layer equation and the Page's equation were used to predict moisture loss during convective drying.

Experimental data and predicted values of relative moisture content were compared as shown in Fig. 10. The results showed some discrepancies between experimental data and prediction with the thin-layer model, which could result from not taking necessary assumptions into consid-

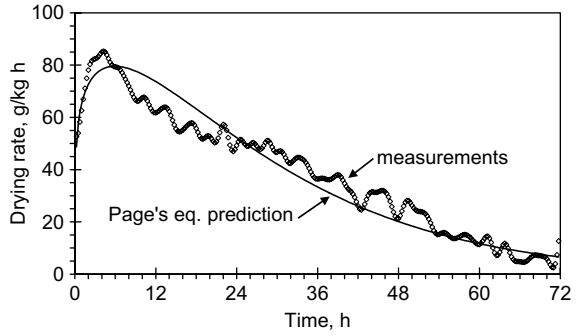

Fig. 10. Drying rate vs. time: (a) experimental; (b) prediction.

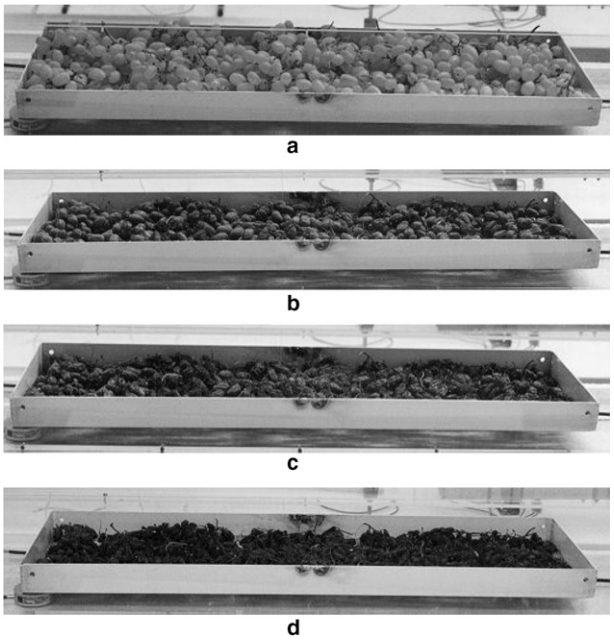

Fig. 11. Sultana grapes at different drying stages showing the decrease in bed thickness due to the shrinkage effect: (a) fresh; (b) after 24 h; (c) after 48 h; (d) after 72 h.

eration. However, good agreement was found with Page's model prediction. It is possible that negligible shrinkage effect, dependence of the effective diffusivity on moisture content or heat transfer effect could contribute to the observed discrepancies.

Finally, some pictures showing the tray with grapes at different stages of drying are presented in Fig. 11. The decrease of the bed thickness due to the shrinkage effect can be easily observed. Even if in this paper the phenomenon is not experimentally studied from the quantitative point of view, it should be taken into consideration when more sophisticated prediction models than Page's or thin-layer equations are used.

5. Conclusions

Dehydration offers highly effective and practical means of preserving fruits and vegetables that reduce post-harvest losses and abate shortages in supply. The main objective of this research was to experimentally investigate the drying characteristics for Sultana grapes due to the lack of data concerning the properties of this product.

A small laboratory dryer was designed and constructed in order to evaluate the drying behaviour of different fruits and vegetables. Experimental drying curves showed that the drying of Sultana seedless grapes occurs in the falling rate period only. Thin-layer equation and Page's equation were used to determine the drying and product constants from experimental data. In the first case, drying constant was evaluated to $K_1 = 4.7222 \times 10^{-2}\ h^{-1}$, and in the second case to $K_2 = 1.9255 \times 10^{-2}\ h^{-1}$. The product constant in Page's equation was found to be $N = 1.1908$.

Knowing drying and product constants, it is possible to estimate the moisture content as a function of time, or the drying time after which the product reaches certain moisture content. Even if prediction with thin-layer equation was not so accurate, Page's equation estimated values very closed to experimental data.

Finally, the measurement data helped in validation of the DrySAC numerical code, used for effective design and control of industrial drying units. A very good agreement between measurements and simulation was found.

Acknowledgements

This research was carried out in the framework of the Bilateral Science & Technology Cooperation Program for the years 2002–2005 between the General Secretariat for Research & Technology of the Greek Ministry for Development and the Romanian Ministry of Education and Research.

References

Bruin, S., & Luyben, K. Ch. A. M. (1980). Drying of food materials: a review of recent developments. In A. S. Mujumdar (Ed.). *Advances in drying* (Vol. 1, pp. 155–215). Washington: Hemisphere Publishing Corp.

Chirife, J. (1983). Fundamentals of the drying mechanism during air dehydration of foods. In A. S. Mujumdar (Ed.). *Advances in drying* (Vol. 2, pp. 73–102). Washington: Hemisphere Publishing Corp.

Ghiaus, A.-G., Margaris, D. P., & Papanikas, D. G. (1997). Mathematical modeling of the convective drying of fruits and vegetables. *Journal of Food Science, 62*, 1154–1157.

Ghiaus, A.-G., Margaris, D. P., & Papanikas, D. G. (2000). Validation of drying simulation algorithm of fruits and vegetables. In *Proceedings of 3rd European thermal science conference – Eurotherm 2000* (pp. 561–565). Germany: Heidelberg.

Hall, C. W. (1980). Drying and storage of agricultural crops. Westport, Conn.: AVI Publishing Co., Inc.

Hallstrom, B., & Skjoldebrand, C. (1983). Heat and mass transport in solid foods. In S. Thorne (Ed.), *Developments in food preservation – 2* (pp. 61–94). London: Appl. Sci. Publ. Ltd.

Karathanos, V. T., & Belessiotis, V. G. (1999). Application of a thin-layer equation to drying data of fresh and semi-dried fruits. *Journal of Agricultural Engineering Research, 74*, 355–361.

Morey, R. V., & Li, H. (1984). Thin-layer equation effects on deep-bed drying prediction. *Transactions of the ASAE, 27*(6), 1924–1928.

Mujaffar, S., & Sankat, C. K. (2005). The air drying behaviour of shark fillets. *Canadian Biosystems Engineering, 47*, 3.11–3.21.

Pavese, F., & Molinar, G. (1992). *Modern gas-based temperature and pressure measurements. International cryogenics monograph series*. Portland: Book News Inc.

Rahman, M. S., Guizani, N., & Al-Zakwani, I. (2005). Pore formation in apple during air-drying as a function of temperature: porosity and pore-size distribution. *Journal of the Science of Food and Agriculture, 85*, 979–989.

Roberts, J. S., & Tong, C. H. (2003). The development of an isothermal drying apparatus and the evaluation of the diffusion model on hygroscopic porous material. *International Journal of Food Properties, 6*(1), 165–180.

Saravacos, G. D., & Maroulis, Z. B. (2001). *Transport properties of foods*. New York: Marcel Dekker.

Srikiatden, J., & Roberts, J. S. (2006). Measuring moisture diffusivity of potato and carrot (core and cortex) during convective hot air and isothermal drying. *Journal of Food Engineering, 74*, 143–152.

Wang, N., & Brennan, J. G. (1992). Effect of water binding on the drying behavior of potato. In A. S. Mujumdar (Ed.), *Drying 92* (pp. 1350–1359). London: Elsevier Science.

Yusheng, Z., & Poulse, K. P. (1988). Diffusion in potato drying. *Journal of Food Engineering*, 249–261.

15th International Drying Symposium (IDS 2006)
Budapest, Hungary, 20-23 August 2006

IMPACT OF DIC® TEXTURE MODIFICATION ON DRYING KINETICS AND FINAL PRODUCT QUALITY

K. Allaf[1] and A.-G. Ghiaus[2]

[1] *Laboratoire Maîtrise des Technologies Agro-Industrielles, Université de La Rochelle*
Avenue Michel Crépeau, 17042 La Rochelle Cedex 01, France
Tel.:+33 5 46458779, E-mail: karim.allaf@univ-lr.fr

[2] *Thermal Engineering Department, Technical University of Civil Engineering Bucharest*
Bd. P. Protopopescu 66, 021414 Bucharest Sector 2, Romania
Tel.:+40 21 2524280, E-mail: ghiaus@mech.upatras.gr

Abstract: The innovative DIC® technology allows to define a new process named "swell-drying" that leads to very good results in terms of drying kinetics and quality of a large variety of fruits, vegetables, rice, milk, wood, etc. DIC® technology consists of a thermo-hydro-mechanical treatment that modifies the texture of the product and preserves its organoleptic characteristics. This paper presents the swell-drying as a combination of hot air drying and DIC treatment. Using classical hot-air techniques, final stage of drying time decreased significantly compared with the time needed to dry untreated products. End product quality is improved leading to good texture, preserving color and flavor, and assuring a perfect decontamination. Vitamin contents are higher than the non treated ones.

Keywords: swell-drying, dehydration, decontamination, preservation, fruits & vegetables

INTRODUCTION

Drying is one of the oldest and most efficient natural methods for food preservation. In the case of fruits and vegetables, dehydration is generally carried out by hot-air convective drying.

Hot-air dehydration is a slow process for which drying time directly increases with the square of the food piece width (Labuza, 1972). Rehydration of dried products is also a slow process. The taste of rehydrated products is often nowhere near the fresh ones due to the long exposure to high temperature treatment.

Coupled transfer of heat and mass is characteristic to almost all drying processes. Water elimination generates shrinkage and deformation of the final product. The shrinkage induces the increase of thermal conductivity, and thus of internal heat transfer, and the decrease of the pore size and thus of the water diffusivity within the product. Therefore, internal mass transfer becomes the limiting factor that considerably slows down the drying rate and consequently amplifies thermal degradation. A solution for preventing this degradation and for correcting the deformations could be a texture modification by expanding the product. This step would considerably increase the mass transfer and accelerate the drying rate in its last phase (Louka et al., 2004). Expansion has also a fundamental role in the improvement of the final quality of dried foodstuff.

On the other hand, water elimination does not imply any shrinkage of the product during freeze drying process. But, despite quick rehydration and relatively good quality of final dried products, freeze drying is rarely used in food industry because of expensive equipment and high operation costs. This operation is limited to few cases involving high-value products.

Research on foodstuff product expansion (also called explosion-puffing) was carried out for the first time in 1950 on potatoes (Harrington and Griffiths, 1950). Explosion-puffing process incorporated into a hot-air drying step aimed to yield quick cooking dehydrated fruits and vegetables. The process involves placing the product in a kind of canon and treating it at high temperature and pressure (often steam pressure) followed by a decompression toward atmospheric pressure (Clark, 1986). The explosion-puffing phenomenon is directly related to a complex mechanism of alveolation and depends on the actual operating conditions: initial temperature level, final pressure level (just after pressure-dropping) identifying final temperature, and the duration of the decompression. The decompression induces a partial vaporization of the water engendering mechanical constraints within the product which has a visco-elastic behavior and undergoes an irreversible adiabatic transformation. The product water content

determines the amount of generated steam during decompression. Therefore, a large amount may completely disintegrate the treated product, whereas in the opposite case, the product is not well expanded. Consequently, a partial drying step is a prerequisite for the application of the expansion process. Once expanded, the products are subject to further dehydration in order to lower their final moisture content to less than 5%. This final dehydration step can be carried out in a conventional dryer, by microwaves or using infrared rays (Sugisawa et al., 1985).

Puffing provides products that are less deformed, which can be more quickly rehydrated, with good preservation of flavor and lower operation costs. However, from the original idea of expansion by self-vaporization, the treatment cycle did not really evolve. Systematic parametric studies have rarely been performed and there has been little discussion concerning the behavior of the re-textured matter. Also, the treatment of heat-sensitive food products was very delicate.

DÉTENTE INSTANTANÉE CONTRÔLÉE

During 1990's, a new process of texturing by self-vaporization, Détente Instantanée Contrôlée - DIC (Instantaneous Controlled Pressure-Drop) was developed. This process allows various biological products that are heat-sensitive to be expanded while obtaining very good final quality (shape, texture, color and flavor) (Allaf et al., 1992). It involves a thermo-mechanical treatment of the product followed by an instantaneous Pressure-Drop towards the vacuum. This contributes advantageously on three levels. First, a net increase in temperature difference, where the final equilibrium temperature is close to the saturation temperature (30 °C at 0.05 bar) and the amount of generated steam is therefore sufficiently great at a lower treatment temperature (150 °C toward 30 °C instead of 220 °C toward 100 °C). Second, the reduction in the final temperature leads to a reduction in heat-induced deterioration of sensitive products. Third, low final temperature allows the product to easily maintain its new expanded structure. The amount of steam generated by self-vaporization increases as the final equilibrium temperature is lower, and cooling is more intense as the final equilibrium pressure is lower (Louka and Allaf, 2002). DIC texturing of sensitive food products involves a short treatment of around 15 s at a temperature below 150 °C, followed by an abrupt (Instantaneous) Pressure-Drop towards a vacuum of 0.1 bar. The re-texturing carried out in these relatively mild conditions, followed by a very rapid and intense cooling, results in a product that maintains a highly satisfactory color and shape after the final drying.

The reactor, based on the above fundamental approach, consists of the following three main components: 1) the processing vessel where the samples are disposed, equipped with thermocouples and a pressure detector. All these elements are linked to a data acquisition system. Within the processing vessel, a controlled pressure can be obtained from a primary vacuum. 2) the vacuum system, which consists of a vacuum tank 60 times greater than the processing vessel and an airlock system that enable one to evacuate the condensed water in the tank. The processing vessel and the vacuum tank are connected through a pneumatic valve that can be operated instantaneously. 3) the decompression system. Figure 1 shows a photo of a tubular reactor, with manual feeding that is used for testing and treatment of limited amounts of products.

Fig. 1. DIC tubular reactor

Numerous parameters involved in DIC technology have special importance concerning the quality of final products. There are two parameter categories that influence the process: inherent and operating parameters. The inherent parameters, such as initial steam pressure, vacuum tank pressure and duration of the pressure-drop, contribute to the definition of the DIC technology itself. These parameters have to be set up for all products at optimal levels that depend in particular on the apparatus capacity. The operating parameters depend on both the steam treatment and the product itself and include: saturation pressure of the treatment steam (which also determines the treatment temperature), treatment time, initial water content of the product and thickness of the product pieces.

Specific food products that generally fail to give a desirable final quality after DIC expansion belong in particular to the following three cases: a) Very heat-sensitive products. Although treated under relatively mild conditions (temperature below 150 °C for a short time), some fragile products are likely to undergo certain degree of thermal degradation. b) Products with a very low hardening temperature. Although the final temperature after dropping pressure is about 30 °C, certain products do not reach their hardening level, are not able to maintain their own new expanded structure, shrinkage takes place

and will then have a shriveled surface after final drying. c) Products treated in thick layer. After treatment under preset operating conditions, the products are quite well expanded at the surface of the layer while not expanded far from the periphery, with no improvement in volume recovery. A prolonged treatment may expand the whole sample but the outer layers will lose their color. Some modifications of the standard DIC treatment cycle were made to overcome the above problems (Louka and Allaf, 2004). The establishment of an initial vacuum phase prior to the steam treatment, a treatment by step-wise increases in temperature and an atmospheric air injection as a last phase, enable to obtain good results for product pieces in thick layer, very heat-sensitive and with a low hardening temperature.

DRYING KINETICS

DIC treatment is followed by a final drying in order to bring the product to the water content that is required for storage. The impact of DIC technology on final drying kinetics was studied by Louka and Allaf (2002) for three samples of potato pieces: A, B and C. Sample A was dried only by conventional hot-air drying and needed 600 min to decrease the water content from 805% d.b. to 4% d.b. Sample B was initially dried, in the same conditions as Sample A, up to 25% d.b. for 220, directly followed by DIC processing and them, finally dried for other 220 min to reach 4% d.b. It was considered that change in water content during DIC processing was negligible. Last sample was similarly treated to sample B but including an equilibration step before the DIC step; the final drying time was in this case only 100 min. The values of the drying kinetics for the three samples are given in Table 1.

Table 1. Drying kinetics for three potatoes samples

Water content [% d.b.]	from 805 to 25	from 25 to 4
A - without DIC	220 min	380 min
B - with DIC	220 min	220 min
C - DIC + equilib.	220 min	100 min

The study was done on two levels: first one consisted in evaluation the inherent effect of expansion by DIC (comparing samples A with B), and the second one concerned the effect of the repartition of alveolation in the expanded product, as a result of the distribution form of residual water in the product (comparing samples B with C). The reduction in final drying time for samples B and C compared to A is a direct consequence of the expansion by DIC processing. The porosity acquired by expansion certainly improves the mass transfer and allows water trapped within the product to escape more easily than in normal hot-air drying. Final drying time of sample C was significantly decreased compared to B due to the homogeneous alveolation in the product generated by the equilibration step before expansion.

FINAL PRODUCT QUALITY

The quality of the expanded products can be expresses in terms of three response parameters: expansion ratio, color and degree of cooking. These parameters were systematically studied as a function of saturated steam pressure, treatment time and water content of the product just before DIC treatment. The combination of time and temperature determines the intensity of the treatment.

Pressure is the parameter that establishes the level of the decompression for a given final pressure and, in particular, the treatment temperature using saturated steam. For vegetables, pressure seems to be the parameter that exerts the most significant effect on the expansion ratio. Pressure defines the treatment temperature and the extent of the fall in temperature that determines the amount of steam generated by self-vaporization and thus the intensity of the mechanical constraints which provoke the expansion of the product's structure. In the general pattern evolution of the expansion ratios as a function of pressure, three phases can be distinguished. During the first phase, at low pressure, corresponding to very small expansion ratios, the amount of steam generated is not sufficient to give rise to the intense mechanical constraints capable of provoking the expansion of the product. During the second one, characterized by a rapid increase in the expansion ratio, the mechanical forces induced by the steam become sufficiently strong to brake through the resistance threshold of the matter. The expansion ratio variation is proportional to the amount of steam generated and varies almost linearly. During the third phase, there is an almost complete stabilization of the expansion ratio. The amount of steam is so great that it enlarges the existing pores considerably and creates fissures in the product, which reaches the limits of its elasticity. A part of the steam escapes out of the product and consequently stabilizes the level of the expansion ratio. Most of the expanded products have volumes ranging from 2 to 5 times the volumes obtained after drying by hot air only. For carrots, onions, broccolis and tomatoes, the expansion ratio reaches a stabilization at around 5 bar and for potatoes at a pressure of 9 bar due to the very dense structure of the potato after hot air drying in comparison with the other vegetables (Louka et al., 2004).

The variation in expansion ratio with time have four distinct phases. First phase corresponds to short treatments during which the product expands little and reaches thermal equilibrium. The mechanical constraints created by the steam generated during the Pressure-Drop are not sufficient to swell the product, which remains still hard and plastic. During the

second phase, the product starts to acquire a viscoelasticity that allow it to be expanded. The expansion ratio increases rapidly in an almost linear manner. Third phase corresponds to a period of optimal expansion and in the last phase the expansion ratio begins to fall down and two phenomena could occur: the product may become too elastic and so the volume shrinks after expansion, or the structure of the product may collapse due to a prolonged treatment at high temperature. A extended treatment can lead to a total collapse of the structure or even a liquefaction of the product.

The variation in expansion ratio as a function of water content has also four distinct phases. First one consists in an extremely fast increase in the expansion ratio. The presence of water in the product before treatment is indispensable for the production of steam: the higher the initial water content, the greater is the quantity of water that could be evaporated during the abrupt Pressure-Drop. The second phase is very short and stabilizes the expansion ratio followed by a sharp drop phase. During the last one, corresponding to very high water content, a large amount of steam may be generated, which could partially or totally disintegrates of the product.

Thickness seems to play a very important role in terms of expansion ratio. It has two variation phases: first in which it increases and second in which it decreases, with a maximum at around 3 mm thickness. In the first phase, escape of the generated steam seems to be more and more difficult with the increase of the piece thickness and the expansion is therefore grater. The decrease of the expansion ratio during second phase is due to a greater resistance of the matter to deformation.

Color can be expressed on a scale from 0 to 4, where 4 corresponds to the color of the control product. Modification in color only occurs at the end of the second expansion ratio phase as a function of pressure and becomes more obvious at the beginning of the last phase, being different from one product to another. Naturally, a long treatment at high temperature can lead to a change in the color of the product. The presence of water in the product protects against thermal alterations. Low water content (< 5%) can lead to a drastic deformation, which can seriously discolor the product. A water content of around 15% is indispensable to avoid a major modification of the color of the product.

Cooking rate is considered to be a quality criterion in the preparation of soups and ready-made meals for which rehydration is called "instantaneous". An evaluation of the cooked product can be done by people trained in sensorial analyses. The dried product is dipped in a bowl with boiling water and left covered for one minute. After tasting, it is evaluated as: uncooked, well cooked or overcooked. For the last one, the products have a mushy structure due to severe heat degradation and their structure is weakened by the abrupt pressure - drop and the rupture of their cells (Debs-Louka et al., 1996). These products can be very quickly rehydrated but water is not efficiently retained by the matrix, which corresponds to a rather spongy look. With the exception of very low water content (< 5%) when the products are often caramelized, the treatment time has no major influence on the product degree of cooking.

Fig. 2. Example of swell-dried products

Fig. 3. Swell-dried kiwis

Fig. 4. Swell-dried red peppers

Some examples of fruits and vegetables, i.e. onions, tomatoes, strawberries, apples, kiwis, red peppers, bananas and carrots, treated by DIC technology are presented in Figure 2. Figures 3 and 4 gives detail image of swell-dried kiwi and red pepper.

CONCLUSIONS

Internal resistance limits the dehydration rate of capillary-porous materials especially during the last drying stage. Most of the products reveal an important degree of shrinkage that contributes to the decrease of effective moisture diffusivity with drying time. Expanding partially dried foods (water content around 20% -dry basis) is a valuable alternative both for increasing the drying rate and improving final product quality.

Drying kinetics shows the beneficial effect of DIC incorporation into the hot-air drying process. The introduction of an equilibration step during which the water of the product is homogenized after initial drying, significantly reduces the duration of final drying step.

General patterns were discussed for the variation in the expansion ratio as a function of saturated steam pressure, exposure time to high pressure and temperature, initial water content of the product and thickness of the pieces. DIC technology can be used to control the quality of the final product and also to provide dried vegetables with a cooking time of one minute compared with approximately 15 min immersion in boiling water needed for vegetables classically dried with hot-air to cook them properly. The use of atmospheric air flow injected just after decompression may intensify cooling effect; it may allow low hardening temperature products to avoid final shrinking and fixes them in an expanded state. Creation of a vacuum in the processing vessel before the steam injection enables DIC to be successfully used with thick pieces of product (approx. 15 cm).

The overall impact of DIC technology results in saving time and drying costs together with an improvement in finished product quality. It was successfully industrialized for different types of vegetables such as tomatoes, red and green peppers, green beans, peas, onions, leaks, garlic, cabbage, cauliflower, broccoli, carrots, potatoes, turnips, parsnip as well as many fruits such as strawberries, apples, kiwis, bananas.

ACKNOWLEDGEMENTS

The research was partially supported by the Poitou-Charentes Region (France) through a post-doc scholarship awarded to Mr. Adrian-Gabriel GHIAUS. We studied various DIC dried products from ABCAR-DIC Process (www.abcar-dic.com).

REFERENCES

Allaf, K., N. Louka, J.-M. Bouvier, F. Parent and M. Forget (1992), Définition d'un nouveau procédé de traitement thermo-mécanique par détente instantanée contrôlée TTMDIC, French Patent, no. 92 04940.

Clark, J.P. (1986), Texturization process in the cereal foods industry, Food Technology, Vol. 40, pp. 91-93.

Debs-Louka, E., W. Sahyoun, H. Adenier, J.-N. Barbotin, N. Louka, H. Chaveron, D. Thomas and K. Allaf (1996), Etude de la composition lipidique et de la structure de la carotte prétraitée en vue du séchage thermique, Sciences des Aliments, Vol. 16, pp. 491-503.

Harrington, W.O. and F.P. Griffiths (1950), Puffs potatoes, Food Industry, Vol. 22, p.1872.

Labuza, T.P. (1972), Nutrient losses during drying and storage of dehydrated foods, Food Technology, Vol. 3, p. 217.

Louka, N. and K. Allaf (2002), New process for texturizing partially dehydrated biological products using Instantaneous Controlled Pressure-Drop towards vacuum: application on potatoes, Journal of Food Science, Vol. 67, pp. 3033-3038.

Louka, N. and K. Allaf (2004), Expansion ratio and color improvement of dried vegetables textured by a new process " Instantaneous Controlled Pressure-Drop ". Application to potatoes, carrots and onions, Journal of Food Engineering, Vol. 65, pp. 233-243.

Louka, N., F. Juhel and K. Allaf (2004), Quality studies on various types of partially dried vegetables textured by Instantaneous Controlled Pressure-Drop - General patterns for the variation of the expansion rate, Journal of Food Engineering, Vol. 65, pp. 245-253.

Sugisawa, K., Y. Matsumura and K. Taga (1985), Process for drying foods under reduced pressure, US patent.

17th International Drying Symposium (IDS 2010)
Magdeburg, Germany, 3-6 October 2010

INDUSTRIAL DRYING OF WOODEN PALLETS - CFD ANALYSIS OF AIR FLOW

A.-G. Ghiaus[1], A. Filios[2], D.P. Margaris[3], D. Tzempelikos[3]

[1]*Thermal Engineering Department, Technical University of Civil Engineering Bucharest*
Bd. Pache Protopopescu 66, Bucuresti Sector 3, RO-021414, Romania
Tel.:+40 21 2524280, E-mail: ghiaus@instal.utcb.ro

[2]*Fluid Mechanics and Turbomachinery Laboratory, School of Pedagogical and Technological Education*
ASPETE N. Heraklion, Athens, GR-141 21, Greece
Tel.:+30 210 2896744, E-mail: fmtulab@gmail.gr

[3]*Fluid Mechanics Laboratory, University of Patras*
Panepistimioupoli Rio, Patras, GR-265 04, Greece
Tel.:+30 2610 997202, E-mail: margaris@mech.upatras.gr

Abstract: This paper presents the results of the airflow 2D numerical simulation inside an industrial unit designed for drying of wooden pallets. The airflow field profile was examined in different operation conditions by plotting velocity vector distribution, path lines and pressure contours for both loaded with the wooden pallets and unloaded drying room. The analysis of the obtained results shows the presence of stagnation zones between and above the pallet columns and recirculation regions in different zones of the drying room. Further work will focus on validation of the predicted CFD results by means of local measurements that will be taken on a full scale dryer.

Keywords: wood drying, airflow, CFD analysis, wooden pallets

INTRODUCTION

Improvement and optimization of air flow and air-distribution systems in industrial convective dryers contribute to the overall quality of the drying process, homogeneity of the final product and important reduction of energy consumption and exploitation costs.

Airflow design is potentially important in the design of drying kilns which operate as closed, fully recirculatory systems. In industrial wood drying kilns, the effect of non-uniform airflows is particularly difficult to resolve. The airflow distribution is dependent on the drying process, the drying medium, the geometry and equipment of the drying kiln. Although the performance of a drying kiln can be studied experimentally, the time-consuming and costly methodology restrict the generalization of the outcomes and certainly is not applicable in an early design phase of the drying chamber. In contrary, with the aid of the computational fluid dynamics (CFD) that spans in a wide range of industrial and non-industrial applications, the complex flow field can be solved numerically.

Various researchers have considerably contributed in revealing the flow mechanics inside of a closed enclosure, aiming to improve and optimize the air distribution systems. Sun et al. (2004) simulating velocity and pressure distributions in an industrial dehumidifier wood drying kiln showed that for high efficiency it is important to avoid air recirculation. Smit et al. (2007) simulated a two dimensional pore-scale model in order to predict air flow through a wood drying stack and the predicted results are favorably compared with experimental measurements. Langrish and Keey (2004) modeling the air flow patterns in a timber kiln, intended to predict the distribution of the airflow in the fillet spaces between the boards in a hydraulic model of a timber kiln.

Margaris and Ghiaus (2006) simulated extensively the air flow inside a full-scale industrial dryer and the predicted parameters for different configuration contributed in the optimization of the drying space and led to a substantial improvement of the quality of the dried product along with the reduction of energy consumption. Mureh et al. (2009) studied the numerical and the experimental characterization of airflow within a semi-trailer enclosure loaded with pallets. The experiments were carried out on a

reduced-scale model of a refrigerated air duct systems. The numerical predictions show reasonable agreement with experimental data and moreover the results saw that the supply air duct system improves significantly the homogeneity of ventilation in the semi-trailer enclosure. Mathioulakis et al. (1998) simulated the air movement inside the drying chamber of an industrial batch-type, tray air dryer. The pressure and the air velocities above the product were found to have a lack of spatial homogeneity. Tapsoba et al. (2007) studied a reduced-scale model in order to investigate experimentally and numerically the airflow patterns within a ceiling-slot ventilated enclosure loaded by slotted boxes. The numerical predictions with the application of the Reynolds stress model show rather good agreement with experimental data.

However, little research on the prediction and measurements of flow field in a wood drying room loaded with pallets has been performed. The lack of experiments can be attributed to the complexity of direct measurement of local air velocities and flow rates in the thin air spaces located between the pallets.

In this study, CFD is used to develop and solve the physical and mathematical problem that describes the steady two-dimensional flow field in a wood pallets drying system of industrial type that is used for the effective preservation of wood by the withdrawing of microorganisms. The prediction of air flow field is examined inside the empty and pallet loaded drying room. Improvement of airflow distribution is achieved by different arrangements of the wooden pallet stacks as well as by using screen walls. The Fluent® commercial CFD code is used in all numerical simulations for which the steady state RANS equations are solved in combination with standard k-ε and rng k-ε turbulence models. The effect of the selected turbulence model is analyzed through direct comparisons of the predicted airflow patterns.

MODELS AND METHODS

Drying system configuration

Figure 1 presents a longitudinal cross section of the considered industrial type wood drying system which consists of an insulated drying chamber with pallet stacks, an air recirculation axial fan with six blades (37.5° pitch angle) and 872 mm impeller diameter, and a dehumidifier module (refrigeration cycle coupled with an electric air heater. Because energy and mass transfer does not significantly affect the air flow analysis, it was adopted a simplified configuration in which the dehumidifier, the electric air heater and the air recirculation fan were incorporated within a unique module. The drying chamber contains pallets arranged in four columns (PC-1 to PC-4) of 2.1 m height each.

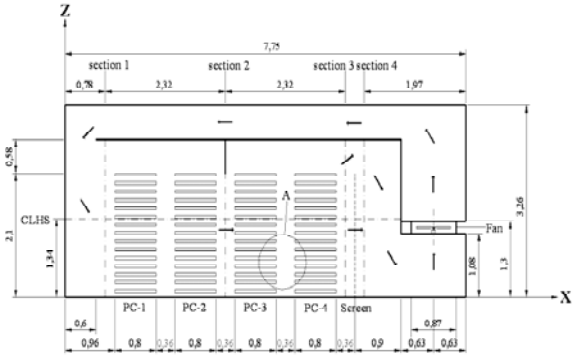

Fig. 1. Longitudinal cross section of the industrial wood pallet drying system (units in meters)

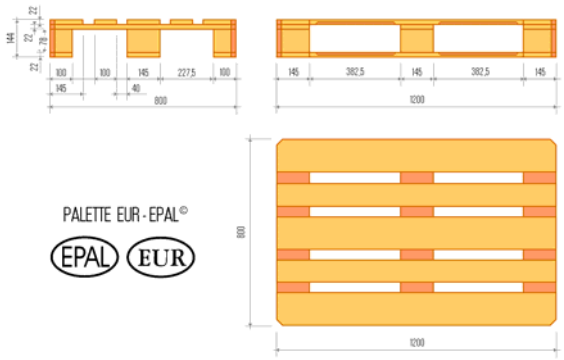

Fig. 2. EUR-EPAL pallet (units in millimeters)

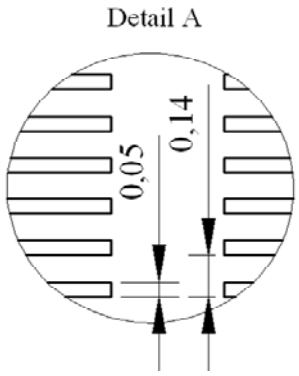

Fig. 3. Detail of pallet stack arrangement (units in meters)

The distance between the pallet stacks is 36 cm. Each stack has fifteen EUR-EPAL type pallets (see Fig. 2) placed one above the other.

For the simulation purpose, the pallet thickness was considered uniform and constant of 5 cm and the free space between the pallets of 9 cm. A detail of the pallet arrangement is shown in Figure 3.

Boundary condition and domain discretization

The boundary condition at the inlet is set as uniform velocity (U_0=16.3 m/s) that corresponds to a volume flow rate Q_0=35,000 m^3/h. At the outlet, the pressure is assumed to be uniform. The porosity of the round hole metal screen with 2 mm thickness is 40%, resulting a resistance coefficient of 7.4.

Turbulence models apply in fully turbulent regions. Close to the wall, where viscous effects become dominant, the models are used in conjunction with wall functions. In this study, the convectional equilibrium logarithmic law is used.

The computational domain is structured meshed with the aid of Fluent Gambit® pre-processor. In order to resolve steep gradients close to all walls, fine grid spacing has been applied. The final grid for the drying room discretization consists of 276,000 cells for the empty configuration and 227,000 cells for the pallet loaded configuration.

Numerical simulation procedure

Numerical simulation was performed using Fluent® commercial code. The steady-state RANS equation system was solved using two turbulence models: standard k-ε and renormalization group (rng) k-ε. The semi-empirical standard k-ε model based on model transport equations for the turbulence kinetic energy (k) and its dissipation rate (ε) is valid only for fully turbulent flows where the effects of molecular viscosity are negligible. The rng k-ε model employs a differential form of the effective viscosity relation, yielding to accurate description of how the effective Reynolds number affects the effective turbulent transport. This allows accurate model extension to low-Reynolds-number and near-wall flows where standard logarithmic wall functions were used. The SIMPLE algorithm was used in conjunction with the Fluent® solver to find the solution for pressure-velocity coupling equations. Solution accuracy was improved by using the second-order-upwind scheme.

Numerical solution control

The code was run using a Intel® Core 2 platform at 2.4 GHz. The number of iterations was adjusted to reduce the scaled residual below the critical value of 10^{-5}. Depending on the case, the convergence was achieved at different iterations using result history of previous running to initialize the new one. Aiming to smooth convergence, various runs were attempted by varying the under-relaxations factors. In this way, a direct control regarding the update of computed variables through iterations was achieved. Initializing with low values for the first iteration steps and observing the progress of the residuals, their values were modified and the convergence was accelerated.

RESULTS AND DISCUSSION

The prediction of the airflow pattern (velocity vectors and path lines) in the unloaded drying room is shown in Figures 4 to 7. The air coming out from the axial fan reaches the ceiling, passes through the distribution channel and spreads out at the upper left entrance of the drying room. The air flow downwards and reaches the bottom of the room with high velocity. The air flow recirculation eddies are produced at the top and the bottom side corners of the room, as can be seen in Figures 6 and 7. At the centre of the room there is a recirculating zone with low velocities. In this part of the room the flow is weak and the velocity magnitude did not exceed 10% of the initial fan velocity. The numerical results indicate that air flow recirculation eddy is produced at all top and bottom corners of the room as well as near the fan aspiration. Both turbulence models, i.e. k-ε and rng k-ε, well predict the regions with air recirculation presence.

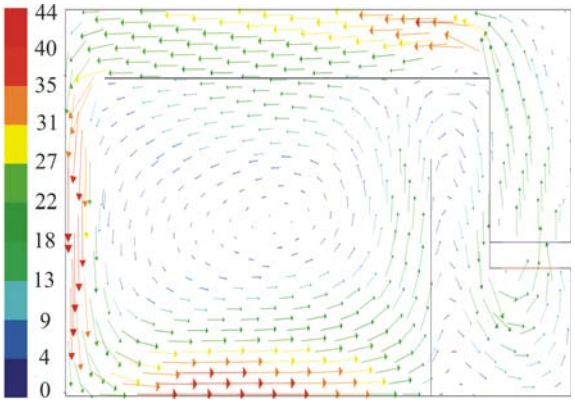

Fig. 4. Velocity vector distribution inside the empty drying room predicted with k-ε model

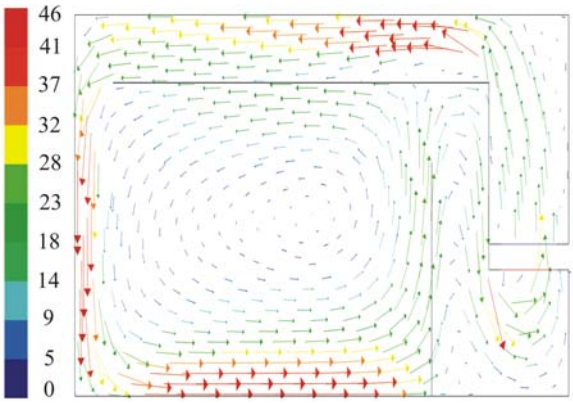

Fig. 5. Velocity vector distribution inside the empty drying room predicted with rng k-ε model

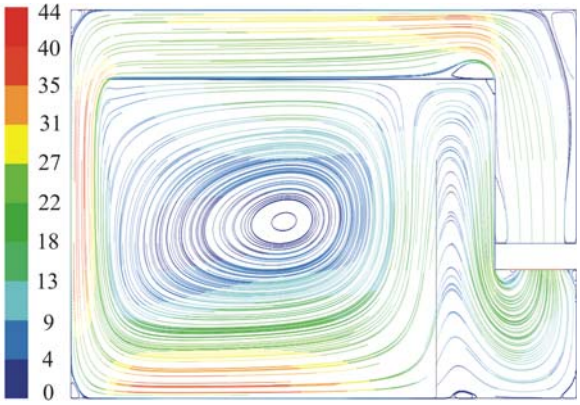

Fig. 6. Path lines inside the empty drying room predicted with k-ε model

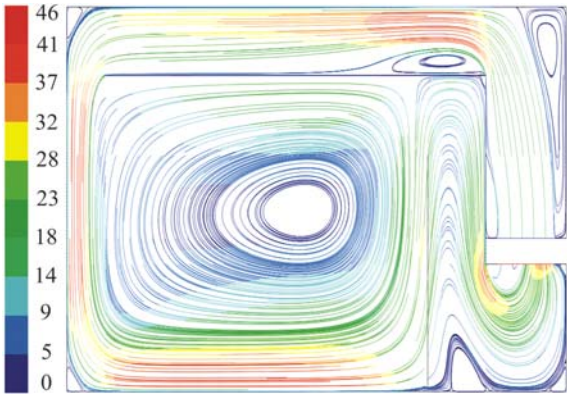

Fig. 7. Path lines inside the empty drying room predicted with rng k-ε model

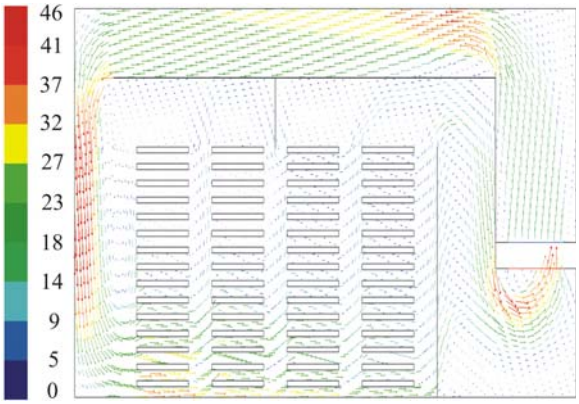

Fig. 8. Velocity vector distribution inside the pallet loaded drying room predicted with k-ε model

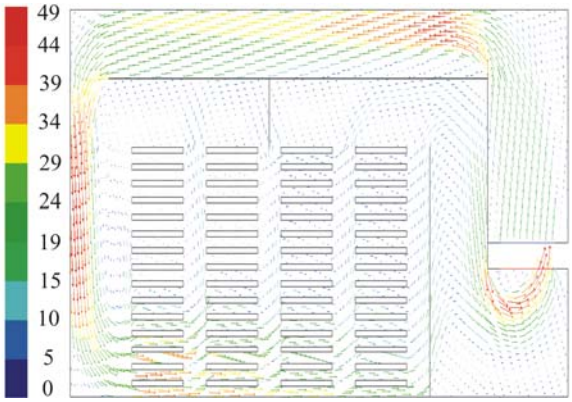

Fig. 9. Velocity vector distribution inside the pallet loaded drying room predicted with rng k-ε model

The prediction of the airflow pattern inside the drying room loaded with pallets is shown in Figures 8 to 11. The path line structure for both turbulence models, shows the complexity of the airflow with high velocity downstream of the room and air flow recirculation zones (near the corners, at the left side of the first pallet stack (PC1), above of the four series of the pallet stacks and between the pallets, especially at upper middle part, at the right side of the room and finally close to the fan aspiration).

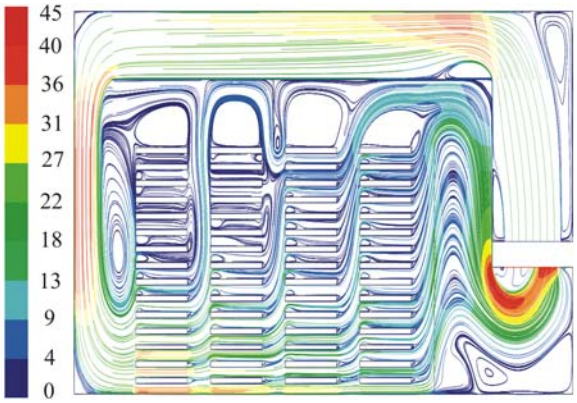

Fig. 10. Path lines inside the pallet loaded drying room predicted with k-ε model

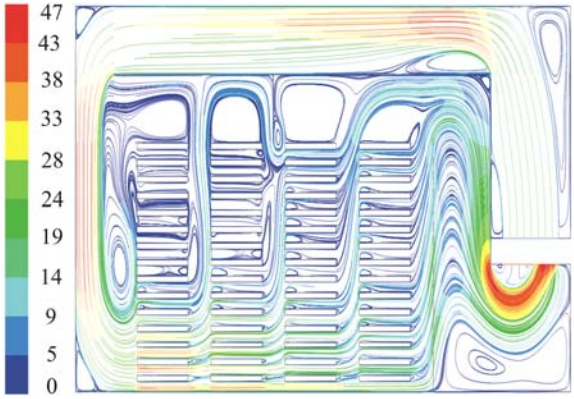

Fig. 11. Path lines inside the pallet loaded drying room predicted with rng k-ε model

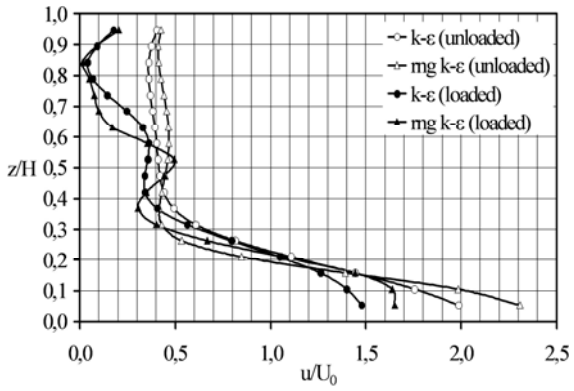

Fig. 12. Horizontal components of velocity vectors in Section 1

Profiles of the velocity vector horizontal component in four different vertical sections for the two turbulence models with and without pallets are given in Figures 12 to 15. For the pallet loaded configuration, the velocity distribution in Section 1 (at the entrance region of the first PC) is not uniform. The variation appears to be caused by the non-uniform flow at the entrance of the drying room. The flow patterns of the airflow on the top entrance of the second PC are similar to those of the first PC, but the velocities are smaller.

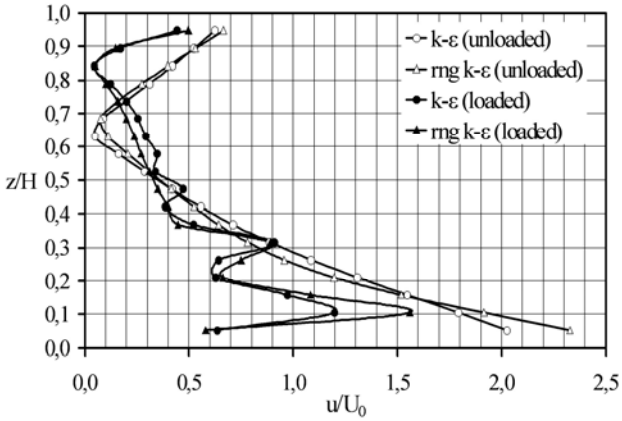

Fig. 13. Horizontal components of velocity vectors in Section 2

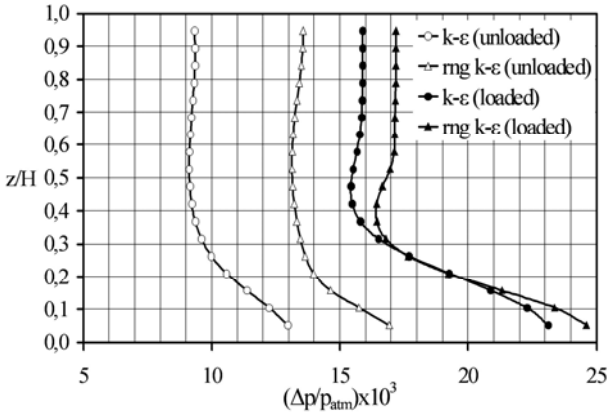

Fig. 16. Static pressure distribution in Section 1

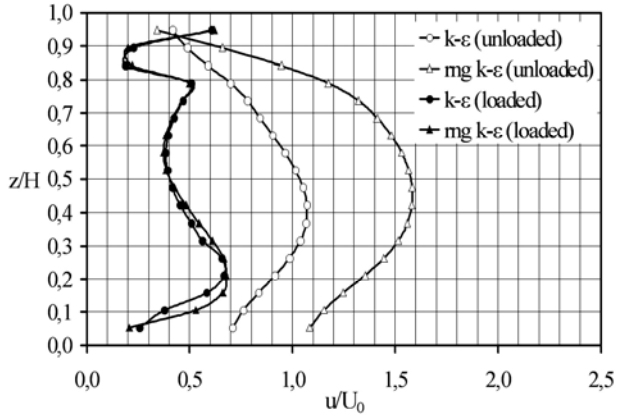

Fig. 14. Horizontal components of velocity vectors in Section 3

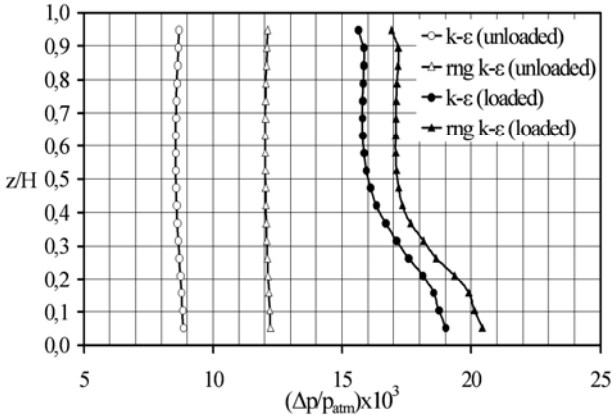

Fig. 17. Static pressure distribution in Section 2

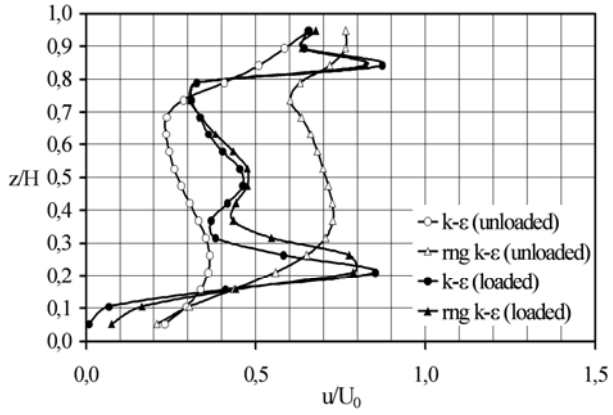

Fig. 15. Horizontal components of velocity vectors in Section 4

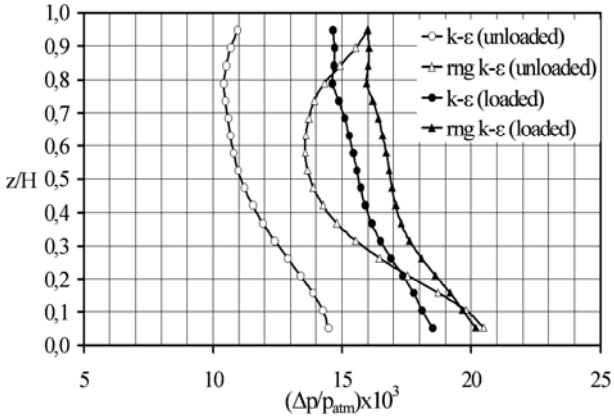

Fig. 18. Static pressure distribution in Section 3

At the entrance of the third PC, the velocity magnitude is smaller than those at the entrances of the first and second PC. However the large span in velocity magnitude in the exit area of the third PC indicates the presence of recirculation eddies at the exit of the PC.

At the entrance of the fourth PC, the velocity magnitude is smaller again, than those at the entrances of the first, second and third pallet columns.

The static pressure distribution at four different vertical sections (Section 1 to 4) of the room is

illustrated in Figures 16 to 19. The distribution of the static pressure in the chamber reflects the presence of a low velocities regime especially from the seventh row pallet and upwards.

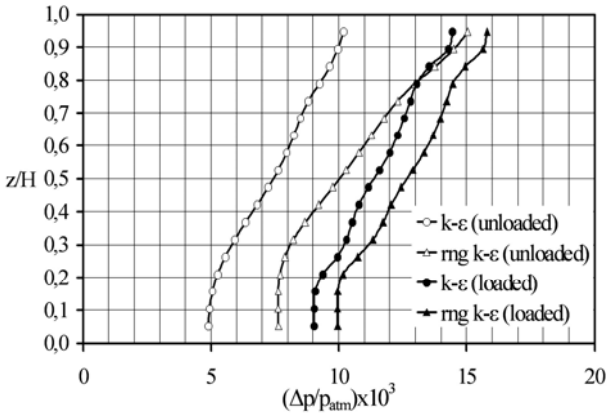

Fig. 19. Static pressure distribution in Section 4

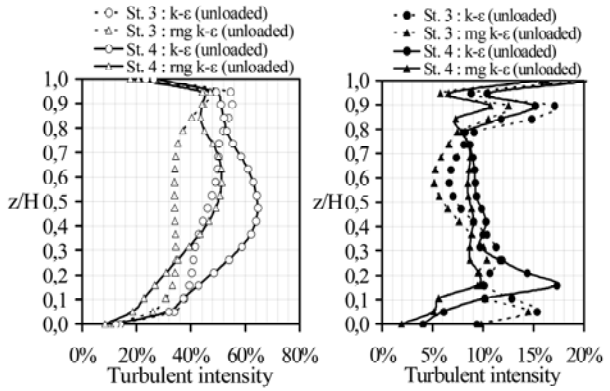

Fig. 20. Comparison of turbulent intensity between Section 3 and Section 4

Comparison of the turbulent intensity between two vertical Sections, is illustrated Figure 20. For the unloaded configuration the turbulent intensity is 64% in Section 4, in reverse to the loaded case where the turbulent intensity reaches almost 17%. This difference between the two configurations could be explained by the presence of the pallets.

CONCLUSIONS

Air flow patterns in an industrial drying system have been investigated using a commercial CFD code for two cases: empty room and loaded with wood pallets. In order to avoid the grid generation difficulties for the industrial dryer loaded with wood pallets, a simplified configuration has been chosen in which the actual pallets were replaced by rectangular solids. The turbulent flow regime was modeled by using standard k-ε and rng k-ε models. The simulation results obtained with the two turbulence models predict the presence of low velocities zones inside the pallets stacks and above them and the presence of recirculation regions in different zones of the drying room. The rng k-ε model provides more accurate flow prediction for low velocity zones (recirculation and near-walls) even if, generally, the two turbulence models give similar results. Further work will focus on experimental validation of the CFD results followed by extensive simulation of different proposed configuration, such as perforated walls, aiming to improve the drying room geometry.

ACKNOWLEDGEMENTS

The authors would like to express their thanks to Mr. George Varsos from Vencon Varsos S.A. (Athens, Greece) for collaboration and assistance during preliminary investigations.

REFERENCES

Langrish T.A.G. and Keey R.B. (2004), Progress in the modeling of air flow patterns in softwood timber kilns, Dev. Chem. Eng. Mineral Process, Vol. 12 (3/4), pp. 249-261.

Margaris D.P. and Ghiaus A.G. (2006), Dried product quality improvement by air flow manipulation in tray dryers, Journal of Food Engineering, Vol. 75, pp. 542-550.

Mathioulakis E., Karathanos V. T. and Belessiotis V. G. (1998), Simulation of air movement in a dryer by computational fluid dynamics : Application for the drying if fruits, Journal of Food Engineering, Vol. 36, pp. 183-200.

Moureh J., Tapsoba S., Derens E. and Flick D. (2009), Air velocity characteristics within vented pallets loaded in a refrigerated vehicle with and without air ducts, International Journal of Refrigeration, Vol. 32, pp. 220-234.

Smit G.J.F., Plessis J.P. and Plessis Sr.J.P. (2007), Modelling of airflow through a stack in a timber-drying kiln, Applied mathematical modelling, Vol. 31, pp. 270-282.

Sun Z.F., Carrington C.G., Anderson J.A. and Sun Q. (2004), Air flow patterns in dehumidifier wood drying kilns, IChemE, Chemical Engineering Research and Design, Vol. 82 (A10), pp. 1344-1352.

Tapsoba M., Moureh J. and Flick D. (2007), Airflow patterns in a slot-ventilated enclosure partially loaded with empty slotted boxes, International Journal of Heat and Fluid Flow, Vol. 28, pp. 963-977.

4th GRACM Congress on Computational Mechanics
GRACM 2002
Patra, 27-29 June, 2002

NUMERICAL MODELLING OF TWO-PHASE FLOW INSIDE INVOLUTE SEPARATORS

Adrian-Gabriel V. Ghiaus [1] and Dionissios P. Margaris [2]

[1]Thermal Engineering Department, Faculty Building Services and Equipments
Technical University of Civil Engineering of Bucharest
Bd. P. Protopopescu, 66, 73232 Bucharest, Romania

[2] Fluid Mechanics Laboratory, Mechanical Engineering and Aeronautics Department
University of Patras, GR-26500 Patras, Greece
e-mail: margaris@mech.upatras.gr, web page: http://fml.mech.upatras.gr

Keywords: Two-phase flow, separation processes, numerical simulation

Abstract. *A novel compact separator, I-SEP is proposed as a cost-effective alternative to conventional separators. In order to evaluate its performance, the new apparatus has to be tested over a wide range of flow conditions (velocity, flow-rate, gas-liquid ratio, back pressure, particle size and distribution), which cover most of the industrial applications. The limits of the experimental tests require the use of numerical simulation, which implies the development of a mathematical model to describe the flow inside the separator. Furthermore, the achieved differential equations have to be integrated in order to obtain the space distribution of the involved parameters. To solve the system of equations for the two-phase inter-penetrating continua flow, the Inter-Phase Slip Algorithm (IPSA), which entails solving the full Navier-Stokes equations for each phase, was chosen. The two phases are taken as having the same pressure and each having, at each point in the domain under consideration, its own velocity components, temperature, composition, density, viscosity and volume fraction. Numerical simulation was carried out using PHOENICS commercial code. Graphical results from the numerical simulation present, for different operation conditions, pressure contours, velocity vectors and volume-fraction distribution of each phase, and help in a better understanding of the influence of each involved parameter.*

1 INTRODUCTION

Separation processes have a wide range of applications in the oil and gas industry related to separation of gas, liquid and/or sand from multiphase mixture. A novel compact separator, I-SEP is proposed as a cost-effective alternative to conventional separators. Compared with these, the new involute separator has several advantages: it is very compact and free from the effect of the motion on floating platforms, it can be modularized in series to remove liquid or gas carry-over, it generates high "g" forces and is more tolerant to flow fluctuations.

There are a number of details and dimensions crucial to the design and performance of the system. In order to evaluate its performance, the new apparatus has to be tested over a wide range of flow conditions (velocity, flow-rate, gas-liquid ratio, back pressure, particle size and distribution), which cover most of the industrial applications. The limits of the experimental tests require the use of numerical simulation, which implies the development of a mathematical model to describe the flow inside the separator.

Results both from numerical simulation and from tests under real field production conditions, where the fluids, flow-rates, temperatures and pressures are representative, have to be compared and interpreted in order to validate and improve the mathematical model which will be used as an essential tool both for designing and for predicting the performance of the system.

2 PHISICAL MODEL (I-SEP CONFIGURATION)

The novel separator consists of two involutes connected through a separation chamber (see Figure 1). The mixture, on entry tangentially into the first involute, is spun around with high angular velocity and enters the separation chamber where light and denser phases are separated under the generated high "g" forces.

The fluids then enter the second involute where the dense phase is spun around and exits tangentially, and the light phase is axially evacuated. In cases when slug flow and flow fluctuations are expected, some liquid will

normally be carried-over into the separated gas phase. If this level of carry-over is not acceptable, a second involute may be added to the end of the gas outlet line. The pressure of the mixture at the centre core of the

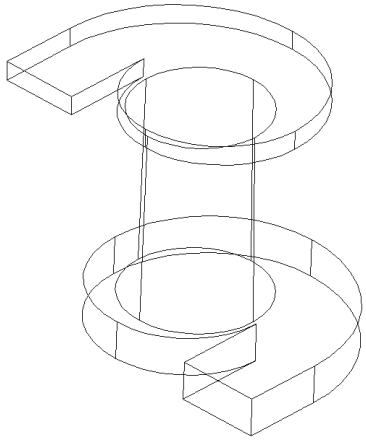

Figure 1. Outline of the I-SEP separator

involute is low because of high angular velocities generated, and will practically suck-in the liquid phase fed at this point. The unit is modularized with identical sections and several can be stacked up and manifolded to handle high flow-rates at optimum efficiency.

3 MATHEMATICAL MODEL

Multiphase flows are characterized by two or more phases in motion relative to each other. In addition, the phases will usually have different physical properties - temperature, density, conductivity, etc. Flows where the phases are not mixed, but are separated by a sharp interface, can be also solved using multiphase techniques [1].

A phase is an identifiable class of material in a mixture, which can be characterized by size (e.g. all particles between 200 and 500 μm), geometric shape (e.g. all round particles), velocity (e.g. all downward moving particles) or temperature (e.g. all particles above 100 ºC). However, the most common identifier is the thermodynamic phase (solid, liquid or gas).

In a general form, the transport equation (including momentum, kinetic energy, dissipation rate, etc.) can be written as given in equation (1):

$$\frac{d}{dt}(\rho\cdot\Phi)+div(\rho\cdot\vec{w}\cdot\Phi)=div[\Gamma_\Phi\cdot grad(\Phi)]+S_\Phi \tag{1}$$

$$transient + \ convection = \ diffusion + source$$

where ρ is the density, $\vec{w}$ is the velocity vector and Φ, Γ_Φ, and S_Φ are the general transport equation parameters, i.e.: Φ the variable in question, Γ_Φ the diffusive exchange coefficient for Φ and S_Φ the source term [2]. For our purpose, it is necessary to solve only the momentum and continuity equations. For the momentum equation, the particular transport parameters are: Φ = u, v, w (velocity components), Γ_Φ = $\rho\cdot(\nu_l+\nu_t)$ and $S_\Phi=-\frac{dp}{dn}$, where ν_l and ν_t are the laminar and turbulent kinematic viscosities:

$$\frac{d}{dt}(\rho\cdot u)+div(\rho\cdot u^2)=div[\rho\cdot(\nu_l+\nu_t)\cdot grad(u)]-\frac{dp}{dx} \tag{2}$$

and for the continuity equation $\Phi = 1$ and $\Gamma_\Phi = S_\Phi = 0$:

$$\frac{d\rho}{dt}+div(\rho\cdot\vec{w})=0 \tag{3}$$

The prediction of multiphase phenomena involves, for each phase, computation of the values of up to 3 velocity components (u_i, v_i, w_i), 1 volume fraction (r_i) and possibly pressure, turbulence quantities, particle size,

chemical composition, temperature, etc.

Eulerian-Eulerian techniques using a fixed grid, employ the concept of "interpenetrating continua" to solve a complete set of equations for each phase present. The volume fraction of phase "i", r_i, is the proportion of volumetric space occupied by phase "i". It can also be interpreted as the probability of finding phase "i" at the point and instant in question. All volume fractions must sum the unity. This method is embodied in the Interphase Slip Algorithm, IPSA which has been implemented for two thermodynamic phases only.

The treatment is impartial between the phases, i.e. if either phase volume fraction goes to 1.0, the equation for that phase reduces to the single phase form. The transient, convective and diffusive terms all contain the appropriate volume fraction multiplier, upwinded or averaged as required. The links between the phases -mass, momentum and heat transfer- are introduced via an interphase source.

Concerning the linked phase equations, each phase is regarded as having its own distinct velocity components. Interphase momentum transfer - droplet drag, film surface friction, etc, influences phase velocities. Each phase may have its own temperature, enthalpy, and mass fraction of chemical species. Pressure (p_1) is common to all phases. The equation describing the state of a phase are basically the Navier-Stokes Equations, generalised to allow for the facts that each of the phases occupies only a part of the space, given by the volume fraction; and the phases are exchanging mass and all other properties.

The phase continuity is regarded as the equations governing the phase volume fractions. They are the counterparts of the single phase continuity equation.

$$\frac{d(r_i \rho_i)}{dt} + div\left[r_i \rho_i \vec{w}_i - \Gamma_{ri} grad(r_i)\right] = \dot{m}_{ji} \tag{4}$$

transient + convection - phase diffusion = mass source

where r_i is the phase volume fraction (m^3/m^3), ρ_i is the phase density (kg/m^3), $\vec{w}_i$ is the phase velocity vector (m/s), Γ_{ri} is the phase diffusion coefficient (Ns/m^2) and $\dot{m}_{ji}$ is the net rate of mass entering phase *i* from phase *j* (kg/m^3s). The phase diffusion term models the turbulent dispersion of particles by random motion mechanism. It is not present in laminar flows.

The conservation equations for any variable of phase *i*, Φ_i is:

$$\frac{d(r_i \rho_i \Phi_i)}{dt} + div\left[r_i \rho_i \Phi_i - r_i \Gamma_{\Phi_i} grad(\Phi_i) - \Phi_i \Gamma_{r_i} grad(r_i)\right] = S_i + S_{ip} \tag{5}$$

transient + convection - within-phase diffusion - phase diffusion = sources

where Φ_i is the phase variable, Γ_{Φ_i} is the within-phase diffusion coefficient (Ns/m^2), S_i is the within-phase volumetric sources (kg [Φ]/m^3s) and S_{ip} is the interphase volumetric sources (kg [Φ]/m^3s). The volume fraction multiplier allows for the 'diluting' effect of the other phase. The within-phase diffusion term represents the molecular and turbulent mixing present in the phase. The phase diffusion term represents the transport of the variable Φ_i brought about by the turbulent dispersion of the phase itself.

In the case of two-phase flow, the two inter-penetrating continua have at each point in the space-time domain under consideration its own velocity components, temperature, composition, density, viscosity, volume fraction, etc. [3]. Because the sum of the two volume fractions is equal with unity ($r_1 + r_2 = 1$), it is possible to solve one of r_1 or r_2, and only store the other. This works well if both phases are present in finite quantities throughout the domain. If one of the phases can disappear, it is better to solve both r_1 and r_2 for numerical reasons. Each phase can be characterized by a "fragment size". This could be a droplet or bubble diameter, film thickness or volume/surface area [4]. Phase equations include mathematical expressions for the rates of the interphase transport processes. These are sometimes called the "constitutive relationships". The expressions are often empirical, and mainly come from experiment.

A numerical technique called Partial Elimination Algorithm (PEA) is used to procure convergence for tightly linked phases. In two-phase flow, the expression of mass flow is affected by the volume fraction of each phase.

The normal within-phase diffusion treatment for two phase flow is very similar to that for the single phase. The diffusion coefficient for each phase is written as:

$$\Gamma_{\Phi i} = \rho_i \cdot \left(\frac{\nu_l}{Pr_l(\Phi_i)} + \frac{\nu_t}{Pr_t(\Phi_i)} \right) \tag{6}$$

where Pr_l, Pr_t are the laminar and turbulent Prandtl numbers. The term includes both laminar and turbulent mixing but there is only one laminar and one turbulent viscosity corresponding to phase 1. If one of the phases, normally phase 2, is a dispersed one, say droplets or particles, then within-phase turbulent effects are absent.

The phase diffusion term accounts for turbulent dispersion of particles or droplets due to turbulence in the continuous phase and represents the turbulent flux associated with correlations between fluctuating velocity and volume fraction. Therefore, the diffusion coefficient is written as:

$$\Gamma_{ri} = \rho_i \cdot \left(\frac{\nu_l}{Pr_l(r_i)} + \frac{\nu_t}{Pr_t(r_i)} \right) \tag{7}$$

where $Pr_l(r_i)$, $Pr_t(r_i)$ are the laminar and turbulent Prandtl numbers for the volume fractions, the later being taken as unity by default.

The turbulence variables, k and ε are always phase-1 variables, and the generation rate is calculated from phase-1 velocity gradients [5]. The presence of particles will normally have a damping effect on the turbulent field. Strictly speaking, this effect is not completely modelled in the built-in k-ε model. Only the generation and dissipation terms are reduced by the volume fraction, but there is no explicit damping. This can be introduced via additional source/sink terms.

The interphase source contains the diffusive (e.g., friction, heat transfer) and convective (mass transfer related) links between the phases and in the general form it is formulated as follows:

$$S_{ip} = \left(f_{\Phi_i} + \dot{m}_{ji} \right) \cdot \left(\Phi_i^{int} - \Phi_i \right) \tag{8}$$

where f_{Φ_i} is the interphase (diffusive) transfer coefficient (kg/s), $\dot{m}_{ji}$ is the net mass transfer rate between phases (kg/s), Φ_i^{int} is the value of Φ at the interface between the phases, and Φ_i is the bulk phase value of conserved variable Φ. The unit of S_{ip} is (kg/s) · (unit of Φ), which means that if Φ is velocity, the units of S_{ip} are Newtons and if Φ is enthalpy, the units of S_{ip} are Watts [6].

The value of Φ_i at the i-j interface, Φ_i^{int} can be a function of space, time, or local bulk phase values. It is a property, and not a variable obtained from a conservation equation. In the case of interphase momentum transfer, the concept of an interface value is not helpful, and it is more meaningful to think of direct transfer between bulk phase values. In this case, the interface value of current phase is made equal to the bulk value of another phase, i.e. $\Phi_i^{int} = \Phi_j$. Then, interphase source becomes:

$$S_{ip} = \left(f_{\Phi_i} + \dot{m}_{ji} \right) \cdot \left(\Phi_j - \Phi_i \right) \tag{9}$$

The interphase (diffusive) transfer coefficient, f_{Φ_i} is actually the interphase flux per cell per unit conserved variable difference. The specific interphase fluxes are made proportional to f_{ip}, which is termed the reference interphase transfer coefficient (kg/s = Ns/m), the force per cell per unit velocity difference. It appears as multiplier, in the built-in formulations of all specific f_{Φ_i}, and $\dot{m}_{ji}$. This multiplier is introduced because of the analogy between friction, heat and mass transfer.

Ignoring the interphase mass transfer, for bulk-to-bulk transport of momentum, the interphase source term becomes:

$$S_{ip} = f_{ip} \cdot \left(u_j - u_i \right) \tag{10}$$

where S_{ip} has units of Newton and f_{ip} is now the interphase drag coefficient [7] between phases in units of Ns/m or kg/s. For the dispersed flow, wherein phase 1 is the carrier and phase 2 is dispersed, the interphase drag coefficient is calculated using the following expression:

$$f_{ip} = 0.75 \cdot C_d \cdot \rho_1 \cdot r_2 \cdot r_1 \cdot V_{cell} \cdot u_{slip} / d_p \tag{11}$$

where C_d is a dimensionless particle drag coefficient, V_{cell} is the free cell volume (m^3), u_{slip} is the absolute slip velocity between the two phases (m/s), and d_p is the particle diameter (m).

4 NUMERICAL SIMULATION

The simulation trials have been carried out under conditions as close as possible to actual field conditions in terms of fluid used, pressure, flow rate, gas-liquid ratio and operation conditions.

Because of the complex three-dimension geometry of the separator, consisted of three distinct sections (inlet involute, separation chamber and outlet involute) as provided by CAL TEC, the standard configuration (scale 2) was designed in AutoCAD and afterward imported through an implementation procedure into Phoenics code.

A parallelepiped having in X-direction 0.225 m, in Y-direction 0.3048 m and in Z-direction 0.247 m was chosen for the computational domain. The I-SEP mask created in Auto-CAD was imported through an CAD interface as a blockage-type object assimilated with solid material with smooth-wall friction. This object is represented in all the graphics by black lines wires. The object tolerance is 0.1 mm, which means that object edges lying closer than this will be assumed to be coincident. The code is running in the steady-state mode of operation. The coordinate system is Cartesian having a total number of computational cells equal with 21,000, arranged in the three directions as follows: 30 in X-direction, 35 in Y-direction and 20 in Z-direction. The last corresponds to the direction of the separation chamber axis.

Boundary conditions must be specified for whichever phase is to be affected. The practice is to use the mass flow for each phase as inlet condition and the pressure as outlet conditions.

The simulation code solver applies wall function boundary conditions on all faces of solids, without the need for explicit commands. The type of turbulent wall functions used to calculate shear stress on plates and blockages is Logarithmic Law of the wall. The global wall roughness is the absolute "sand-grain roughness" size for rough walls, according to the formula of Nikuradse.

The equations were formulated in Elliptic-CCM form, which allows for recirculations. As it was mentioned before, the simulation is based on the IPSA-Full method, which solves the full equations for the two phases. A number of 12 turbulence models was tested, i.e. KECHEN, KECHEN-LOWRE, KEMODL, KEMODL-2L, KEMODL-LOWRE, KEMODL-LOWRE-YAP, KEMODL-YAP, KERNG, KLMODL, KOMODL, KOMODL-LOWRE, KWMODL. The best results were achieved with the Standard 2-equations K-E model.

The total number of iterations was set up to 2000 and the solution in all the solved equations will stop when the errors have fallen below 0.01 %.

Phase-1 (gas) was chosen as air at 20 ºC with a density of 1.189 kg/m^3 and a viscosity of $1.544 \cdot 10^{-5}$ m^2/s. Phase-2 (liquid) was chosen as water at the same temperature, 20 ºC and having a density of 998.23 kg/m^3.

5 RESULTS AND DISCUSSIONS

The results of the simulation are presented by means of pressure contours, liquid-volume-fraction (R2) contours and velocity vectors distribution of the gas-phase and liquid-phase, for different values of the inlet liquid-phase volume fraction (Figure 2 and 3). In these 3-D images, pressure, liquid-volume-fraction and velocities are given in three X-Y planes: one at the bottom of the inlet involute, another at the middle of the separation chamber and the last at the top of the outlet involute. The X-Y plane is the one perpendicular to the separation chamber axis. The 2-D images, (Figure 4) give the top view of the inlet involute (X-Y plane) and the front view of the Y-Z plane passing through the axis of the separation chamber. Figure 5 is a 3-D also figure showing the influence of the inlet velocity on pressure distribution for a specific value of the inlet liquid-phase volume fraction.

6 CONCLUSIONS

As an aid to improve the design, the modelling work has explore the effect of changes to parameters related to the flow conditions, such as inlet velocity and gas-volume-fraction and has identified and quantified to an extent the impact of the separation chamber length on performance.

The simulation code covered testing of the standard configuration of the I-SEP compact separation (scale 2) under a wide range of operation conditions involving two-phase (gas-liquid) separation.

The cross analysis of all the images could lead to a better understanding of the two-phase flow inside each of the separator component. For each operation condition and configuration it is possible to have details at certain zone of interest inside the I-SEP.

ACKNOWLEDGEMENTS

Part of this research was carried out in the framework of the Contract no. OG/206/98 UK/HE "

Demonstration and Testing of a Novel Compact Separator" supported by the European Commission - Directorate General for Energy.

REFERENCES

[1] Hetsroni, G. (1982), *Handbook of Multiphase Systems*, Hemisphere, Washington.

[2] Bird, R.B., Stewart, W.E. and Lightfoot, E.N. (1960), *Transport phenomena*, John Wiley & Sons, New York.

[3] Ishii, M. (1975), *Thermo-fluid dynamic theory of two-phase flow*, Book Publication, Eyrolles.

[4] Clift, R., Grace, J.R. and Weber M.E. (1978), *Bubbles, Drops and Particles*, Academic Press, New York.

[5] Goldberg, U.C. (1996), "Exploring a Three-Equation R-k-ε Turbulence Model", Journal of Fluids Engineering, pp. 795-799.

[6] Spalding, D.B. (1981), *Numerical Computation of Multiphase Flow and Heat Transfer,* C. Taylor & K. Morgan, Pineridge Press, Swansea.

[7] Ishii, M. and Zuber, N. (1979), "Drag coefficient and relative velocity in bubbly, droplet or particulate flows", AIChE Journal, Vol.25, No.5, p. 843.

I-SEP Scale 2 - standard

inlet velocity: 10 m/s, inlet liquid-phase volume fraction: 50%

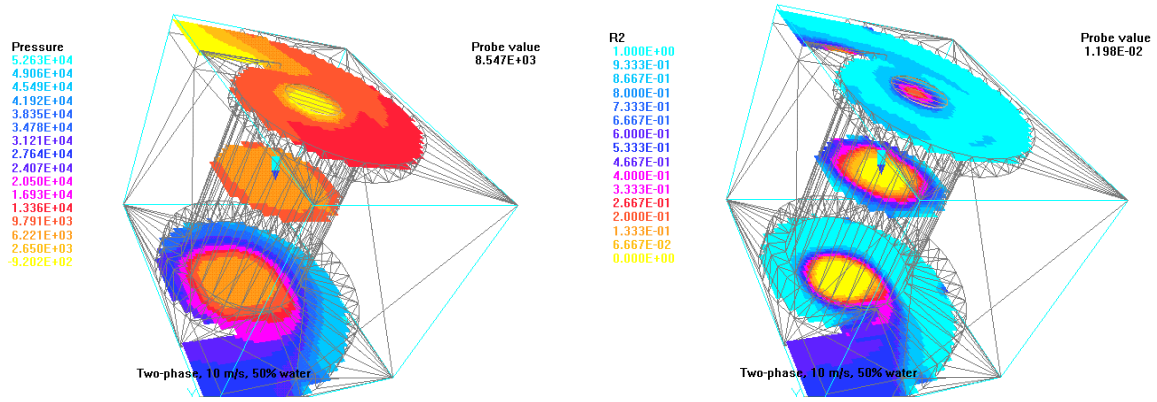

a) Pressure distribution

b) Liquid-phase volume fraction

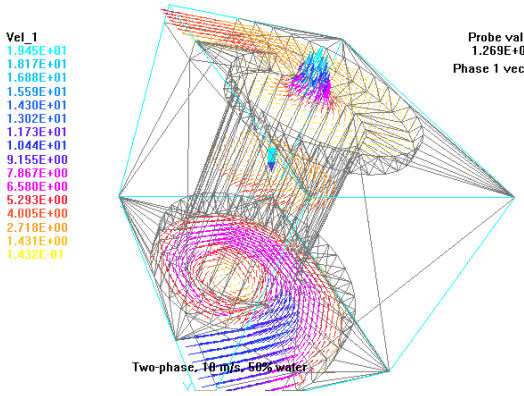

c) Gas-phase velocity

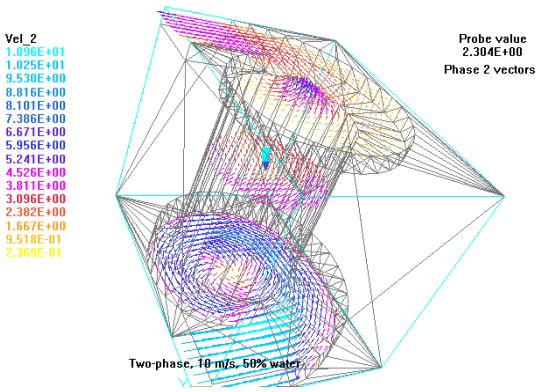

d) Liquid-phase velocity

Figure 2. Pressure, volume fraction and velocity distributions.

I-SEP Scale 2 - standard
inlet velocity: 10 m/s, inlet liquid-phase volume fraction: 80%

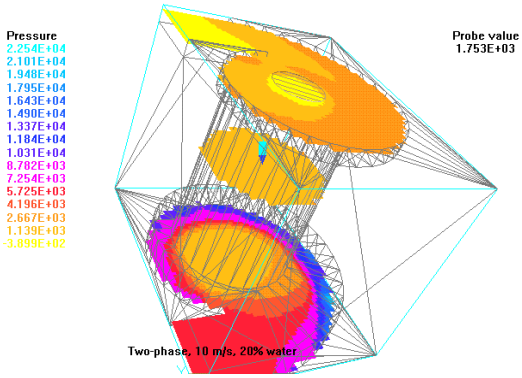

a) Pressure distribution

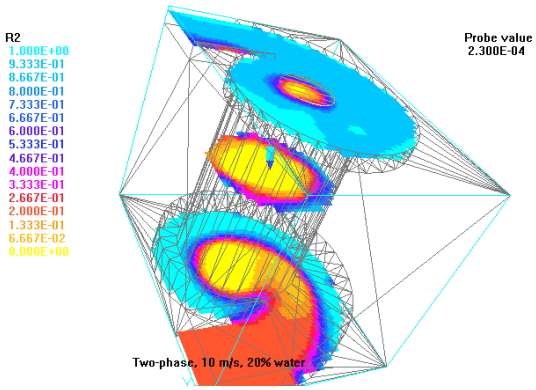

b) Liquid-phase volume fraction

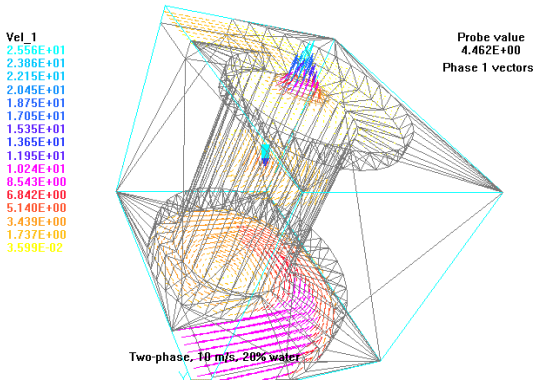

c) Gas-phase velocity

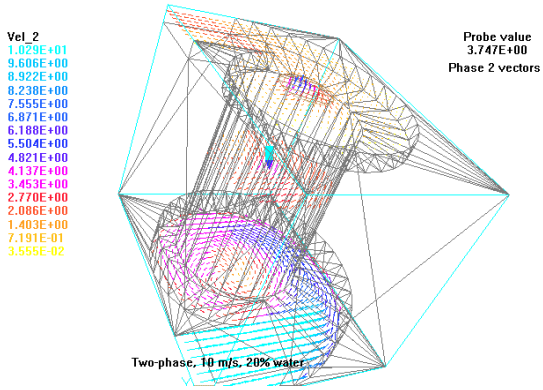

d) Liquid-phase velocity

Figure 3. Pressure, volume fraction and velocity distributions.

Top view - inlet involute

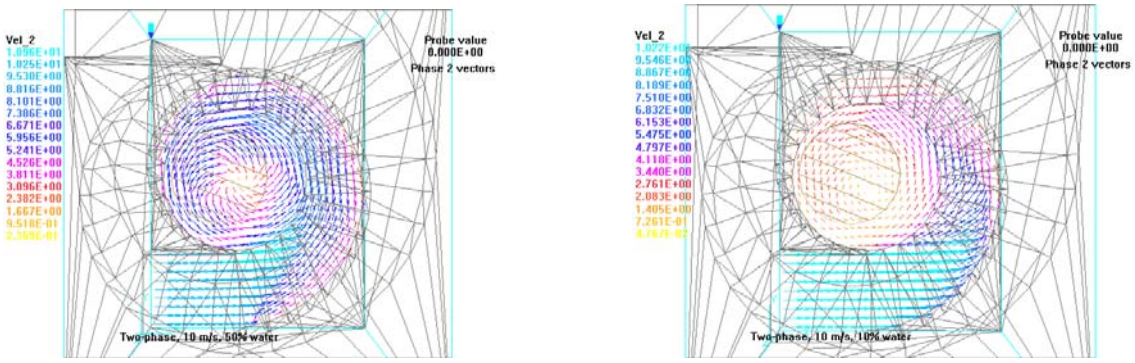

a) inlet gas-phase volume fraction: 50 %

b) inlet gas-phase volume fraction: 90 %

Front view

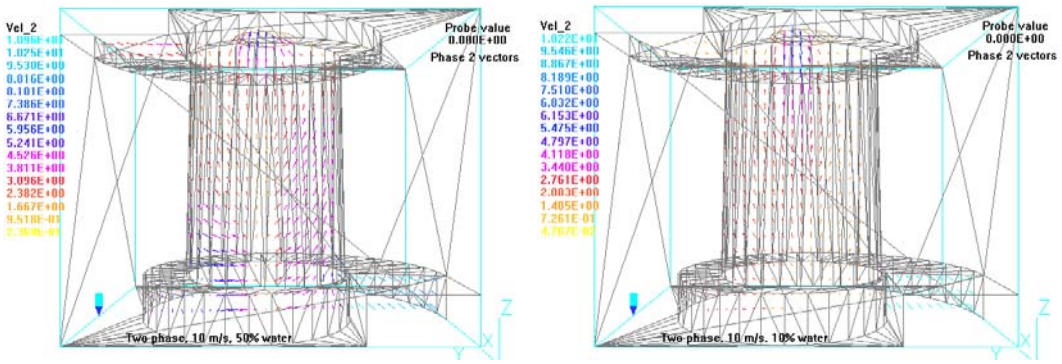

a) inlet gas-phase volume fraction: 50 %

b) inlet gas-phase volume fraction: 90 %

Figure 4. Top and front views of the liquid-phase velocity.

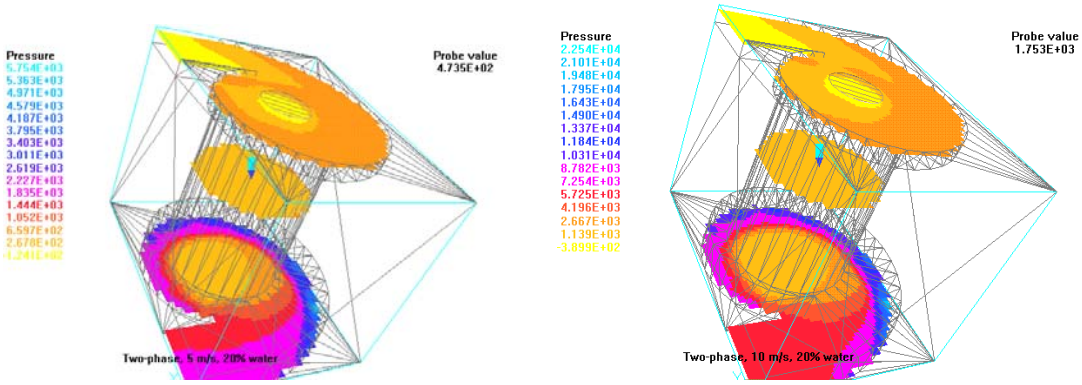

a) inlet velocity 5 m/s
Pressure drop inlet-outlet: 1.724 kPa

b) inlet velocity 10 m/s
Pressure drop inlet-outlet: 6.115 kPa

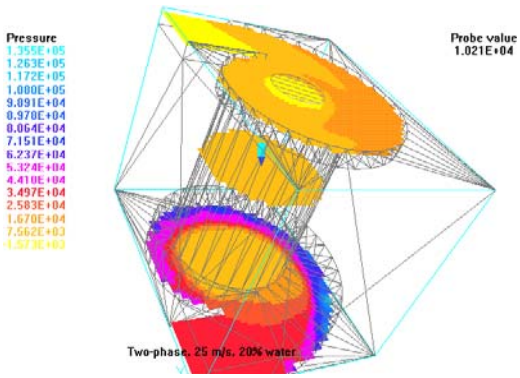

c) inlet velocity 25 m/s
Pressure drop inlet-outlet: 36.543 kPa

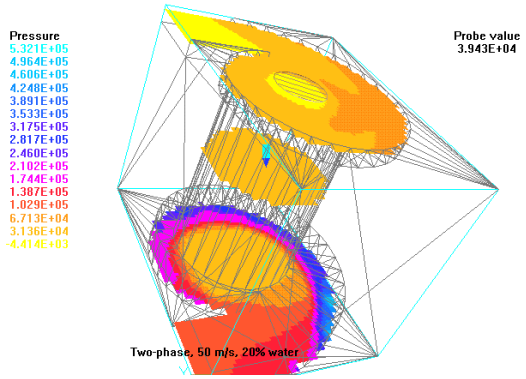

d) inlet velocity 50 m/s
Pressure drop inlet-outlet: 107.314 kPa

Figure 5. Influence of inlet velocity on pressure distribution (inlet liquid-phase volume fraction: 80%).

PERGAMON

Building and Environment 34 (1999) 671–679

BUILDING AND ENVIRONMENT

Evaluation of the indoor temperature field using a given air velocity distribution

C.M. Ghiaus, A.G. Ghiaus*

Technical University of Civil Engineering—Bucharest, Building Services Engineering Faculty, Bd. P. Protopopescu, 66, RO-73 232 Bucuresti-39, Romania

Received 8 October 1997; received in revised form 6 April 1998; accepted 14 September 1998

Abstract

A new method for compensating the space discretization error introduced when the fixed flow field is considered for the dynamic models of temperature distribution is presented. It is proved that the method generally used in literature is a particular solution of the proposed one. Moreover, it results in a continuous-time model, for which the integrating method becomes a free choice and a state-space representation is possible. The numerical model was experimentally validated, the comparison, both in the time and in the frequency domains, between simulation and measured results showing good agreement. The presented dynamic model increases the calculation speed and it can be analysed with the tools developed in control theory. © 1999 Elsevier Science Ltd. All rights reserved.

Keywords: Dynamic models; Computational fluid dynamic; Air conditioning; Control theory

Nomenclature

S_Φ source term in general transport equation
S_q source term in thermal energy equation
$\mathbf{V}$ velocity vector
u, v, w velocity components in x-, y- and z-directions, respectively
x, y, z space co-ordinates

Greek symbols

Γ effective thermal diffusivity coefficient
Γ_Φ effective diffusivity coefficient
θ temperature
ρ density
Φ potential in the general transport equation

Subscripts

e, w, n, s, h, l east, west, north, south, high, and low frontier, respectively, for an elementary cell
E, W, N, S, H, L east, west, north, south, high and low elementary cell, respectively
i, j, k the current indexes for x-, y-, and z-directions, respectively

1. Introduction

In order to evaluate the indoor thermal comfort, it is desirable to know the air flow field and the room temperature distribution [1]. As an alternative to experiment, the computational fluid dynamic (CFD) theory supplies numerical techniques for studying indoor temperature distribution and air flow field (and consequently the thermal comfort) in a computational grid [2–4]. However, since the mass, energy and especially momentum balance equations need thousands of grid cells to be solved by iteration procedure, and since the iterative process should be continued until all dependent variables converge to some satisfactory extent, the CFD calculation takes so much time that it is practically suitable only for some steady state evaluations. Although the future development of computer technology will eventually make fast dynamic CFD calculation possible, at present we have to find some trade-off methods concerning the calculation of the dynamic temperature distributions which is essential for the simulation of indoor climate control systems.

For the problem of indoor air flow, Peng et al. [5] proposed a method to calculate the dynamic temperature distribution in a fixed flow field, provided that it is correctly calculated for the steady state. By assuming that the air flow field is not changing in time and can be correctly calculated by the CFD code, only the dynamic

* Corresponding author: University of Patras, School of Engineering, Fluid Mechanics Laboratory, GR-265 00, Patras, Greece. Tel.: 0030-61-99 7193; fax: 0030-61-99 7202; e-mail: ghiaus@mech.upatras.gr

PII: S0360-1323(98)00051-1

energy balance equation needs to be solved. But Peng et al. [5] used the implicit (backward difference) method to solve the energy balance equation, thereby the iteration method for all grid cells has to be used. However, the given flow field may not satisfy the continuity equation, a problem which appears in the discretized continuity equation, also mentioned by Patankar [2], who stated that the rule of sum of neighbour coefficients should be satisfied. To correct the discretization error, Patankar [2] considers that the new values (at time $t+\Delta t$) prevail during the time step. The old value (i.e. the one at time t) appears only through its time derivative. The new values are initially guessed. Then, an iterative procedure is applied in order to obtain the values at the instant $(t+\Delta t)$. But the iterative procedure is very time consuming. This paper discusses a new method to correct the discretization error, i.e. the mass compensation idea. A mass flow is considered in a supplementary (fictitious) direction so that the continuity equation for each control volume (or cell) and the ones for the overall system are satisfied. This idea will be used in solving the dynamic energy equation when the explicit (forward finite difference) method is used.

2. Mathematical modelling

2.1. Correct of mass balance equation

The prediction of air flow in ventilated rooms is based on the solution of the general transport equation:

$$\frac{\partial}{\partial t}(\rho\Phi)+\operatorname{div}(\rho\mathbf{V}\Phi)=\operatorname{div}[\Gamma_\Phi \operatorname{grad}(\Phi)]+S_\Phi \tag{1}$$

where Φ, Γ_Φ and S_Φ (for the k–ε model) are given in Table 1 [4].

According to Peng et al. [5], the dynamic model of temperature distribution is mathematically expressed by the thermal energy balance:

$$\frac{\partial}{\partial t}(\rho\theta)+\operatorname{div}(\rho\mathbf{V}\theta)=\operatorname{div}(\Gamma \operatorname{grad}(\theta))+S_\theta \tag{2}$$

with the following assumptions:
constant density:

$$\frac{\partial}{\partial t}\rho=0;\quad \frac{\partial}{\partial x}\rho=0;\quad \frac{\partial}{\partial y}\rho=0;\quad \frac{\partial}{\partial z}\rho=0; \tag{3}$$

static velocity field:

$$\frac{\partial}{\partial t}\mathbf{V}=0 \tag{4}$$

2.2. Continuity equation in steady-state for continuous- and discrete-space systems

Computational fluid dynamics (CFD) computer programs solve numerically the set of transport eqns (1), evaluating the flow field. The problem is that the computed velocity field does not satisfy the continuity equation.

A steady-state solution in a discrete space is usually given by CFD programs. The dependent variables Φ (see Table 1) are evaluated at the grid nodes (a typical grid is shown in Fig. 1). This discretization method is known as 'finite volume' method. The grid node convention, presented in Fig. 2, is used to derive the equivalent discretization of eqn (2). The grey area represents the 'control volume' which, for a three-dimensional space, has the faces denoted by e, w, h, l, n and s for east, west, high, low, north and south faces, respectively. For a two-

Table 1
Dependent variables, effective diffusion coefficients and source terms in the general transport equation [4]

Equation	Φ	Γ_Φ	S_Φ
Continuity	1	0	0
u Momentum	u	μ_e	$-\frac{\partial p}{\partial x}+\frac{\partial}{\partial x}\left(\mu_e\frac{\partial u}{\partial x}\right)+\frac{\partial}{\partial y}\left(\mu_e\frac{\partial v}{\partial x}\right)+\frac{\partial}{\partial z}\left(\mu_e\frac{\partial w}{\partial x}\right)$
v Momentum	v	μ_e	$-\frac{\partial p}{\partial y}+\frac{\partial}{\partial x}\left(\mu_e\frac{\partial u}{\partial y}\right)+\frac{\partial}{\partial y}\left(\mu_e\frac{\partial v}{\partial y}\right)+\frac{\partial}{\partial z}\left(\mu_e\frac{\partial w}{\partial y}\right)-g(\rho-\rho_0)$
w Momentum	w	μ_e	$-\frac{\partial p}{\partial z}+\frac{\partial}{\partial x}\left(\mu_e\frac{\partial u}{\partial z}\right)+\frac{\partial}{\partial y}\left(\mu_e\frac{\partial v}{\partial z}\right)+\frac{\partial}{\partial z}\left(\mu_e\frac{\partial w}{\partial z}\right)$
Temperature	θ	Γ_e	q/C_p
Kinetic energy	k	Γ_k	$G_s-\rho\varepsilon+G_B$
Dissipation rate	ε	Γ_ε	$C_1\frac{\varepsilon}{k}(G_S+G_B)-C_2\rho\frac{\varepsilon^2}{k}$

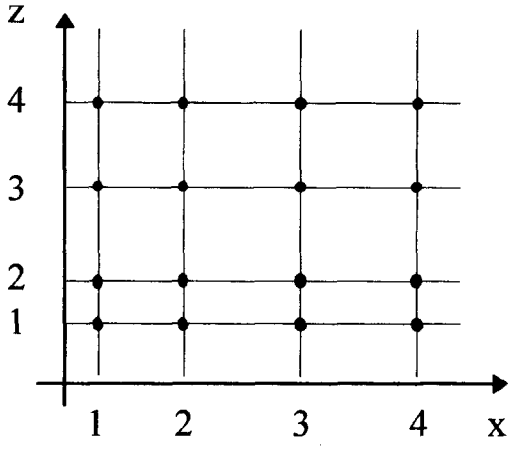

Fig. 1. Grid generation for the two-dimensional numerical simulation.

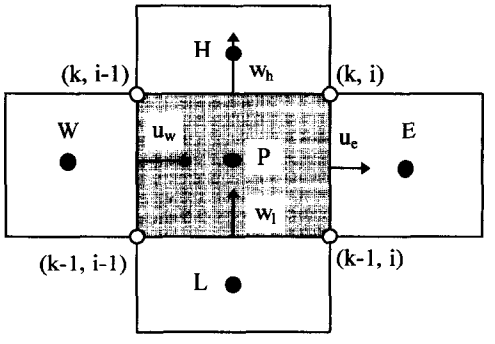

Fig. 2. The control volume for a two-dimensional cell.

dimensional space, the faces are denoted by e, w, h, and l. Integrating eqn (2) over the control volume, it becomes:

$$\frac{\partial}{\partial t}(\rho\theta) = -\frac{(\rho u\theta)_e-(\rho u\theta)_w}{\Delta x} - \frac{(\rho v\theta)_n-(\rho v\theta)_s}{\Delta y} - \frac{(\rho w\theta)_h-(\rho w\theta)_l}{\Delta z} + \frac{\left(\Gamma\frac{\partial\theta}{\partial x}\right)_e-\left(\Gamma\frac{\partial\theta}{\partial x}\right)_w}{\Delta x} + \frac{\left(\Gamma\frac{\partial\theta}{\partial y}\right)_n-\left(\Gamma\frac{\partial\theta}{\partial y}\right)_s}{\Delta y} + \frac{\left(\Gamma\frac{\partial\theta}{\partial z}\right)_h-\left(\Gamma\frac{\partial\theta}{\partial z}\right)_l}{\Delta z} + S_\theta \quad (5)$$

Let us call 'discrete divergence' the form derived by integrating the differential equation over the control volume shown in Fig. 2. Then, the discrete divergence of the velocity field, as calculated by CFD codes for steady-state conditions, may be not identically null when the continuous divergence of the velocity field is null. This may be due to:

- Insufficient convergence achieved by the applied iterative procedure. More iterations will decrease the value of discrete divergence.
- Error introduced by discretization. Since the velocity is a non-linear function with respect to space co-ordinate, the difference between the divergence and its numerical approximation is present in the most of the cases.

We will prove that the discrete divergence may be not identically null, when the continuous divergence is null, i.e. $\exists(i,j,k)$ so that:

$$\operatorname{div} d(\mathbf{V}_{ijk}) \equiv \frac{u_e-u_w}{\Delta x} + \frac{v_n-v_s}{\Delta y} + \frac{w_h-w_l}{\Delta z} \neq 0 \quad (6)$$

when $\operatorname{div}(\mathbf{V}) = 0$.

If the velocity function is not linear, then it is possible for the derivative in point P′ and the finite difference in point P to be different (see Fig. 3):

$$\frac{\partial}{\partial x}u \neq \frac{u_e-u_w}{\Delta x};\quad \frac{\partial}{\partial y}v \neq \frac{v_n-v_s}{\Delta y};\quad \frac{\partial}{\partial z}w \neq \frac{w_h-w_l}{\Delta z}; \quad (7)$$

and consequently the divergence may differ its discrete form.

But, when continuous-time discrete-space steady flow models are considered, the conservation of mass must be satisfied for each elementary cell volume, that is:

$$\forall(i,j,k)\ \operatorname{div} d(\mathbf{V}_{ijk}) = 0 \quad (8)$$

2.3. Correction of discrete continuity equation

The space discretization introduces an error in the mass balance equation. This error should be corrected so that the continuity equation is also satisfied in discrete space [6].

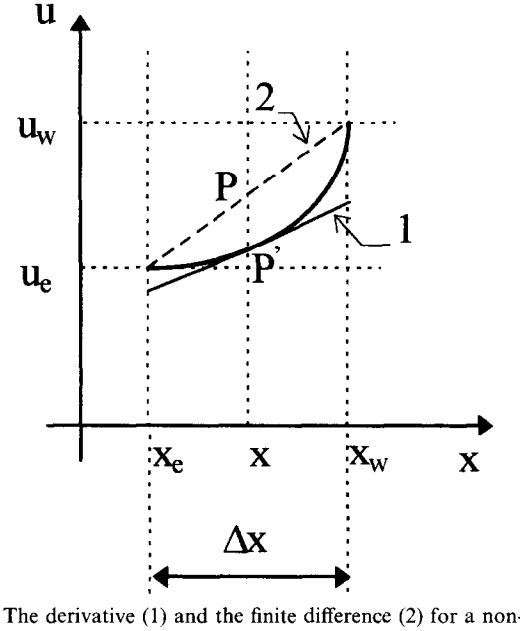

Fig. 3. The derivative (1) and the finite difference (2) for a non-linear velocity function.

The continuity equation in discrete form, for a three-dimensional space, without internal mass sources:

$$\rho\Delta y\Delta z(u_e-u_w)+\rho\Delta x\Delta z(v_n-v_s)+\rho\Delta x\Delta y(w_h-w_l)=0 \tag{9}$$

will be considered as the continuity equation (or mass balance equation) for the discrete-space. To simplify the presentation, let us assume a two-dimensional space (x, z), which is the vertical plane. In this space, the unbalanced mass of a cell is compensated in order to have the continuity equation satisfied for a continuous-time discrete-space steady flow model. This compensation is achieved by considering for each cell a flow in a third fictitious direction, y, resulting a three-dimensional space (x, y, z) that will correspond to the two-dimensional space (x, z). For the mathematical calculation convenience, the dimension of the cell in the fictitious direction is taken equal with 1:

$$\Delta y = 1 \tag{10}$$

By noting:

$$\Delta v \equiv v_s - v_n \tag{11}$$

eqn (9) becomes:

$$\rho\Delta z(u_e-u_w)+\rho\Delta x(w_h-w_l)=\rho\Delta x\Delta z\Delta v \tag{12}$$

For the cell denoted by indices (i, k), the above equation may be written as:

$$\rho\Delta z_k(u_{k,i-1}-u_{k,i})+\rho\Delta x_i(w_{k-1,i}-w_{k,i})=\rho\Delta x_i\Delta z_k\Delta v_{k,i} \tag{13}$$

where: $\rho\Delta x_i\Delta z_k\Delta v_{k,i}$ represents the mass algebraically added to cell (i, k) in order to correct the mass balance equation. Let us demonstrate that the algebraic sum of the mass added to each cell is null for overall system. That is:

$$\sum_{i=1}^{l}\sum_{k=1}^{n}\Delta x_i\Delta z_k\Delta v_{k,i}=\sum_{i=1}^{l}\sum_{k=1}^{n}[\Delta z_k(u_{k,i-1}-u_{k,i}) +\Delta x_i(w_{k-1,i}-w_{k,i})]=0 \tag{14}$$

By convention, for the overall system, the flow which enters in through the boundaries is denoted by indices '0' and the flow which goes out through the boundaries is denoted by indices 'l' and 'n' for x- and z-directions, respectively (Fig. 4).

In steady state, the conservation of mass for the whole system states that the flow of mass which enters in and goes out through the whole system boundaries is balanced, that is:

$$\sum_{i=1}^{l}\Delta x_i(w_{0i}-w_{ni})+\sum_{k=1}^{n}\Delta z_k(u_{k0}-u_{k1})=0 \tag{15}$$

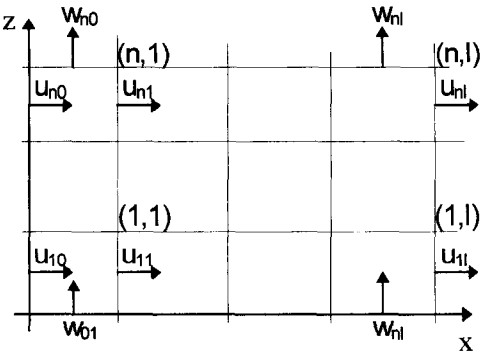

Fig. 4. Conventional notation of the velocity components in a two-dimensional grid.

The mass flow from one cell to another is added when the velocity is towards the cell and subtracted when the velocity is away from the cell. For internal boundaries of the cells, the total sum of the flow will be null, since the flow is added to a cell and subtracted from a neighbouring cell (Fig. 4). With eqn (15), eqn (14) becomes:

$$\sum_{k=1}^{n}\left[\Delta z_k\left(\sum_{i=0}^{l-1}u_{ki}-\sum_{i=1}^{l}u_{ki}\right)\right]+\sum_{i=1}^{1}\left[\Delta x_i\left(\sum_{k=0}^{n-1}w_{ki}-\sum_{k=1}^{n}w_{ki}\right)\right] =\sum_{k=1}^{n}\left[\Delta z_k\left(u_{k0}+\sum_{i=0}^{l-1}u_{ki}-\sum_{i=0}^{l-1}u_{ki}-u_{kl}\right)\right] +\sum_{i=1}^{1}\left[\Delta x_i\left(w_{0i}+\sum_{k=1}^{n-1}w_{ki}-\sum_{k=1}^{n-1}w_{ki}-w_{ni}\right)\right]=0 \tag{16}$$

The mass correction affects the other transport equations in which mass is involved.

2.4. Correction of energy balance equation

The correction introduced in the continuity equation will be reflected by a term in the energy equation. This correction term is related to the energy transported by the corrected mass. In the three-dimensional discrete space (x, y, z), the conservation of mass for a cell states that:

$$\operatorname{div} d(\mathbf{V})\equiv\frac{u_e-u_w}{\Delta x}+\frac{v_n-v_s}{\Delta y}+\frac{w_h-w_l}{\Delta z}=0 \tag{17}$$

Since the correction may be seen as a flow on only one surface in the fictitious direction, then:

$$v_s=0\Rightarrow v_s-v_n\equiv\Delta v=-v_n \tag{18}$$

and considering the temperature in the fictitious direction to have the same value as the one in the control volume, then the temperature on this surface is the temperature of the cell centre (point P in Fig. 2), and

$$\frac{(\rho v\theta)_n-(\rho v\theta)_s}{\Delta y}=\frac{(\rho v\theta)_n}{\Delta y}=\rho\theta\frac{v_n}{\Delta y} \tag{19}$$

From eqn (17) results:

$$\frac{u_e-u_w}{\Delta x}+\frac{w_h-w_l}{\Delta z}=-\frac{v_n-v_s}{\Delta y}=-\frac{v_n}{\Delta y} \tag{20}$$

therefore the equation of energy balance becomes:

$$\rho\frac{\partial\theta}{\partial t}=-\rho\frac{(u\theta)_e-(u\theta)_w}{\Delta x}-\rho\frac{(w\theta)_h-(w\theta)_l}{\Delta z}+\frac{\left(\Gamma\frac{\partial\theta}{\partial x}\right)_e-\left(\Gamma\frac{\partial\theta}{\partial x}\right)_w}{\Delta x}+\frac{\left(\Gamma\frac{\partial\theta}{\partial z}\right)_h-\left(\Gamma\frac{\partial\theta}{\partial z}\right)_l}{\Delta z}+S_\theta+\rho\theta\left(\frac{u_e-u_w}{\Delta x}+\frac{w_h-w_l}{\Delta z}\right) \tag{21}$$

Equation (21) describes the dynamic behaviour of temperature in a two-dimensional discrete-space (x,z) in which the (continuous) divergence of velocities is null.

Equation (21) may be considered a general representation. The numerical integration method for this differential equation with respect to time and differencing scheme for discretization in space becomes a free choice. The finite difference equations presented by Patankar [2] and considered by Awbi [4] are obtained as a particular solution of eqn (21) by applying the upwind difference scheme for space and Euler implicit method for time numerical integration.

3. Numerical simulation

The discretization of eqn (21) requires the application of a finite difference scheme. From the set of differencing schemes that may be used only the upwind scheme will be given as an example. Applying a finite differential scheme, eqn (21) becomes an ordinary differential equation with respect to time. Numerical integration of this equation by using Euler implicit method yields the same equation as the one presented by Patankar [2], Awbi [4] and used by commercial CFD programs.

In the upwind difference scheme (or donor cell method), the values of θ at the control surface (i.e. w, e, l and h surfaces) are taken as the value of upstream node point:

$$\theta_e=\theta \quad \text{for } u_e>0 \quad \text{and} \quad \theta_e=\theta_E \quad \text{for } u_e<0 \tag{22}$$

and similarly for θ_w, θ_l and θ_h. Using notation $|[A]|$ to denote the greater of A and 0, the first and the second term of eqn (21) may be written as:

$$-\rho\left[\frac{(u\theta)_e-(u\theta)_w}{\Delta x}+\frac{(w\theta)_h-(w\theta)_l}{\Delta z}\right]=\left[\frac{1}{\Delta x}(|[u_w]|\theta_w-|[-u_w]|\theta-|[u_e]|\theta+|[-u_e]|\theta_E\right]+\rho\left[\frac{1}{\Delta z}(|[w_l]|\theta_L-|[-u_l]|\theta-|[u_h]|\theta+|[-u_h]|\theta_H\right] \tag{23}$$

The third and the fourth right-hand terms of eqn (21) may be written as:

$$\frac{\left(\Gamma\frac{\partial\theta}{\partial x}\right)_e-\left(\Gamma\frac{\partial\theta}{\partial x}\right)_w}{\Delta x}\cong\frac{1}{\Delta x}\left(\Gamma_e\frac{\theta_E-\theta}{\delta x_e}-\Gamma_w\frac{\theta-\theta_W}{\delta x_w}\right)$$

$$\frac{\left(\Gamma\frac{\partial\theta}{\partial z}\right)_h-\left(\Gamma\frac{\partial\theta}{\partial z}\right)_l}{\Delta z}\cong\frac{1}{\Delta z}\left(\Gamma_h\frac{\theta_H-\theta}{\delta z_h}-\Gamma_l\frac{\theta-\theta_L}{\delta z_l}\right) \tag{24}$$

With the notations:

$$a=-\frac{|[-u_w]|}{\Delta x}-\frac{|[u_e]|}{\Delta x}-\frac{|[-w_l]|}{\Delta z}-\frac{|[w_h]|}{\Delta z}+\frac{u_e-u_w}{\Delta x}+\frac{w_h-u_l}{\Delta z}-\frac{1}{\rho\Delta x}\left(\frac{\Gamma_e}{\delta x_e}\right)-\frac{1}{\rho\Delta x}\left(\frac{\Gamma_w}{\delta x_w}\right)-\frac{1}{\rho\Delta z}\left(\frac{\Gamma_h}{\delta z_h}\right)-\frac{1}{\rho\Delta z}\left(\frac{\Gamma_l}{\delta x_l}\right) \tag{25}$$

$$a_W=\frac{|[u_w]|}{\Delta x}+\frac{1}{\rho\Delta x}\frac{\Gamma_w}{(\delta x)_w} \tag{26}$$

$$a_E=\frac{|[-u_e]|}{\Delta x}+\frac{1}{\rho\Delta x}\frac{\Gamma_e}{(\delta x)_e} \tag{27}$$

$$a_L=\frac{|[u_l]|}{\Delta z}+\frac{1}{\rho\Delta z}\frac{\Gamma_l}{(\delta z)_l} \tag{28}$$

$$a_H=\frac{|[-u_h]|}{\Delta z}+\frac{1}{\rho\Delta z}\frac{\Gamma_h}{(\delta z)_h} \tag{29}$$

eqn (21) may be written:

$$\frac{d}{dt}\theta=a\theta+a_W\theta_W+a_E\theta_E+a_L\theta_L+a_H\theta_H \tag{30}$$

or, if there are internal sources, S, eqn (21) becomes:

$$\frac{d}{dt}\theta=a\theta+a_W\theta_W+a_E\theta_E+a_L\theta_L+a_H\theta_H+\frac{S}{\rho} \tag{31}$$

It is easy to observe that:

$$a = a_W + a_E + a_L + a_H \tag{32}$$

or the rule of coefficients mentioned by Patankar [2] is respected.

If the Euler implicit method is used to integrate numerically eqn (31), then:

$$\frac{\theta - \theta^\circ}{\Delta t} \cong \frac{d}{dt}\theta = a\theta + a_W\theta_W + a_E\theta_E + a_L\theta_L + a_H\theta_H + \frac{S}{\rho} \tag{33}$$

where $\theta \equiv \theta(t)$ and $\theta^\circ \equiv \theta(t-\Delta t)$. Then eqn (33) may be written as:

$$\left(\frac{1}{\Delta t} - a\right)\theta = a_W\theta_W + a_E\theta_E + a_L\theta_L + a_H\theta_H + \frac{S}{\rho} + \frac{\theta^\circ}{\Delta t} \tag{34}$$

Writing the source term as $S = S_C + S_P\theta$ and multiplying eqn (34) by $\rho\Delta x\Delta y$ it becomes exactly the same as the final finite difference equation presented by Patankar [2] and widely used in CFD programs:

$$a'\theta = a'_W\theta_W + a'_E\theta_E + a'_L\theta_L + a'_H\theta_H + b' \tag{35}$$

with:

$$a'_W = \rho\,\Delta x\,\Delta z\,a_W; \quad a'_E = \rho\,\Delta x\,\Delta z\,a_E;$$
$$a'_L = \rho\,\Delta x\,\Delta z\,a_L; \quad a'_H = \rho\,\Delta x\,\Delta z\,a_H; \tag{36}$$

$$b' = S_C\Delta x\Delta z + a'^\circ\theta^\circ; \quad \text{with } a'^\circ = \frac{\rho^\circ\Delta x\Delta z}{\Delta t} \tag{37}$$

$$a' = a'_W + a'_E + a'_L + a'_H + a'^\circ - S_P\Delta x\Delta z \tag{38}$$

The energy eqn (31) is implemented in MATLAB, having the flow field given as computed by CFD software PHOENICS. As the numerical integration method is a free choice, any method available in MATLAB can be used. The details regarding the implementation are given by Ghiaus et al. [7]. Figure 5 presents a sequence of temperature distribution as obtained by the model. The number of nodes for the numerical grid generation is 24 (in x-axis) by 24 (in y-axis). The velocity field is fixed during the simulation of temperature distribution. The implementation is achieved in MATLAB and can be run on the same platforms as MATLAB (Windows or Unix). On a Windows platform (Pentium 133 MHz) the numerical simulation time is approximately 5 s for a process that lasts in reality 60 s.

4. Experimental facility and results

In order to validate the mathematical model, experiments were performed in a test-cell, located at Delft University of Technology, 52°N and 4°6′E. The cell room has internal dimensions of 3.2 × 3.9 × 2.68 (m) and exter-

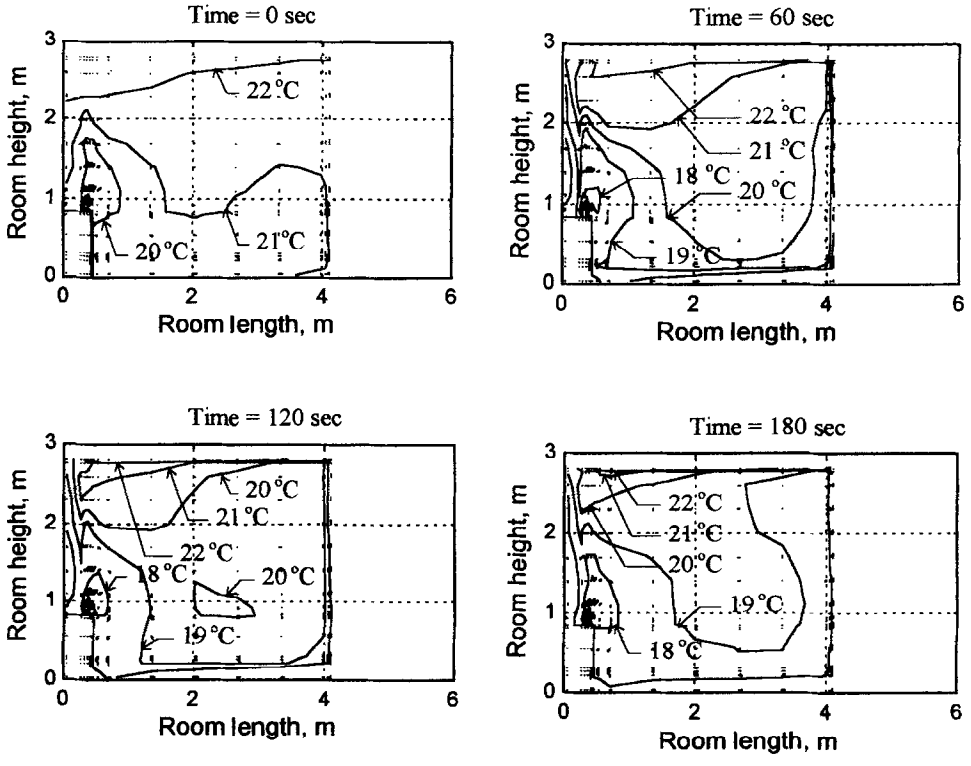

Fig. 5. Room temperature distribution numerically simulated with a sample time-step of 60 s.

Table 2
Specifications of the materials used for the roof, walls and floor

Layer type	Thickness [mm]	Conductivity [W m^{-1} K^{-1}]	Density [kg m^{-3}]	Heat capacity [J kg^{-1} K^{-1}]
Roof and walls:				
Steel	0.6	52	7800	500
Polystyrene	148	0.034	20	1300
Floor:				
Carpet	5	0.06	160	2500
Aluminium	2.5	200	2800	880
Plywood	18	0.17	700	1880
Polystyrene	150	0.034	20	1300

nal ones of $3.4 \times 4.2 \times 3.0$ (m). The room window (3.1×1.9 m^2), with the glazing global heat transfer coefficient of 2.7 W m^{-2} K^{-1}, has the azimuth 30°E. The roof and the walls are constructed from light-weight sandwich plates, (polystyrene with steel plate layers on both sides) having the heat transfer coefficient equal to 2.7 W m^{-2} K^{-1} and the floor is made of polystyrene, plywood, aluminium and carpet on top. The global heat transfer coefficient of the floor is 1.9 W m^{-2} K^{-1}. The specifications of the above materials are given in Table 2. The temperature was measured at points on a nine-node grid, symmetrically distributed in a perpendicular plane on the window surface. A fan-coil, installed under the window introduces, by means of two separate coils, cool or warm air for cooling or heating, respectively. The operation characteristics of the fan-coil are given in Table 3. The simulation results were compared with the experimental ones, both in time and in frequency domain. A comparison of a step response at the start-up (in the morning) is shown in Fig. 6. The model gives a good response at the beginning, but, because the simulated wall temperature was assumed to be constant, in the last part of the response the influence of the actual variable wall temperature can be observed. However, from the point of view of controlling the temperature it is more important to consider a frequency response comparison. Using the tools of control theory, the frequency response (Bode diagrams) can be easily achieved. To obtain the frequency response, the inlet air temperature was varied according to a function obtained as a sum of sine waves of different frequency, which are typical for normal operation of a fan-coil. The comparison for a point in the occupied zone is given in Fig. 7. The response was achieved by varying the inlet temperature of the air so that the frequencies contained in the signal covered the domain of interest for control purposes.

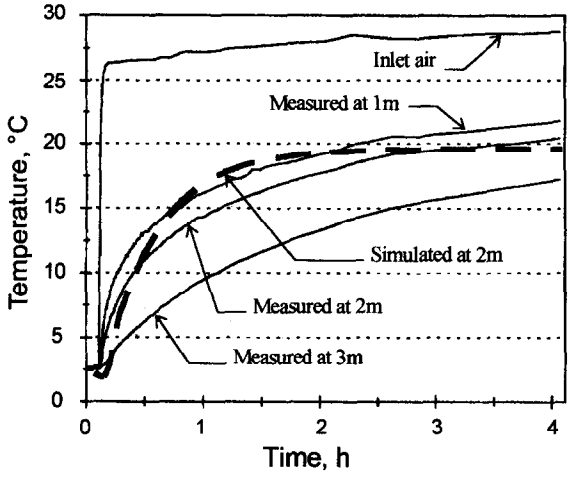

Fig. 6. Mean temperature step response simulated and measured in several horizontal planes.

Table 3
Operation characteristics of the fan-coil

Fan-coil characteristics	Low speed	Medium speed	High speed
Air volume flow rate [m^3 h^{-1}]	225	330	600
Heating power at 90/70°C [kW]	2	3	4
Cooling power at 6/12°C [kW]	1	1.2	2

5. Conclusions

The discretization of the continuity equation introduces an error due to non-linear velocity field. The method presented corrects the continuity and energy equations for discrete space models. The correction term may be seen either as a flow in a fictitious direction or as a source of mass, so that:

- If the correction term is positive, it means that there was a removal of mass from the elementary cell and some mass should be added to compensate.

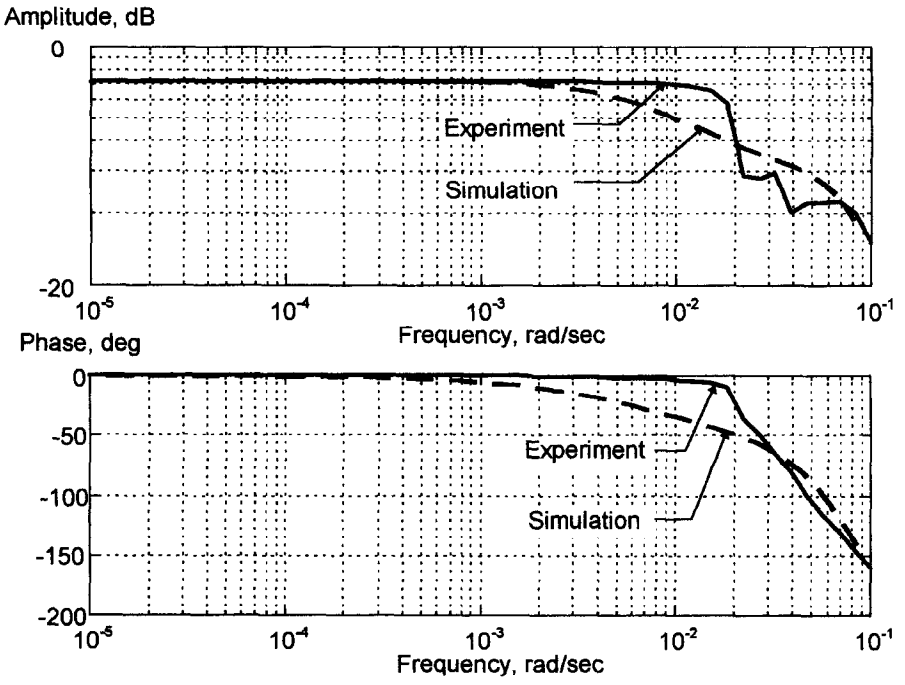

Fig. 7. Comparison between simulation and experimental results in frequency domain for a point in the occupied zone.

- If the correction term is negative, it means that there was an addition of mass to the elementary cell and some mass should be removed to compensate.

A remark should be made: accepting that the stationary velocity field is correct, that is the divergence of velocities is null, it is possible that the conservation of mass will not be respected for some elementary cells of the discrete space system. However, since the model is in discrete space from, the conservation of mass should be respected for each elementary cell. The mass conservation law in steady state for constant density, continuous space systems is:

$$\frac{\partial}{\partial x}u+\frac{\partial}{\partial y}v+\frac{\partial}{\partial z}w=0 \tag{39}$$

and for constant density, discrete space systems is:

$$\frac{u_e-u_w}{\Delta x}+\frac{v_n-v_s}{\Delta y}+\frac{w_h-w_l}{\Delta z}=0 \tag{40}$$

Accepting eqn (39) to be true means that eqn (40) does not necessarily stand for each cell. In fact, eqn (39) should be satisfied for continuous systems. Reciprocally, accepting eqn (40) to be true means that eqn (39) does not necessarily stand for each point in the continuous system. However, eqn (40) should be satisfied in a discrete space system. However, the mass conservation law should be respected in the system, whether it is described in continuous or discrete form. In fact, accepting that the velocity field is correct, then eqn (39) stands and a correction is introduced to have the mass conservation respected also in each elementary cell. Since the conservation of mass should be respected also in the system as a whole, if the velocity field is correct, the total algebraic sum of mass exchanged in the fictitious direction should equal zero.

The corrected dynamic model of temperature may be integrated using any numerical integration method (e.g. Euler implicit or explicit, Runge–Kutta, Adams or Gear). As these integration methods use variable time steps, the time efficiency of these methods is very good. In literature, the energy differential equation is discretized using implicit method. When the flow field is changed, a set of algebraic equations is to be solved in one step (by inverting the matrix of coefficients) or by iteration (an initial guess followed by an iterative calculation). The inverse of the matrix and the iterative procedure are far more time consuming than integrating with an explicit method with variable time step (for a standard size room about 10^3–10^5 times faster).

Acknowledgements

The experimental measurements were carried out at Laboratory of Refrigerating Engineering and Indoor Climate Technology, Deft University of Technology, The Netherlands, X. Peng and A.H.C. van Paassen, from the same laboratory, provided the flow field calculations.

References

[1] Fanger PO. Thermal comfort. Malabar (Florida): Robert E. Krieger Publishing Company, 1982.
[2] Patankar V. Numerical heat transfer and fluid flow. New York: McGraw–Hill Inc., 1980.
[3] Chen Q. Indoor airflow, air quality and energy consumption of buildings. Ph.D. thesis, Delft University of Technology, Delft, 1988.
[4] Awbi HB. Ventilation of buildings. E and FN Spon, 1991.
[5] Peng X, van Paassen AHC, Chen Q. A type of calculation of indoor dynamic temperature distribution. Proceedings of System Simulation of Buildings Conference, Liege, 1994.
[6] Ghiaus C. Numeric and expert control of air conditioning installations. Ph.D. thesis, Technical University of Civil Engineering, Bucharest, 1996.
[7] Ghiaus C, Peng X, van Paassen AHC. A state-space representation of the dynamic model of air temperature distribution. Proceedings of 19th International Congress of Refrigeration, The Hague, 1995.

Clădiri inteligente (I) - Mediul urban, energia şi clădirile

Smart buildings (I) - Urban environment, energy and buildings

Cristian Ghiauş, conferenţiar dr.-ing., Universitatea Tehnică de Construcţii Bucureşti, inginer-cercetător, Universitatea La Rochelle, LEPTAB, Franţa, (Université de La Rochelle, LEPTAB), e-mail: cristian.ghiaus@univ-lr.fr
Adrian-Gabriel Ghiauş, şef de lucrări dr.-ing., Universitatea Tehnică de Construcţii Bucureşti, Facultatea de Instalaţii, (Technical University of Civil Engineering - Bucharest, Faculty of Building Services and Equipment), e-mail: ghiaus@mech.upatras.gr

1. Introducere

În orice ţară din lume, spatiul amenajat constituie în mod normal mai mult de jumătate din totalul investiţiei de capital naţional iar construcţiile reprezintă nu mai puţin de 10 % din PIB [1]. Consumurile de energie definesc calitatea vieţii urbane şi calitatea globală a mediului înconjurător din oraşe. Energia este corelată cu toate aspectele dezvoltării şi are un impact imens asupra bunăstării locuitorilor urbei, a sănătăţii, educaţiei, productivităţii, oportunităţilor economice, etc. Din păcate, situaţia actuală legată de producerea şi consumul de energie este extrem de injustă, existând largi deosebiri între lumea dezvoltată şi cea în curs de dezvoltare. Aproape un sfert din populaţia globului nu are acces la electricitate, în timp ce al doilea sfert are un acces sărac [2]. Cu toate că 75 de milioane de oameni obţin anual accesul la electricitate, numărul total al celor care duc lipsa acesteia nu se schimbă [3]. Caracteristic este faptul că partea bogată a lumii consumă aproape de 25 de ori mai multă energie pe persoană decât partea săracă [3].
Energia este cel mai important motor pentru a ridica calitatea vieţii şi a lupta împotriva sărăciei. Considerând că în 2020 aproape 70 % din populaţia globului va locui în oraşe iar 60 % va fi sub pragul sărăciei, se estimează de către Banca Mondială [4] că mulţi dintre aceştia vor fi săraci în energie. Astfel, în următoarele decenii, noi capacităţi cu puteri instalate de mii de megawaţi, trebuiesc realizate.
Estimările arată că, în următorii 30 de ani, costurile pentru noile generatoare de energie vor însuma peste 2 mii de miliarde de dolari americani [4]. Cu toate acestea, tările în curs de dezvoltare plătesc deja prea mult pentru energie. Locuitorii acestor ţări cheltuiesc 12 % din venituri pentru energie, de cinci ori mai mult decât media ţărilor OECD [1].

1. Introduction

In every country in the world, the built environment normally constitutes more than half of the total national capital investment and construction represents as much as 10% of GNP [1]. Energy consumption defines the quality of urban life and the global environmental quality of cities. Energy is linked with all aspects of development and has a tremendous impact on the well being of urban citizens, health, education, productivity, economic opportunities, etc. Unfortunately, the current situation on energy supply and consumption is extremely unfair and wide disparities exist between the developed and the developing world. Almost one third of the world's population has no access to electricity while the second third has very poor access [2]. Although 75 million people gain annually access to electricity, the total number of people lacking electricity does not change [3]. It is characteristic that the reach part of the world consumes almost 25 times as much energy per person as the poorest people [3].
Energy is the most important engine to improve the quality of life and fight poverty. Given that by 2020 almost 70 % of the world population will be living in cities and 60% will be below poverty, it is estimated by the World Bank [4] that many of those will be energy - poor. Thus, for the next decades, thousands of megawatts of new electrical capacity have to be added.

Estimates show that the cost of the new power generation plants over the next 30 years will amount over 2 trillion USD [4]. However, developing countries pay already too much for energy.
Citizens in these countries spend 12 % of their income for energy services, i.e. five times more than the average in OECD countries [1].

În paralel, importurile de energie reprezintă una dintre sursele majore ale datoriilor externe. Aşa cum a fost prezentat în raportul summitului de la Johannesburg, "în peste 30 de ţări, importurile de energie depăşesc cu 10 procente valoarea întregului export" în timp ce "în aproximativ 20 de ţări, cheltuielile pentru importurile de petrol le depăşesc pe cele pentru servicii" [5].
Astfel, este evident că trebuiesc utilizate surse alternative de energie. Utilizarea surselor noi în combinaţie cu tehnologii energetice eficiente, poate furniza energia necesară pentru două treimi din populaţie în vederea îmbunătăţirii calităţii vieţii şi poate contribui esenţial la scăderea consumurilor de resurse în ţările dezvoltate. Un studiu efectuat de Laboratorul Lawrence Berkeley [6] arată că ţările în curs de dezvoltare pot evita cheltuirea a 1700 miliarde USD pentru rafinarea petrolului, mine de cărbune şi noi centrale electrice prin cheltuirea, în următorii 30 de ani, a 10 miliarde USD anual pentru îmbunătăţirea eficienţei şi conservării energiei [6]. O altă estimare, făcută de US Office of Technology Assessment, arată că ţările în curs de dezvoltare ar putea reduce la jumătate producţia lor de electricitate dacă energia ar fi utilizată mai eficient.

2. Impactul sectorului de construcţii

Domeniul construcţiilor este pe departe unul dintre cele mai importante sectoare economice. Se estimează că producţia mondială anuală în construcţii se apropie de 3 mii de miliarde USD şi constituie aproape o zecime din economia mondialã [7]. Aproape 30 % din capital este din Europa, 22 % din Statele Unite, 21 % din Japonia, 23 % din ţările în curs de dezvoltare şi 4 % din restul ţărilor dezvoltate.
Construcţiile reprezintă mai mult de 50 % din investiţia de capital naţional şi, pentru cei peste 111 milioane de angajaţi, ele reprezintă aproape 7 % din forţa de muncă şi 28 % din numărul global al angajaţilor industriali. Cu toate aceste, având în vedere că fiecare loc de muncă din sectorul de construcţii generează două noi locuri de muncă în economia mondială, se poate spune că sectorul de construcţii este în mod direct sau indirect corelat cu aproape 20 % din numărul global al angajaţilor [7].

In parallel, energy imports are one of the major sources of foreign debt. As reported during the Johannesburg summit "in over 30 countries, energy imports exceed 10 percent of the value of all exports," while "in about 20 countries, payments for oil imports exceed those for debt servicing" [5].

It is thus evident that alternative energy patterns have to be used. The use of renewable sources, in combination with energy efficient technologies, can provide the necessary energy supply to the two thirds of the world's population to improve their quality of life and can contribute highly to decrease over-consumption of resources in the developed countries. A study by Lawrence Berkeley Laboratory [6], shows that developing countries may avoid spending 1.7 trillion USD on oil refineries, coal mines and new power plants by spending, for the next 30 years, 10 billion USD annually to improve energy efficiency and conservation [6]. Other estimate by the US Office of Technology Assessment shows that developing counties could have the potential to half their electricity production if energy is used more effective.

2. The impact of the construction sector

Construction is by far one of the most important economic sectors. It is estimated that the total world annual output of construction is close to 3000 billions USD and constitutes almost one tenth of the global economy [7]. About 30 % of this capital is from Europe, 22 % from the United States, 21 % from Japan, 23 % from developing countries and 4 % from the rest of the developed countries.
Construction represents more than the 50 % of the national capital investment and, with more than 111 million of employees, it accounts for almost the 7 % of the total employment and 28 % of the global industrial employment. However, given that every job in the construction sector generates two new jobs in the global economy, it can be said that the construction sector is directly or indirectly linked to almost 20 % of the global employment [7].

În paralel, aproape o şesime din resursele mondiale majore sunt consumate în sectorul de construcţii [8]. Clădirile consumă aproape 40 % din energia mondială, 16 % din apa proaspătă mondială şi 25 % din lemnul de pădure, şi emit în atmosferă aproape 70 % din oxidul de sulf şi 50 % din bioxidul de carbon.

În Europa, circa 30 % din energie este consumată în clădiri, o mare cantitate fiind utilizată pentru încălzire (Fig. 1a). Sursa de energie primară principală este cea fosilă (cărbune, petrol şi gaz), cu o pondere redusă de surse nucleare şi neconvenţionale (Fig. 1b). Consumurile de energie cresc în mod constant în Uniunea Europeană şi se estimează că în 2020 importurile de energie vor depăşi producţia. Două soluţii importante există: dezvoltarea producţiei şi controlul cererii.

Dezvoltarea surselor neconvenţionale este împiedicată de aspecte financiare şi structurale. Deşi preţul energiei obţinute din surse neconvenţionale a scăzut considerabil şi se aşteaptă să scadă în continuare (Fig. 2b), va fi cu 50 % mai scumpă decât electricitatea generată de arzătoarele de gaz [9]. Dezvoltarea viitoare a surselor neconvenţionale necesită eforturi financiare importante şi ajutor prin subvenţionare [9]. În plus, structura producţiei de energie este centralizată în jurul surselor convenţionale (cărbune, petrol şi gaze) şi a centralelor nucleare. Pe termen scurt şi mediu, combustibilii convenţionali se estimează că vor rămâne predominanţi pentru sursele de energie. Uşurinţa utilizării şi valoarea energetică ridicată a petrolului explică consumul mare în economia occidentală după cel de al doilea război mondial.

In parallel, almost one sixth of the world major resources are consumed by the construction sector [8]. Buildings consume almost 40 % of the world's energy, 16 % of the world's fresh water and 25 % of the forest timber, while it is responsible for almost 70 % of sulphur oxides and 50 % of the CO_2 emissions [8].

In Europe, about 30 % of energy is consumed in buildings, a large amount being used for heating (Fig. 1a). The main primary energy source is fossil (coal, oil and gas), with a small share of nuclear and renewable sources (Fig. 1b). The energy consumption increases constantly in European Union and it is estimated that by 2020 the import of energy will be larger than the production. Two important solutions are opened: development of energy production and demand management.

The development of renewable sources is hindered by financial and structural aspects. Although the price of energy obtained from renewable sources decreased considerably and it is expected to decrease further (Fig. 2b), it will be with 50 % more expensive than the electricity generated by gas burners [9]. Further development of renewable sources needs important financial efforts and aid by subsidies [9]. In addition, the structure of the energy production is centralized around conventional sources (coal, oil and gas) and nuclear plants. On short and medium term, it is estimated that the conventional fuels will remain predominant for the energy sources. The ease of use and the high energetic value of oil explains its extensive consumption in the western economies after the Second World War (Fig. 2a).

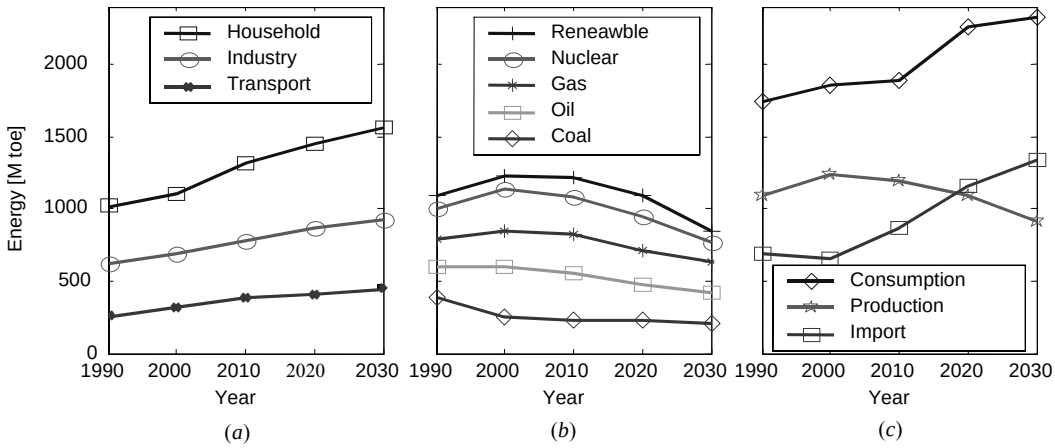

Fig. 1 Utilizarea energiei în Europa: a) Consumul de energie finală, b) Producţia de energie, c) Energia totală
Use of energy in Europe: a) Final energy consumption, b) Energy production, c) Total energy

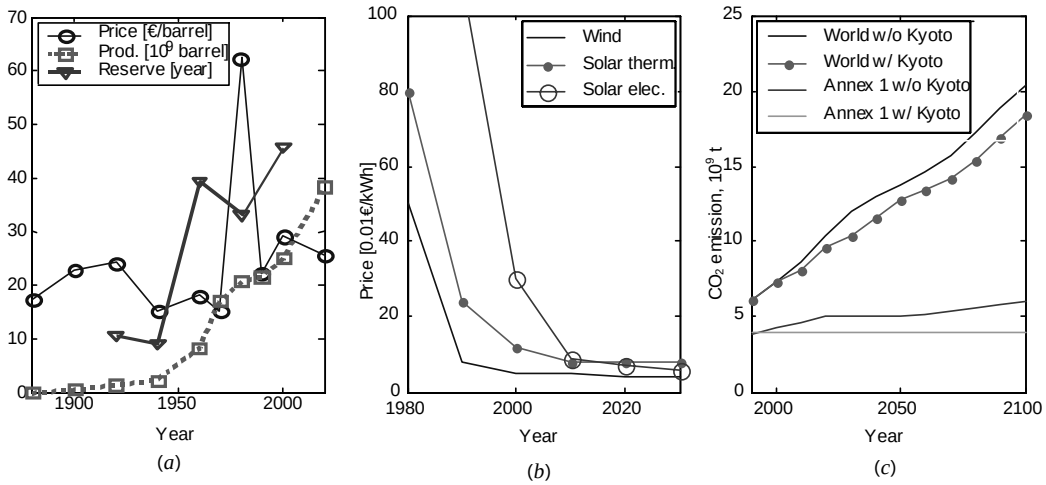

Fig. 2 Energia şi emisiile de CO_2: a) Prețul petrolului în dolari/br, producția de petrol în Mbr şi rezervele în ani, b) Prețul pe kWh pentru energia neconvențională, c) Emisiile de CO_2
Energy and CO_2 emissions: a) Oil price in dollar/barrel, oil production in Mbarrel and reserves in years, b) Price per kWh for renewable energy, c) CO_2 emissions

În ciuda creşterii exponențiale a producției şi consumului, rezervele cunoscute cresc şi ele exponențial. Pe de altă parte, prețul a crescut numai liniar, cu excepția crizei petrolului din anii '70, depăşind 20 USD/br după anul 2000 (Fig. 2a). Utilizarea intensivă a combustibilului fosil pare să aibă efecte asupra schimbărilor climatice datorită emisiilor gazelor de seră. Protocolul de la Kyoto urmăreşte să reducă emisiile de CO_2 ale țărilor dezvoltate care sunt specificate în Anexa 1 a protocolului. Dar, deoarece emisiile de CO_2 ale țărilor în curs de dezvoltare vor creşte considerabil în următoarele decenii, contribuția relativă a țărilor dezvoltate se va diminua (Fig. 2c). Datorită problemelor pe care le ridică dezvoltarea surselor, managementul cererii este considerat că rămâne singura cale pentru întrunirea cerințelor privind modificările climatice [9].

3. Eficiența energetică şi conservarea energiei în clădiri

Sectorul de construcții este considerat a fi o sursă majoră pentru economisirea energiei. În Europa, această reducere poate ajunge la cel puțin 20 % , ceea ce reprezintă 40 de milioane t/an sau echivalentul a 10 % din consumul de petrol şi 20 % din emisia de gaze de seră a anului 2000 [9]. Economiile de energie pot fi obținute prin creşterea eficienței produselor şi prin stoparea consumurilor.
Termenii "eficiența energetică" şi "conservarea energiei", folosiți câteodată ca echivalenți,

Despite the exponential growth in production and consumption, the known reserves increased also exponentially. Meantime, the price increased only linearly, save during the oil crises of the 70's, exceeding 20 USD/br after the year 2000 (Fig. 2a). The intensive use of fossil fuels seems to have effects on climate change due to greenhouse gas emissions. The Kyoto protocol aims to reduce CO_2 emissions of the developed countries which are specified in Annex 1 of the protocol. But since the CO_2 emissions of the developing countries will increase considerably in the next decades, the relative contribution of the developed countries will diminish (Fig. 2c). Due to the problems raised by the development of the supply, the demand management is considered to be the only way to meet the challenges of climate change [9].

3. Energy efficiency and energy conservation in buildings

The building sector is believed to be a major source for energy savings. In Europe, this reduction can be at least 20 % which will represent 40 million t/year or the equivalent of 10% of the oil consumption and 20 % of greenhouse gas emission of the year 2000 [9]. Energy savings may be obtained by increasing the efficiency of the products and by not consuming.
The terms “energy efficiency” and “energy conservation,” sometimes used interchangeably,

au conotații total diferite. În timp ce "eficiență" înseamnă a obține cât mai mult din fiecare joule, "conservarea" înseamnă a face fără. Eficiența energetică poate duce la conservare, dar poate deasemeni să incurajeze consumul [10]. Eficiența energetică pare a fi o măsură obiectivă deoarece este definită ca raportul dintre toate energiile de intrare şi energiile de ieşire utile. Dar acest concept distrage atenția de la sursele reale ale consumurilor de energie deoarece poate duce la concluzia că consevarea energiei ar putea fi mai degrabă o problemă tehnologică decât una comportamentală [10]. De exemplu, un sistem de aer condiționat poate fi mai eficient energetic decât altul, în timp ce o fereastră nu poate fi.

Eficiența energetică în clădiri este legată de productivitate. Productivitatea în birourile moderne poate fi definită în multe feluri, de la numărul colilor de hârtie completate într-o oră, la importanța ideilor create. Conceptul de productivitate este studiat în prezent prin activitatea mintală, cum ar fi atenția, vigilența, memoria, creativitatea, calculul mintal, înțelegerea, şi procese psihologice, ca motivația, perseverența, efortul [11]. Condițiile locului de muncă au o influența importantă asupra productivității în birouri (Fig. 3).

have quite different connotations. While “efficiency” means to get the most out of every joule, “conservation” means doing without. Energy efficiency may result in conservation but it may also encourage to consume [10]. Energy efficiency seems to be an objective measure because it is defined as the ratio of all energy input to that of useful energy output. But this concept draws attention from the real sources of energy consumption because it may lead to the conclusion that energy conservation should be entirely a technological problem rather a behavioral one [10]. For example, an air conditioning system may be more energy efficient than another, while a window will be not.

Energy efficiency in buildings is related to productivity. Productivity in modern offices may be defined in many ways, from number of paper sheets completed per hour, to importance of ideas generated. The concept of productivity is studied in present by mental activity, such as attention, vigilance, memory, creativity, mental computation, comprehension, and psychological processes, like motivation, persistence, effort [11]. Workplace conditions were found to have important influence in productivity in office buildings (Fig. 3).

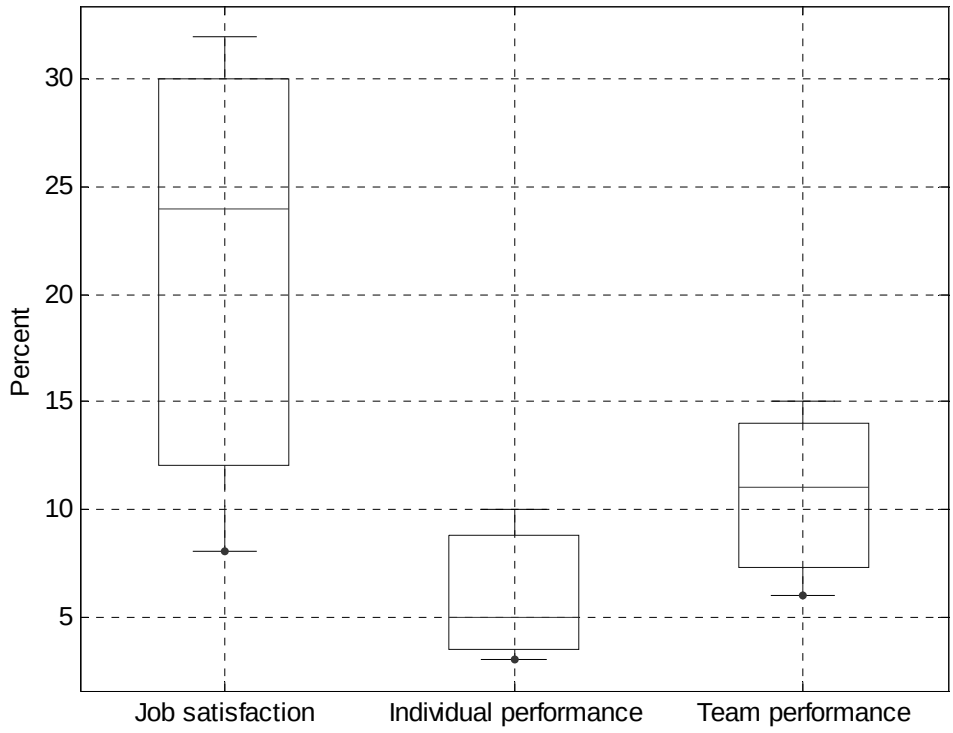

Fig. 3 Contribuția locului de muncă asupra productivității în clădirile de birouri
Contribution of workplace to productivity in office buildings

Bâtiments intelligents (I) L'environnement urbain, l'énergie et les bâtiments

Résumé

Dans le monde, le domaine du bâtiment constitue à peu prés la moitie de l'investissement de capital, 10 % du PNB, 1/6 des ressources naturelles consommées, et 7 % de l'emploi. En Europe, 1/3 de l'énergie est consommée par le secteur du bâtiment, la grande majorité pour le chauffage, mais des réductions de 20 % sont visées comme objectif par la Commission Européenne. La consommation de l'énergie dans le bâtiment représente moins de 5 % des coûts globaux dans les bâtiments tertiaires et le confort obtenu peut augmenter la productivité de 5 à 17 %. L'objectif des bâtiments intelligents est de consommer moins en s'adaptant activement aux conditions météorologiques et à l'usage.

Bibliografie
References

[1]. CICA: *Construction*, UK, Beacon Press, **2002**.

[2]. WEHAB: *A Framework for Action on Energy*, World Summit on Sustainable Development, WEHAB Working Group, **2002**.

[3]. ALBOUY, Y., NADIFI, N.: *Impact of Power Sector Reform on the Poor: A Review of Issues and the Literature,* Washington, D.C., World Bank, Energy, Mining, and Telecommunications Department, **1999**.

[4]. SERAGELDIM, R. B., BROWN, J. M.: *The Business of Sustainable Cities*, Environmentally Sustainable Development Proceedings, Series No 7, Washington, DC, The World Bank, **1995**.

[5]. SAGHIR, J.: *Multilateral Financing of Sustainable Energy*, The WSSD Summit. German Parallel Event on North-South Cooperation for a Sustainable Energy Future, German Stand, Ubuntu Village, Johannesburg, **2002**.

[6]. DER PETROSSIAN, B.: *Conflicts between the construction industry and the environment*, The 6th Sharjah Urban Planning Symposium, Habitat Debate, **1999**.

[7]. LEITMAN, J.: *Energy Environment Linkages in the Urban Sector*, UNDP, **1991**.

[8]. BITAN, A.: *The high climatic quality of city of the future,* Atmospheric Environment 26(8), pp. 313-329, **1992**.

[9]. EC: *Green Paper: Towards a European strategy for the security of energy supply*, European Communities, **2001**.

[10]. MOEZZI, M.: *The Predicament of Efficiency,* ACEEE, Summer Study on Energy Efficiency in Buildings, **1998**.

[11]. DILOUIE, G.: *Personal Control*, Boosting Productivity, Energy Savings, Lighting Controls Association, **2002**.

Clădiri inteligente (II) - Confortul termic în clădiri adaptive

Smart buildings (II) - Thermal comfort in adaptive buildings

Cristian Ghiauş, conferenţiar dr.-ing., Universitatea Tehnică de Construcţii Bucureşti, inginer-cercetător, Universitatea La Rochelle, LEPTAB, Franţa, (Université de La Rochelle, LEPTAB), e-mail: cristian.ghiaus@univ-lr.fr
Adrian-Gabriel Ghiauş, şef de lucrări dr.-ing., Universitatea Tehnică de Construcţii Bucureşti, Facultatea de Instalaţii, (Technical University of Civil Engineering - Bucharest, Faculty of Building Services and Equipment), e-mail: ghiaus@mech.upatras.gr

1. Avantajele clădirilor adaptive

Conceptul de clădiri adaptive se referă la acele clădiri care-şi modifică comportamentul în funcţie de condiţiile meteorologice şi de utilizatori. Acest concept include aspectul tehnologic al clădirilor care reacţionează la vreme şi comportamentul uman. Utilizarea forţelor naturale pentru a menţine confortul interior are avantajul evident al reducerii aproape de zero al consumului de combustibil fosil şi al emisiilor de gaze cu efect de seră. Utilizarea ventilării pentru răcire are un potenţial important în ţările europene. Se poate estima economia de energie necesară condiţionării aerului în cazul utilizării ventilării, presupunând că, datorită masei termice, diferenţa dintre temperatura exterioară şi cea interioară poate fi considerată ca medie zilnică. Dacă presupunem în continuare că valoarea medie zilnică a temperaturii în evoluţie liberă este cu aproximativ 5 °C mai mare decât temperatura medie exterioară, economia de energie realizată utilizând ventilaţia naturală în locul răcirii mecanice este între 70 % şi 100 %.
În analiza reducerilor consumurilor de energie în clădiri, trebuiesc luate în considerare cele două roluri ale clădirior: calitatea aerului interior şi confortul. Problemele de sănătate legate de poluarea aerului interior sunt diferite în ţările în curs de dezvoltate faţă de cele dezvoltate (Figura 1a) [1,2]. În ţările în curs de dezvoltate, numărul deceselor datorate poluării aerului interior este mai mare în mediul rural decât în cel urban, în timp ce situaţia este inversă în ţările dezvoltate. Confortul este un factor extrem de important, mai cu seamă în sectorul terţiar unde influenţează major productivitatea şi contribuie la imaginea organizaţiilor. Se estimează că în clădirile de birouri din occident, aproape 80 % din cheltuieli sunt costuri de personal şi 10 %

1. Benefits of adaptive buildings

The concept of adaptive buildings refers to buildings that change their behavior according to the weather conditions and to the users. This concept includes the technological aspect of weather responsive buildings and the human behavior. The use of natural forces for controlling the indoor comfort has the obvious advantage of reducing almost to zero the fossil fuel consumption and the greenhouse gases emissions. The use of ventilation for cooling has an important potential in European countries. We may estimate the energy savings for air-conditioning if ventilation is used instead by assuming that, due to the thermal mass, the differences between outdoor and indoor temperature may be considered as daily mean values. Then, if we assume that the daily mean value of the free running temperature is about 5 °C higher than the mean outdoor temperature, the percentage of energy saved for mechanical cooling by using ventilation is between 70 % and 100 %.

In the analysis of the potential reduction of energy consumption in buildings, the two roles of buildings should be considered: healthy indoor climate and comfort. Health problems related to indoor air pollution are different in the developing countries from the developed ones (Figure 1a) [1, 2]. In developing countries, the death toll due to indoor air pollution is higher in rural areas than in urban areas while the situation is reversed in developed countries. Comfort is a very important factor, especially in the tertiary sector where it highly influences the productivity and contributes to the image of the organizations. It is estimated that in office buildings in western countries, about 80 % of the expenses are personnel costs and about 10 % are costs related to the building (Figure 1b).

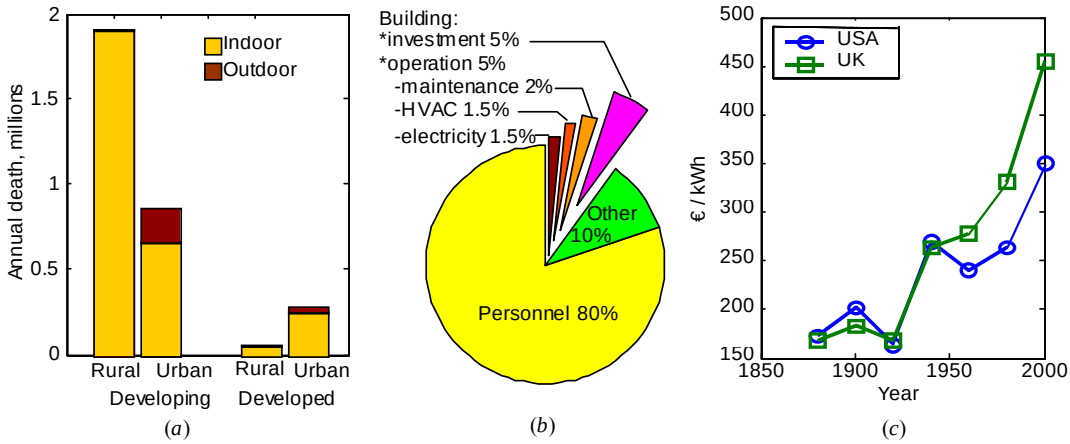

Fig. 1 Impactul socio-economic al energiei asupra clădirilor
Socio-economic impact of energy in buildings

costuri legate de clădire (Figura 1b). Mai puțin de 3 % din costuri sunt legate de consumurile de energie (Figura 1b) [3]. Prin urmare, nu se justifică economic reducerea consumurilor de energie în detrimentul confortului. De fapt, confortul contribuie la creşterea eficienței economice rezultând într-o mai bună utilizare a energiei (Figura 1c) [2]. Importanța confortului şi calității aerului interior şi influența lor asupra sănătății şi eficienței demonstrează că eficiența soluțiilor trebuie judecată global prin considerarea analizei costului pe întreaga durată a vieții sistemului şi a implicațiilor acestuia asupra eficienței.

2. Avantajele vegetației

Alături de rolul său estetic, vegetația are influențe asupra calității aerului, nivelului de zgomot şi microclimatului. Umbra copacilor reduce necesarul de răcire de la 2 % la 30 %, în funcție de climă şi de amplasarea copacilor [4]. Parcurile influențează microclimatul; de exemplu, în Mexico City şi Tokyo, parcuri de aproape 500 ha răcesc aerul cu 1,5–3 °C la o distanță de 1–2 km [5, 6]. Necesarul de electricitate creşte cu 2–4 % pentru fiecare grad Celsius suplimentar al atmosferei exterioare. Se estimează că 5–10 % din consumul de electricitate actuală pentru Los Angeles compensează creşterea temperaturii urbane de 0,3–3,0 °C [7].

3. Avantajele confortului la locul de muncă

Într-un sondaj efectuat în 2002, 79 % dintre cei 1500 directori de corporații, manageri şi proiectanți de profesie au fost de părere că un

Less than 3 % of the costs are related to energy consumption (Figure 1b) [3]. Therefore; it is not economically sound to reduce the energy consumption by affecting the comfort. In fact, comfort contributes to the constant economic efficiency growth resulting in a better use of energy (Figure 1c) [2]. The importance of the indoor air quality and comfort and their influence on health and efficiency demonstrate that the efficiency of the solutions should be judged globally by considering the whole life cost analysis of the system and its implications on efficiency.

2. Benefits of vegetation

Besides the esthetical role, vegetation influences air quality, noise level and the microclimate. The tree shadow reduces the cooling load from 2 % to 30 %, depending on climate and house-tree configuration [4]. The parks also influence the microclimate; parks of about 500 ha in Mexico City and Tokyo cool down the air with 1.5–3 °C at a distance of 1–2 km downstream [5, 6]. Typically, electricity demand increases with 2–4 % for each degree Celsius increase in outdoor temperature. It is estimated that 5–10 % of the current electricity demand for Los Angeles is to compensate the increase of 0.3–3.0 °C in urban temperature [7].

3. Benefits of comfort in workplaces

In a survey conducted in 2002, 79 % of 1500 corporate executives, facility managers and design professionals responded that they believe

rol important asupra satisfacției îl are confortul fizic; 35 % considerau că organizația lor are informații minime în ceea ce privește nivelului de satisfacție creat de mediul fizic. Aceasta arată o mare discrepanță între țelul organizatoric și înțelegerea reală a situației [8].
Într-un studiu efectuat pe un eșantion de 10.000 de lucrători din 100 de organizații s-a stabilit că beneficiile datorate unui loc de muncă "perfect" ar putea fi teoretic 17 % din costurile salariale, cu toate că experiența sugerează că cifra de 2–5 % ar fi o valoare rezonabilă. Din duzina de caracteristici evaluate, contribuția principală asupra performanțelor de muncă a rezultat a fi locurile de munca unde nu este distrasă atentia (care permit oamenilor să se concentreze atât individual cât și în grup) și posibilitatea de comunicare informală. De-a lungul unei perioada de 10 ani, 92 % din costuri au fost pentru personal (salarii și beneficii), 2 % pentru menținerea și funcționarea clădirii și numai 6 % a reprezentat costul în sine al clădirii [9]. Costul pentru tehnologizare (hardware, software, instruire) a crescut după anii '90, depășind în 2000 costurile clădirii: 3,3 % clădire, 0,8 % mobilier, 3,5 % întreținere și funcționare, 10,2 % tehnologizare, 81,6 % personal [10].
Ramura construcțiilor a avut multe eșecuri în ceea ce privește satisfacerea nevoilor de confort ale ocupanților. Diferite studii susțin că nu mai puțin de 68 % dintre angajați se plâng de iluminatul birourilor, 43 % nu sunt satisfăcuți de instalațiile de climatizare, și 56–89 % din angajații guvernamentali privesc instalațiile de climatizare ca pe o problemă [8, 11]. Deoarece costurile salariale sunt de la 8 la 13 ori mai mari decât cele de întreținere a clădirii iar confortul interior are o mare influență asupra productivității, tendința în climatizare este de a menține temperatura interioară la o valoare constantă care să mulțumească pe cât mai mulți oameni.
Tendința către un control mai riguros al temperaturii interiore este accentuată de dezvoltarea sistemelor de automatizare a clădirilor (SAC). Un SAC permite controlul temperaturii în limite restrânse în întreaga clădire. Această tendință rezultă din ideea că menținând temperatura în limite restrânse se va reduce numărul de plângeri ale ocupanților.
Menținerea temperaturii interioare la o valoare constantă necesită costuri ridicate de investiție

that physical comfort has an important impact on satisfaction; 53 % believed that their organization had minimal information regarding the level of satisfaction with the physical environment. This shows a large discrepancy between the organizational goal and actual understanding of the situation [8].
In a study involving 10,000 workers in 100 organizations, it was found that the benefits of a “perfect” workplace could theoretically equal 17 % of the salary, although experience at the time suggested that 2–5 % would be a reasonable value. Out of about a dozen features evaluated, the primary contributors to job performance were found to be the distraction-free workplace (which allows people to concentrate both as individuals and as a group) and informal communication opportunities. Over a ten year period, 92 % of costs were for people (salaries and benefits), 2 % to maintain and operate the building and only 6 % was the cost of the building itself [9]. The cost of technology (hardware, software, training) increased after the 90’s, surpassing the facility costs in 2000: 3.3 % building costs, 0.8 % furniture, 3.5 % maintenance and operation, 10.2 % technology, 81.6 % people costs [10].
The building industry failed in many cases to satisfy the comfort needs of the occupants. Different studies claim that as much as 68 % of employees complain about the light in their offices, 43 % are dissatisfied with ventilation and air conditioning, and 56-89 % of government workers regarded ventilation and air conditioning as a problem [8, 11]. Since the cost of salaries is 8 to 13 times the cost for building operation and the indoor climate highly influences the efficiency, the tendency in ventilation and air conditioning is then to keep the indoor temperature at a constant value that would dissatisfy the least number of people.

The tendency to a higher control of indoor temperature is accentuated by the development of the building management systems (BMS). The BMS allow controlling the temperature within narrow limits in the whole building. This is induced by the idea that keeping the temperature within narrow limits will reduce the complaints of the occupants.
Keeping the indoor temperature at a constant value has a high investment cost and is energy

şi energetice, cu toate implicaţiile privind consumul de resurse şi impactul asupra mediului. Pot fi obţinute importante economii de energie dacă clădirea are un domeniu larg în care temperatura poate varia liber. Un calcul simplu arată acest fapt. Să presupunem că temperatura medie lunară iarna este de 0 °C. Prin reducerea temperaturii impuse de la 20 °C la 18 °C, se poate obţine o economie de 10 %. Estimările pentru regimul de răcire sunt mult mai greu de obţinut, dar, în regiunile temperate, cele mai multe dintre sistemele mecanice de răcire pot fi înlocuite prin ventilare. În timp ce economiile de energie ale clădirilor în evoluţie liberă sunt evidente, o problemă importantă este dacă menţinerea condiţiilor ambientale predefinite va asigura confortul şi satisfacţia ocupanţilor. Corelaţia statistică dintre factorii de mediu şi senzaţia termică arată că chiar în condiţii optime impuse, gradul de nemulţumire nu este zero. Standardele ASHRAE consideră că dacă mai puţin de 20 % dintre ocupanţi sunt nemulţumiţi, atunci confortul termic este satisfăcut. O altă problemă importantă este la ce se aşteaptă oamenii de la confortul termic. Este rezonabil să ne aşteptăm că toţi oamenii vor fi satisfăcuţi de un sistem central de încălzire, ventilare şi climatizare ? Dacă standardele sunt îndeplinite, vor fi toţi oamenii din toate clădirile, în toate anotimpurilr şi tot timpul satisfăcuţi? Răspunsul este nu: este imposibil să se anticipeze exact, utilizând standardele de confort termic, cum se va simţi într-o zi un individ. Aceste standarde se bazează pe experimente de laborator şi grupuri mari de persoane; ele nu intenţionează să prezică senzaţia unei anumite persoane. Pentru a demonstra acest argument, să presupunem că o doamnă lucrează la un birou îmbrăcată în fustă, conform codului vestimentar al societăţii sau modei momentului. Ea împarte aceeaşi zonă de confort termic cu un domn în costum. Făcând evaluarea confortului, constatăm că nu există o temperatură care să satisfacă ambele persoane şi că diferenţa între temperaturile preferate de cele două persoane este de 3 °C. În absenţa controlului individual al temperaturii, compromisul este de a controla clădirea la o temperatură constantă bazată pe valorile medii ale vestimenţiei şi activităţii metabolice. Această temperatură va nemulţumi atât doamna cât şi domnul din exemplul dat [12].

-intensive, with all the implications on resources consumption and environment damaging. Important energy savings can be obtained if the building has a larger range in which its temperature can run freely. A simple calculation proves this. Let us assume that the mean monthly temperature in winter is 0 °C. Then, by reducing the set-point temperature from 20 °C to 18 °C, an economy of 10 % can be obtained. The estimation for cooling is more difficult to achieve, but, in temperate climates, most of the mechanical cooling can be replaced by free-cooling. While the energy savings of free-running buildings are evident, an important question is if maintaining predefined environmental conditions would assure the comfort and the satisfaction of the occupants. The statistical relationship between environmental factors and the thermal sensation show that even under given optimal conditions, the percentage of dissatisfaction is not zero. ASHRAE Standard considers that the thermal comfort is fulfilled if no more than 20 % of the occupants are dissatisfied. Another important question is what people expect from thermal comfort. Is it reasonable to expect that all people will be satisfied by a central ventilation and air conditioning system? If the standards are met, will all people be satisfied in all buildings, in all climates, all the time? The answer is no: it is impossible to predict exactly how an individual will feel in a particular day by using thermal comfort standards. These standards are based on laboratory experiments on large groups of persons and represent the average responses; they are not intended to predict the sensation of a person. To demonstrate this point, let us assume that a female sits at her desk wearing a skirt because of the corporate dress code or current fashion. She shares the same thermal comfort zone with a male colleague in a business suit. Evaluating the comfort will show that there is no temperature that will satisfy both persons and that the offset between preferred temperatures of the two persons will be of 3 °C. In the absence of individual temperature control, the compromise is to control the building at a constant temperature based on average values of clothing and metabolic rate. This temperature will dissatisfy both the female and the male from the previous example [12].

4. Confortul termic

Inventarea incălzirii centrale şi aerului condiţionat a făcut posibil controlul climatului interior independent de condiţiile exterioare, arhitectura clădirii şi utilizare. Clădirile au devenit aşa cum propunea Le Corbusier în anii '30: acelaşi tip de clădiri închise ermetic menţinute la 18 °C în toate anotimpurile [13]. Aceasta soluţie energofagă este susţinută de părerea că menţinând condiţii constante se asigură confortul şi satisfacţia ocumanţilor. De fapt, temperatura interioară în clădirile total echipate cu aer condiţionat are o valoare medie de 23 °C cu o deviaţie standard de 1–1.5 °C şi una sezonieră de 0.5–1 °C, care este mai restrânsă decât domeniul de 3 °C cerut de standardele ASHRAE pentru amândouă variaţiille [12]. Aceste valori se bazează pe criterii de confort care sunt importante în deciziile de proiectare. Odată ce clădirea este realizată, hotărârea asupre limitelor de confort este luată de către ocupanţi [14].

5. Controlul confortului termic

Controlul temperaturii şi umidităţii poate fi programat în timp (furnizare numai după program) sau optimizat (bazat pe măsurarea parametrilor în spaţiu). Exemple de control al optimizării încălzirii în funcţie de parametri (temperatură) sunt:

- Controlul temperaturii: protecţie împotriva înghetului; în general implică punerea în funcţiune a cazanelor şi pompelor sistemului de încălzire când temperatura exterioară atinge un nivel prestabilit (0 °C).
- Sisteme compensatorii: controlul temperaturii circuitului de încălzire în funcţie de temperatura exterioară. Aceasta va genera o creştere a temperaturii agentului atunci când temperatura exterioară scade.
- Robineţi de radiator termostataţi: reglarea debitului ce trece prin radiatoare pe care sunt montaţi în funcţie de temperatura ambiantă.
- Controlul proporţional: implică comutarea automata inchis/deschis a dispozitivului pentru a regla ieşirea.
- Alte metode pot include termostate, sesizoare de persoane tip IRP (infra-roşu pasiv) şi contrulul manual de către utilizator.

4. Thermal comfort

The invention of boilers and chillers made technologically possible the total indoor climate control regardless of outdoor conditions, building architecture and use. The buildings became what Le Corbusier proposed in the '30s: the same type of hermetically closed buildings controlled at 18 °C in all climates [13]. This energy-intensive solution is supported by the belief that maintaining constant conditions assures both comfort and satisfaction. In fact, indoor temperature in fully HVAC controlled buildings have a mean value of 23 °C with a standard deviation of 1–1.5 °C and a seasonal shift of 0.5–1 °C which is narrower than the range 3 °C for both of them, as required by ASHRAE Standard [12]. These values are based on comfort criteria which are important in design decisions. Once the building is built, the judgment concerning the comfort range is made by occupants [14].

5. Thermal comfort control

The control of temperature and humidity may be time programmable (delivered only when programmed) or optimized (based on the measurement of a parameter in space). Examples of heating optimizer parameter-based (temperature) control are:

- Temperature control: protection against freezing or frost protection; generally involves running heating system pumps and boilers when external temperature reaches a set level (0 °C).
- Compensated systems: control flow temperature in the heating circuit relative to external temperature. This will give a rise in the circuit flow temperature when outside temperature drops.
- Thermostatic radiator valves: throttle the flow through the radiator or convector to which they are fitted according to the space temperature in a room and accordingly.
- Proportional control: involves switching the equipment on and off automatically to regulate output.
- Other methods can include thermostats, occupancy sensing PIR's (passive infra-red sensors), and manual user control.

6. Controlul tehnologic individual

Opinia generală este că soluția cea mai bună pentru confort şi satisfacție este pe departe controlul parametrilor locali de confort. Controlul individual a arătat o creştere a productivității de 2,8–8,6 % [11]. Dacă se dă ocupaților controlul asupra mediului, nevoia de "condiții standard" va fi eliminată. Prin proiectare va trebui să se asigure posibilitatea de a funcționa într-un domeniu. Deoarece nu pot fi satisfăcute aceleaşi condiții interioare pentru fiecare ocupant, "controlul inteligent" pare mult mai adaptat nevoilor individuale.
Johnson Controls a realizat sistemele "Personal Environment" care permit ocupanților să controleze individual mediul lor de lucru, cum ar fi temperatura, debitul de aer, iluminatul şi acoperirea zgomotelor de fond. S-a constatat că aplicarea acestei soluții a eliminat practic plângerile (de la 40 pe zi la 2 pe săptămână) şi a crescut productivitatea angajaților unei companii de asigurări cu 2,8 % iar perioada de recuperare a investiției a fost de 18 luni [11].

6. Technological individual control

The general agreement is that the individual control of local thermal environment is by far the best solution for comfort and satisfaction. Individual control has shown productivity increases of 2.8–8.6 % [11]. If the occupants are given the control of their environment, the need for 'standard conditions' will be eliminated. The design should then provide the possibility for a range of operation. Since the same indoor conditions may not be satisfactory for every occupant, the "intelligent control" seems more adapted to individual needs.
Johnson Controls developed the "Personal Environment" systems allowing the occupants to control their individual workstation environments, including temperature, air flow, lighting and background noise masking. It is reported that the application of this solution practically eliminated the complaints (from 40 per day to 2 per week) and increased the employee productivity of an insurance company by 2.8 % and the payback period was of 18 months [11].

7. Adaptarea umană

Alături de această abordare tehnologică privind adaptarea, oamenii se adaptează ei înşâşi în trei moduri: comportamental, fiziologic şi psihologic [15]. Adaptarea comportamentală constă în acțiunea pe care o persoană o ia pentru a schimba bilanțul termic al corpului. Această acțiune poate fi tehnologică, precum acționarea unui ventilator, încălzitor, ferestre sau schimbarea îmbrăcăminții. Adaptarea fiziologică sau aclimatizarea constă în răspunsuri biologice care conduc la o mai mare toleranță. Cercetările de laborator arată că aclimatizarea nu joacă un rol prea important [16]. Adaptarea psihologică se referă la aşteptările oamenilor; oamenii se aşteaptă la ceea ce sunt obişnuiți. Aceasta poate fi explicația pentru diferențele dintre temperaturile preferate în clădirile cu aer condiționat şi cele ventilate natural [12].

7. Human adaptation

Besides this technological approach for adjustment, humans adapt themselves in three ways: behavioral, physiological and psychological [15]. Behavioral adjustment consists in the action a person takes to change the thermal balance of the body. This action can be technological, like actuating a fan, a heater, a window, or changing cloths. The physiological adjustment or acclimatization consists of biological responses that lead to higher tolerance. The laboratory evidence shows that acclimatization does not play an important role [16]. The psychological adjustment refers to people's expectations; people will expect what they are already used to. This may be the explanation for the differences between the preferred temperatures in air-conditioned and in naturally ventilated buildings [12].

8. Standarde de confort

Proiectarea clădirilor este făcută în scopul atingerii standardelor de confort.

8. Comfort standards

The design of buildings is meant to achieve the comfort standards.

Alegerea standardelor are implicații foarte importante asupra proiectării clădirilor şi a sistemelor. Cele mai utilizate standarde sunt Standardul ISO 7730 şi Standardul ASHRAE 55. Studiile în domeniul ventilării naturale a clădirilor arată o mai mare plajă de acceptabilitate decât pentru clădirile cu aer condiționat. Ideea standardelor de confort pentru clădiri ventilate natural este aceea că domeniul confortului variază cu temperatura medie lunară. Valorile acesteia pentru Europa variază între –15 °C şi 10 °C în luna ianuarie şi între 0 °C şi 30 °C în luna iulie. Eliminând extremele, putem considera că iarna avem o valoare medie lunară de 2 °C şi vara de aproximativ 22 °C.

Zonele de confort după ASHRAE sunt indicate pentru iarnă şi vară în Figura 2. Deşi temperaturile lunare medii corespunzătoare acestor sezoane nu sunt indicate, putem considera că domeniile de confort pentru iarnă şi vară pot fi aplicate şi pentru Europa.

The choice of the standard has very important implications in the design of the building and of the systems. The standards commonly used are ISO Standard 7730 and ASHRAE Standard 55. Field studies of natural ventilated buildings revealed a larger range of acceptability than in air-conditioned buildings. The idea of comfort standard for naturally ventilated buildings is that the comfort range varies with the mean monthly temperature. The values of mean monthly temperature for Europe in winter (January) is between –15 °C and 10 °C, and in summer (July) between 0 °C and 30 °C. By excluding the extremes, we may consider that winter has a mean monthly value of about 2 °C and the summer about 22 °C.

ASHRAE comfort zones are indicated for winter and summer in Figure 2. Although the mean monthly temperatures corresponding to these seasons are not pointed out, we may assume that winter and summer comfort ranges may also be applicable to Europe.

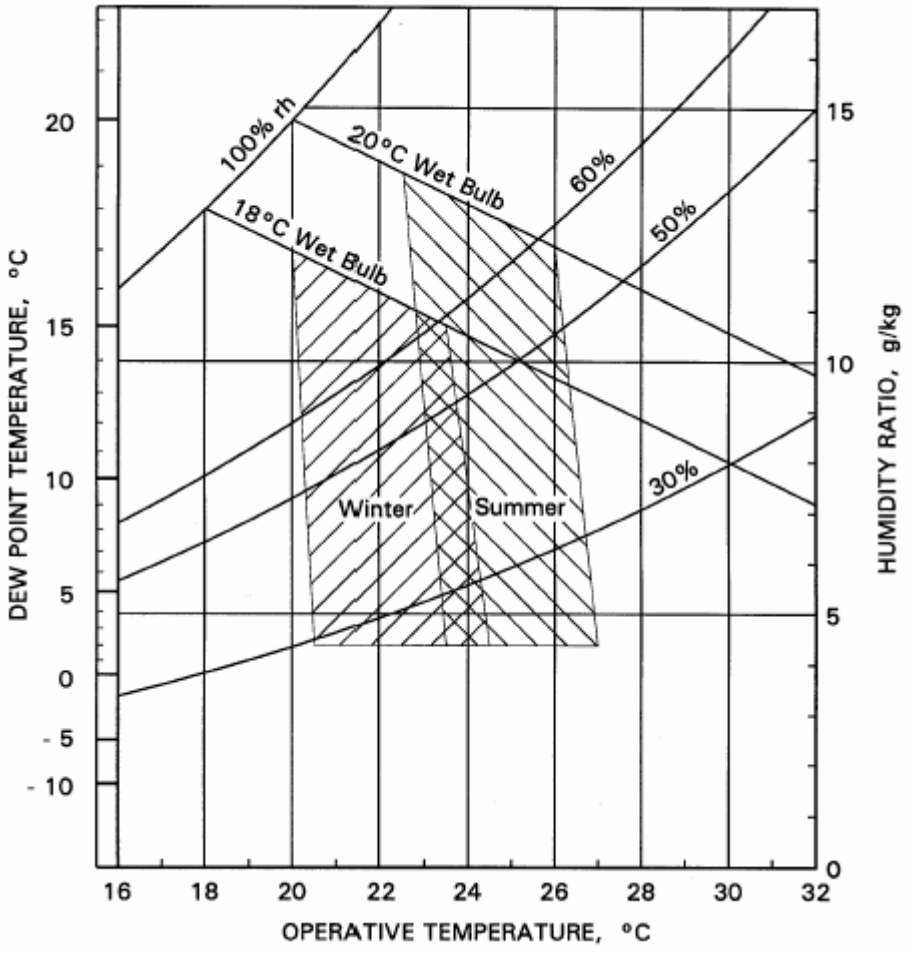

Fig. 2 Zonele de confort pentru vară şi iarnă după ASHRAE
ASHRAE summer and winter comfort zones

Bâtiments intelligents (II) - Le confort thermique dans les bâtiments adaptatifs

Résumé

Les bâtiments adaptatifs changent leur comportement en fonction de conditions météorologiques et de demandes des usagères. L'utilisation de la ventilation pour le refroidissement a un potentiel important en Europe. Néanmoins, l'économie de l'énergie doit se faire en respectant les conditions de confort à l'intérieur pour maintenir la productivité. L'environnement du bâtiment, comme la végétation, peut réduire la demande de refroidissement de 2% à 30%. A l'intérieur, le contrôle local de l'ambiance peut rendre tout le monde satisfait, avec des gains de productivité de 2,8 à 8,6%. Cette approche, corroborées avec les critères de confort adaptatif, est un changement du paradigme actuel qui impose une température quasi-constante dans tout le bâtiment dans le but d'avoir moins de 20% des occupants insatisfaits.

Bibliografie
References

[1]. WHO: *Air quality guidelines,* Geneva, World Health Organisation., **2000**.

[2]. LOMBORG, B.: *The Skeptical Environmentalist*, Cambridge University Press, **2001**.

[3]. HANSSEN, S. O.: *Evaluation of association between indoor air climate, wellbeing and productivity,* Healthy buildings, Espoo, Finland, **2000**.

[4]. AKBARI, H.: *Shade trees reduce building energy use and CO2 emissions from power plants*, Environmental Pollution 116 (Supplement 1), S119-S126, **2002**.

[5]. JAUREGUI, E.: *Influence of a large urban park on temperature and convective precipitation in a tropical city,* Energy and Buildings 15 (3-4), pp 457-463, **1990**.

[6]. CA, V. T., ASAEDA, T., et al.: *Reductions in air conditioning energy caused by a nearby park*, Energy and Buildings 29 (1): pp. 83-92, **1998**.

[7]. AKBARI, H., POMERANTZ M., et al.: *Cool surfaces and shade trees to reduce energy use and improve air quality in urban areas,* Solar Energy 70 (3): 295-310, **2001**.

[8]. DILOUIE, G.: *Personal Control,* Boosting Productivity, Energy Savings, Lighting Controls Association, **2002**.

[9]. BRILL, M.: *Using Office Design to Increase Productivity,* Buffalo, NY,**1985**.

[10]. BOSTI: *Economic benefits*, www.bosti.com/benefits.htm, **2000**.

[11]. LOMONACO, C. and MILLER, D.: *Environmental Satisfaction*, *Personal Control and the Positive Correlation to Increased Productivity*, Johnson Controls, **1996**.

[12]. FOUNTAIN, M., BRAGER, G. et al.: *Expectations of indoor climate control* Energy and Buildings 24, pp. 179-182, **1996**.

[13]. MAHDAVI, A. and KUMAR, S.: *Implications of indoor climate control for comfort, energy and environment,* Energy and Buildings 24, pp. 167-177, **1996**.

[14]. BAKER, N. and STANDEVEN, M.: *Thermal comfort for free-running buildings*, Energy and Buildings 23 (3), pp. 175-182, **1996**.

[15]. BRAGER, G. and DE DEAR R., *A standard for natural ventilation,* ASHRAE Journal (October 2000), pp. 21-28, **2000**.

[16]. BRAGER, G. and DE DEAR R., *Thermal adaptation in the built environment: a literature review*, Energy and Buildings 27, pp. 83-96, **1998**.

Clădiri inteligente (III) - Economia de energie şi calitatea spațiului amenajat

Smart buildings (III) - Energy savings and environmental quality

Cristian Ghiauş, conferențiar dr.-ing., Universitatea Tehnică de Construcții Bucureşti, inginer-cercetător, Universitatea La Rochelle, LEPTAB, Franța, (Université de La Rochelle, LEPTAB), e-mail: cristian.ghiaus@univ-lr.fr
Adrian-Gabriel Ghiauş, şef de lucrări dr.-ing., Universitatea Tehnică de Construcții Bucureşti, Facultatea de Instalații, (Technical University of Civil Engineering - Bucharest, Faculty of Building Services and Equipment), e-mail: ghiaus@mech.upatras.gr

1. Estimarea economiilor de energie

Standardul adoptat pentru confortul interior are implicații asupra soluțiilor tehnologice şi consumurilor de energie. Gradele-zile reprezintă o metodă des utilizată în estimarea consumurilor de energie din clădiri. Ideea de bază a diferitelor variante ale metodei este considerarea consumurilor de energie ca fiind proporționale cu diferența de temperaturi dintre exterior şi interior şi că această diferență este modificată de aporturile interne (precum ocupanții şi aporturile solare). Temperatura modificată este denumită temperatura punctului de echilibru, T_{bal}, care reprezintă temperatura la care, pentru o temperatură interioară dată, clădirea este în echilibru termic cu exteriorul. La această temperatură exterioară, aporturile interne egalează pierderile de căldură [1].

1. Estimation of energy savings

The standard adopted for indoor comfort has implications on the technological solutions and on the energy consumption. A popular method used to estimate the energy consumption of buildings is the degree-day. The basic idea of different variants of this method is to consider that the energy consumption is proportional to the difference between the outdoor and the indoor temperature, and to consider that this difference is modified by the internal gains (such as occupants or solar gains). The modified temperature is called balance point temperature, T_{bal}, that represents the temperature at which, for a given indoor temperature, the building is in thermal balance with the outdoors. At this outdoor temperature, the internal gains equal the thermal losses [1].

$$\dot{Q}_{gain} = K_{tot}(T_i - T_{bal}) \tag{1}$$

unde $\dot{Q}_{gain}$ sunt aporturile de căldură interne totale [W], K_{tot} coeficientul global al pierderilor de căldură [W/K], T_i temperatura interioară {K] şi T_b temperatura punctului de echilibru [K].
Temperatura punctului de echilibru este:

where $\dot{Q}_{gain}$ stands for the total internal heat gains [W], K_{tot} - total heat loss coefficient [W/K], T_i - indoor temperature [K], and T_b - balance point temperature [K].

The balance point temperature is:

$$T_b = T_i - \frac{\dot{Q}_{gain}}{K_{tot}} \tag{2}$$

Considerând variabilele din ecuația (2) pentru încălzire şi răcire, temperatura punctului de echilibru poate fi definită pentru încălzire, T_{bh}, sau răcire, T_{bc}. Încălzirea este necesară atunci când temperatura exterioară este mai mică decât temperatura punctului de echilibru, $T_o < T_{bh}$.

By considering the variables in equation (2) for heating and for cooling, the balance point temperature may be defined for heating, T_{bh}, or for cooling, T_{bc}. Heating is needed when the outdoor temperature is lower than the balance point temperature, $T_o < T_{bh}$.

Răcirea este necesară atunci când temperatura exterioară este mai mare decât temperatura punctului de echilibru, $T_o > T_{bc}$.

Fluxurile temice consumate pentru încălzire, respectiv răcire sunt:

Cooling is needed when the outdoor temperature is higher than the balance point temperature, $T_o > T_{bc}$.

The rates of energy consumption for heating and cooling are respectively:

$$\begin{cases} \dot{Q}_h = \dfrac{K_{tot}}{\eta_h}(T_{bh} - T_o), \text{when } T_o < T_{bh} \\ 0, \text{when } T_o \geq T_{bh} \end{cases} \quad (3)$$

şi

and

$$\begin{cases} \dot{Q}_c = \dfrac{K_{tot}}{\eta_c}(T_o - T_{bc}), \text{when } T_o > T_{bc} \\ 0, \text{when } T_o \leq T_{bc} \end{cases} \quad (4)$$

unde η_h şi η_c reprezintă eficiența energetică a sistemelor de încălzire şi răcire. Consumurile pentru încălzire şi răcire sunt obținute prin integrarea în timp a fluxurilor $\dot{Q}_h$ şi $\dot{Q}_c$.

Pentru o clădire dată dintr-o anumită zonă, consumurile de energie pentru încălzire şi răcire depind de:

- tipul clădirii (prin $\dot{Q}_{gain}/K_{tot}$),
- eficiența sistemului mecanic (prin η_h şi/sau η_c),
- temperatura interioară de confort, T_i şi
- localizarea geografică (prin T_o).

Deoarece adecvanța climatică a unei locații depinde de clădire, pentru calcularea temperaturii punctului de echilibru este necesară o estimare grosieră a raportului $\dot{Q}_{gain}/K_{tot}$.

Temperatura interioară de confort, T_i, are valori diferite în clădirile ventilate natural față de clădirile unde sunt folosite în totalitate sisteme de încălzire, ventilare şi aer condiționat. Temperatura exterioară, T_o, poate fi obținută de la stațiile meteo locale. Atunci când aceste date nu sunt disponibile, se poate utiliza probabilitatea distribuției temperaturii medii zilnice dintr-o lună.

where η_h and η_c are the energy efficiency of the heating and of the cooling systems. The heating and cooling consumption is obtained by integrating $\dot{Q}_h$ and $\dot{Q}_c$ over time.

For a given building in a given location, the energy consumption for heating and cooling depends on:

- building type (through $\dot{Q}_{gain}/K_{tot}$),
- mechanical system efficiency (through η_h and/or η_c),
- indoor temperature for comfort, T_i and
- site (through T_o).

As the climatic suitability of a site depends on the building, a rough estimation of the ratio $\dot{Q}_{gain}/K_{tot}$ is necessary to calculate the temperature balance point. The indoor comfort temperature, T_i, has different values in natural ventilated buildings as compared with buildings where full heating, ventilation and air conditioning systems are used. The outdoor temperature, T_o, can be obtained from local weather stations. When these data are not available, probability distribution of daily mean temperature in a month may be used.

2. Gradele-zile

Numărul gradelor-zile este o indicație reprezentativă a consumurilor de energie pentru

2. Degree-days

The number of degree-days is a representative indication of the energy consumption for

încălzire şi/sau răcire. Pentru încălzire, se defineşte ca suma diferenţelor dintre temperatura punctului de echilibru medie zilnică, T_{bh}, şi temperatura interioară T_i, atunci când $T_{bh} > T_i$:

heating and/or cooling. For heating, it is defined as the sum of the differences between the daily means of temperature point balance, T_{bh}, and indoor temperature, T_i, when $T_{bh} > T_i$:

$$DD_h = \sum_{i=1}^{N} (T_{bh} - T_i) \cdot \delta_h \tag{5}$$

unde

where

$$\delta_h = \begin{cases} 1 & \text{for } T_o < T_{bh} \\ 0 & \text{for } T_o \geq T_{bh} \end{cases}$$

şi N reprezintă numărul de zile al perioadei considerate. Similar, gradele-zile pentru răcire reprezintă suma diferenţelor dintre temperatura interioară medie zilnică, T_i, şi temperatura punctului de echilibru T_{bc}, atunci când $T_i > T_{bc}$:

and N represents the number of days in the considered period. Similarly, the degree-days for cooling represent the sum of the differences between the daily means of indoor temperature, T_i, and temperature point balance, T_{bc}, when $T_i > T_{bc}$:

$$DD_c = \sum_{i=1}^{365} (T_i - T_c) \cdot \delta_c \tag{6}$$

unde

where

$$\delta_c = \begin{cases} 1 & \text{for } T_o > T_{bc} \\ 0 & \text{for } T_o \leq T_{bc} \end{cases}$$

3. Relaţia dintre gradele-zile şi consumurile de energie

Consumurile de energie se obţin prin integrarea în timp a ecuaţiilor (3) şi (4). În intervalul de timp [0, t_{fin}), consumul de energie pentru încălzire este:

3. Relation between degree-days and energy consumption

The energy consumption is obtained by integrating equations (3) and (4) in time. During the time interval $[0, t_{fin}]$, the energy consumption for heating is:

$$Q_h = \int_0^{t_{fin}} \frac{K_{tot}}{\eta_h} \cdot (T_{bh} - T_o) \cdot \delta_h \cdot dt \tag{7}$$

iar pentru răcire este:

and for cooling it is:

$$Q_c = \int_0^{t_{fin}} \frac{K_{tot}}{\eta_c} \cdot (T_o - T_{bc}) \cdot \delta_c \cdot dt \tag{8}$$

Coeficientul total de pierdere de căldură al clădirii, K_{tot}, şi eficienţa sistemelor de încălzire şi răcire, η_h şi η_c, sunt mărimi care variază în timp. Dar, dacă sunt considerate constante, integralele (7) şi (8) devin:

The total heat loss of the building, K_{tot}, and the efficiencies of the heating and cooling systems, η_h and η_c, vary in time. But, if they are considered constant, the integrals (7) and (8) become:

$$Q_h = \frac{K_{tot}}{\eta_h} \int_0^{t_{fin}} (T_{bh} - T_o) \cdot \delta_h \cdot dt \tag{9}$$

şi:

and:

$$Q_c = \frac{K_{tot}}{\eta_c} \int_0^{t_{fin}} (T_o - T_{bc}) \cdot \delta_c \cdot dt \tag{10}$$

Gradele-zile reprezintă aproximarea integralelor (9) şi (10) prin însumarea temperaturilor medii zilnice.

Clădirile obişnuite au constante de timp care variază aproximativ între 10 ore (clădiri cu masă termică scăzută) şi 20 ore (clădiri cu masă termică medie) sau mai mult. Amplitudinea variaţiei temperaturii interioare este mai mică în comparaţie cu variaţia exterioară (Figura 1).

Atunci când este utilizată împreună cu o temperatură de echilibru constantă, numită temperatură de bază, noţiunea de grade-zile pentru încălzire şi răcire furnizează informaţii despre necesarul de combustibil. Gradele-zile au fost calculate pentru multe locaţii utilizând temperatura de bază de 18 °C atât pentru încălzire cât şi pentru răcire. Fiecare grad pentru care temperatura medie zilnică coboară sub 18 °C , este un grad-zi de încălzire; cel pentru care urcă peste 18 °C, este un grad-zi de răcire.

The degree-days represent the approximation of integrals from equations (9) and (10) by summing daily averages of temperature.

Typical buildings have time constants that vary approximately between 10h (for buildings with lower thermal mass) and 20h (buildings with medium thermal mass) or higher. The amplitude of indoor temperature variation is reduced as compared with the outdoor variation (Figure 1).

When used with a constant balance temperature, called base temperature, heating and cooling degree-days provide information about the fuel demand. Degree-days were calculated for many locations by using the base temperature of 18 °C (65 °F) for both heating and cooling. Each degree the average daily temperature falls below 18°C (65°F), is a heating degree-day; each degree the average daily temperature raises above 18°C (65°F), is a cooling degree-day.

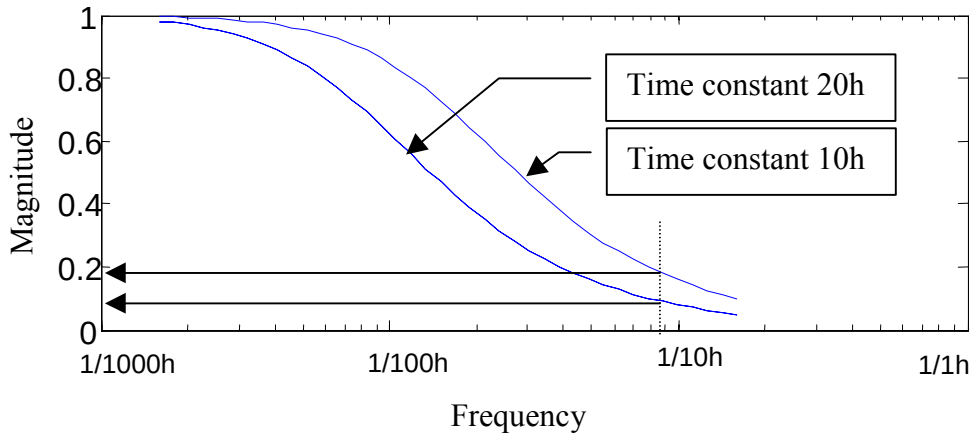

Fig. 1 Răspunsul frecvenţei sistemelor de ordinul întâi pentru constante de timp de 10 şi 20 ore
Frequency response of first order systems for time constants of 10h and 20h

Totuşi, gradele-zile calculate pentru o temperatură fixă de bază de 18 °C nu sunt exacte deoarece ipoteza că temperatura punctului de echilibru este fixă implică că şi temperatura interioară este fixă şi deoarece imbunătăţirile aduse izolaţiei termice şi etanşeităţilor clădirii reduc temperatura de echilibru.

4. Distribuţia probabilităţii temperaturii lunare

Gradele-zile pot fi calculate atunci când se cunoaşte variaţia lunară a temperaturii medii zilnice. Totuşi, această abordare are două dezavantaje: datele sunt greu disponibile şi, dacă sunt accesibile, ele trebuie să fie disponibile pentru mai mulţi ani (normal 5-10) pentru a fi semnificative din punct de vedere statistic. O alternativă la utilizarea seriilor de timp pentru calculul temperaturii medie zilnică este distribuţia probabilistică a temperaturii zilnice. Distribuţia probabilistică este obţinută din măsurări efectuate pe perioade lungi de timp (mai mult de 5 ani).
O histogramă arată distribuţia valorilor de date. Ea prezintă valorile unei variabile în intervale egale şi redă numărul de elemente pentru fiecare interval. Numărul valorilor dintr-un interval împărţit la numărul total de valori reprezintă frecvenţa relativă a acelei variabile pe interval. Densitatea probabilităţii este limita densităţii relative, atunci când numărul valorilor variabilei este infinit (Figura 2):

However, degree-days calculated for a fixed base temperature of 18 °C are misleading because the assumptions that the balance point temperature is fixed implies that the indoor temperature is fixed too, and because the improvements in thermal insulation and airtightness of the building decrease (!) the balance temperature.

4. Probability distribution of monthly temperature

Degree-days may be calculated when we know the monthly variation of daily mean temperature values. However, this approach has two disadvantages: the data are not easily available and, if accessible, they should be available for more years (typically 5-20) in order to be statistically significant. An alternative to using time series of daily mean temperatures is to use the probability distribution of daily mean temperatures. The probability distribution is obtained on measurements achieved during long periods of time (more than 5 years).
A histogram shows the distribution of data values. It bins the values of a variable in equally spaced containers and returns the number of elements in each container. The number of values in an interval (bin) divided by the total number of values represents the relative frequency of that variable for a bin. The probability density is the limit of relative density, when the number of values of the variable is infinity (Figure 2):

$$Pr = \lim_{N \to \infty} \left(\frac{f}{N} \right) \tag{11}$$

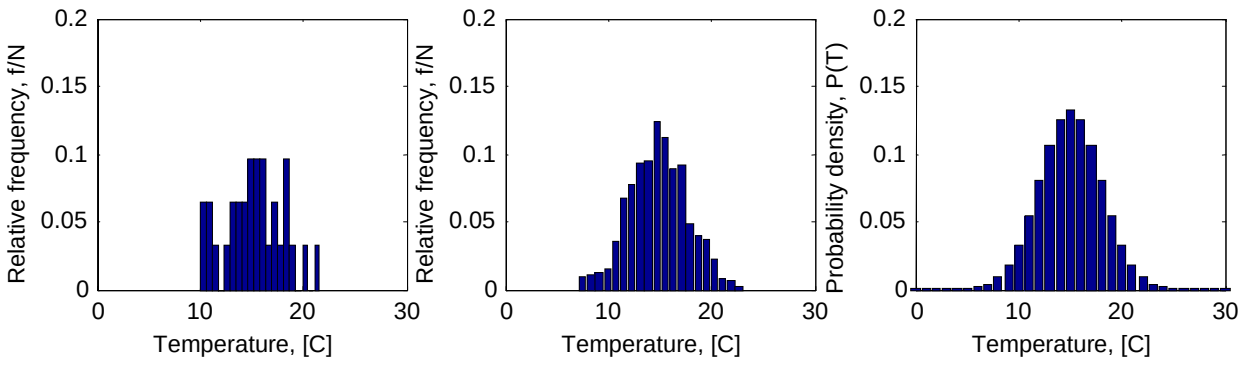

Fig. 2 Frecvenţa distribuţiei relative şi densitatea probabilităţii
Relative distribution frequency and probability density

Funcția densității de probabilitate, *fdp*, (Figura 3) are interpretare diferită în funcție de tipul distribuției: discretă sau continuă. Pentru distribuția discretă, funcția densității de probabilitate este probabilitatea de observare a unui eveniment particular. Să considerăm, de exemplu, că temperatura este măsurată în valori discrete de 1 °C. În cazul funcției densității de probabilitate discretă (*fdp*) prezentată în Figura 3a, probabilitatea ca temperatura să fie 10 °C este dată de valoarea 10 a lui *fdp*. Spre deosebire de distribuțiile discrete, *fdp* pentru o distrubuție continuă la o valoare nu este probabilitatea de observale a acelei valori. Pentru distribuțiile continue, probabilitatea de observare a oricărei valori particulare este zero. Pentru a obține probabilități, trebuie să integrăm *fdp* pe un interval. De exemplu, probabilitatea ca temperatura să fie între 9,5 şi 10,5 °C este integrala *fdp*-ului de la 9,5 la 10,5 °C (Figura 3b).

Pentru o distribuție discretă având intervalele t_{bin}, probabilitatea ca temperatura să fie între $T - t_{bin}/2$ şi $T + t_{bin}/2$, este:

The probability density function, *pdf*, (Figure 3) has a different meaning depending on whether the distribution is discrete or continuous. For discrete distributions, the probability density function is the probability of observing a particular outcome. Let us consider, for example, that the temperature is measured in discrete values of 1 °C. In the case of the discrete probability density function (*pdf*) represented in Figure 3a, the probability that the temperature is 10 °C is given by the value of the *pdf* at 10. Unlike discrete distributions, the *pdf* of a continuous distribution at a value is not the probability of observing that value. For continuous distributions, the probability of observing any particular value is zero. To obtain probabilities, we should integrate the *pdf* over an interval. For example, the probability that the temperature is between 9.5 and 10.5 °C is the integral of the appropriate *pdf* from 9.5 to 10.5 °C (Figure 3b).

For a discrete distribution having bins of t_{bin}, the probability of the temperature being between $T - t_{bin}/2$ and $T + t_{bin}/2$, is:

$$T \in \{T_{min},\ T_{min} + t_{bin},\ T_{min} + 2t_{bin},\ \ldots, T_{max}\}$$
$$Pr\left(T \in \left[T - t_{bin}/2,\ T + t_{bin}/2\right]\right) = t_{bin} \cdot P_{df}(T) \qquad (12)$$

Pentru o distribuție continuă, probabilitatea ca temperatura să fie între $T - t_{bin}/2$ şi $T + t_{bin}/2$, $T \in R$ este:

For a continuous distribution, the probability of the temperature being between $T - t_{bin}/2$ and $T + t_{bin}/2$, $T \in R$, is:

$$Pr\left(T \in \left[T - t_{bin}/2,\ T + t_{bin}/2\right]\right) = \int_{T - t_{bin}/2}^{T + t_{bin}/2} P_{df}(T) \cdot dT \qquad (13)$$

Să considerăm o variabilă aleatoare, *T*, care are *N* valori.

Let us consider a random variable, *T*, that has *N* values.

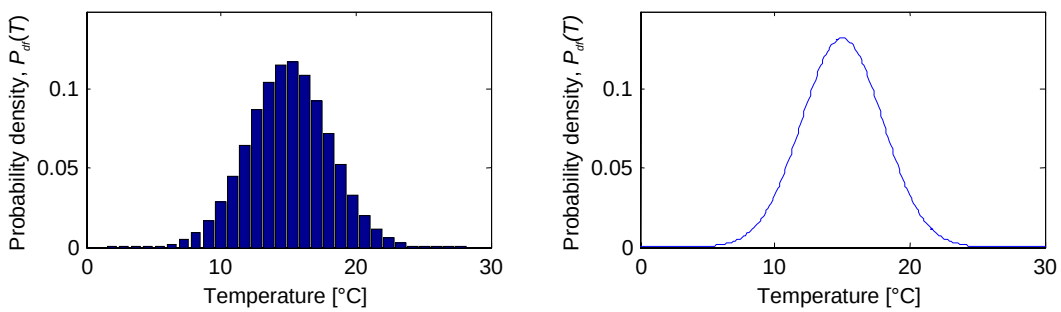

Fig. 3 Funcția densității de probabilitate discretă şi continuă
Discrete and continuous probability density function

Pentru variabila T, frecvența probabilității de a fi în intervalul $\left[T - t_{bin}/2,\ T + t_{bin}/2\right]$ este:

For variable T, the probable frequency of being in the bin $\left[T - t_{bin}/2,\ T + t_{bin}/2\right]$ is:

$$f\left(T \in \left[T - t_{bin}/2,\ T + t_{bin}/2\right]\right) = N \cdot Pr\left(T \in \left[T - t_{bin}/2,\ T + t_{bin}/2\right]\right) \tag{14}$$

Pentru o distribuție discretă, ecuația (14) devine:

For a discrete distribution, eq. (14) becomes:

$$f\left(T \in \left[T - t_{bin}/2,\ T + t_{bin}/2\right]\right) = N \cdot t_{bin} \cdot P_{df}(T) \tag{15}$$

iar pentru o distribuție continuă:

and for a continuous distribution it becomes:

$$f\left(T \in \left[T - t_{bin}/2,\ T + t_{bin}/2\right]\right) = N \cdot \int_{T - t_{bin}/2}^{T + t_{bin}/2} P_{df}(T) \cdot dT \tag{16}$$

Dacă variabila aleatoare T reprezintă temperatura medie zilnică într-o lună, atunci N este numărul total de zile dintr-o lună, $N \in \{28, 30, 31\}$ şi $f\left(T \in \left[T - t_{bin}/2, T + t_{bin}/2\right]\right)$ dă numărul de zile dintr-o lună în care temperatura este $T \in \left[T - t_{bin}/2, T + t_{bin}/2\right]$. Având numărul probabil de zile dintr-o lună cu o temperatură medie dată, putem calcula numărul de grade-zile pentru acea lună.

If the random variable T represents the daily mean temperature in a month, then N is the total number of days in a month, $N \in \{28, 30, 31\}$ and $f\left(T \in \left[T - t_{bin}/2, T + t_{bin}/2\right]\right)$ gives the number of days in a month that have the temperature $T \in \left[T - t_{bin}/2, T + t_{bin}/2\right]$. Having the probable number of days in a month with a given mean temperature, we can calculate the number of degree-days for that month.

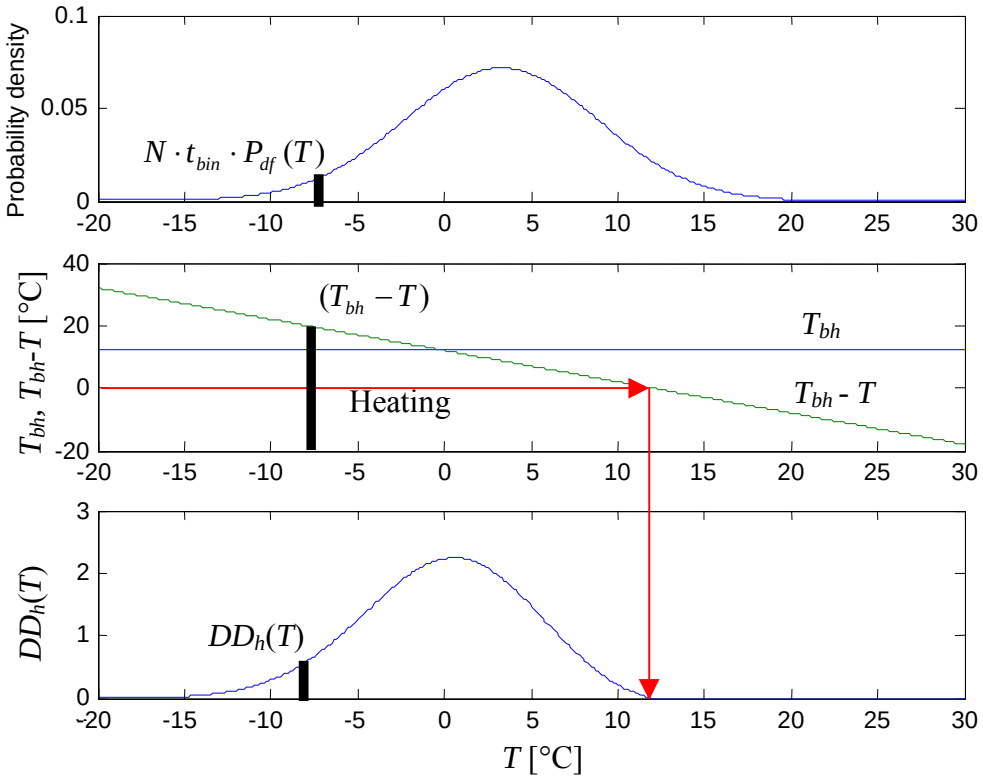

Fig. 4 Obținerea gradelor-zile din funcția densității de probabilitate şi diferența dintre temperatura exterioară şi temperatura de echilibru

Obtaining degree-days from probability density function and the difference between the outdoor temperature and the balance temperature

Gradele-zile sunt o funcție de temperatura exterioară. Pentru o temperatură exterioară dată, *T*, gradele zile reprezintă produsul dintre numărul de zile având temperatura medie T, exprimat prin $N \cdot t_{bin} \cdot P_{df}(T)$ şi diferența de temperatură $(T_{bh} - T)$, atunci când $T_{bh} > T$, condiție dată de δ_h (Figura 4). În mod similar, sunt date gradele-zile pentru răcire.

The degree-days are a function of outdoor temperature. For a given outdoor temperature, *T*, the degree-days are the product of the number of days having mean temperature *T*, number expressed by $N \cdot t_{bin} \cdot P_{df}(T)$ and the temperature difference $(T_{bh} - T)$, when $T_{bh} > T$, condition given by δ_h (Figure 4). Similarly, see the degree-days for cooling.

$$DD_h(T) = N \cdot t_{bin} \cdot P_{df}(T) \cdot (T_{bh} - T) \cdot \delta_h \quad (17)$$

$$DD_c(T) = N \cdot t_{bin} \cdot P_{df}(T) \cdot (T - T_{bc}) \cdot \delta_c \quad (18)$$

5. Metoda înaltei calități a spațiului amenajat

În Franța, înalta calitate a spațiului amenajat din clădiri este definită de metoda HQE® "Haute Qualité Environmentale". Ea constă în controlul impactului clădirii asupra spațiului amenajat şi în creerea unui mediu interior confortabil şi sănătos. Metoda HQE® este aplicată în toate etapele de viața ale clădirii: proiectare, construcție, funcționare şi demolare.
Elementele HQE® sunt definite pe baza standardelor de calitatea managementului [2]. Acest standard defineşte:
- calitatea – capacitatea unei entități de a satisface cerințele explicite sau implicite;
- entitate – ceea ce poate fi descris şi considerat în mod separat;
- cerințe de calitate – exprimarea cerințelor individuale sau ca un grup, calitativ şi cantitativ, pentru o entitate în vederea efectuării unei examinări.

5. High environmental quality approach

In France, the high environmental quality of buildings is defined by the HQE® approach, "Haute Qualité Environmentale". It consists in the control of the impact of the buildings on the environment and in creating a healthy and comfortable indoor environment. The HQE® approach is applied in all stages of building life: design, construction, operation and demolition.
The issues of HQE® are defined based on the standard for quality management [2]. This standard defines:
- quality – the capacities of an entity to satisfy the explicit or implicit needs;
- entity – what can be described and considered separately;
- requirements for quality – the expression of the needs or their expression as a set of needs, qualitatively and quantitatively, for an entity in order to allow the examination.

Bâtiments intelligents (III) - L'économie d'énergie et la haute qualité environnementale

Résumé

L'estimation approximative des consommations énergétiques des bâtiments se peut se faire en utilisant les degrés-jours. Leurs calcule nécessite les valeurs moyennes journalières qui sont difficilement disponible. On propose une méthode alternative qui utilise les distributions de probabilité, disponible suite à des études météorologiques. La consommation énergétique des bâtiments constitue un critère de la haute qualité environnementale, approche qui consiste en l'évaluation de l'impact environnemental des bâtiments pendant toute leurs durée de vie.

Bibliografie
References

[1]. ASHRAE, *Thermal comfort*. ASHRAE Fundamentals, **2001**.

[2]. ISO 9000, *Quality management systems - Fundamentals and vocabulary*, International Organization for Standardization, 29, **2000**.